NASA TECHNICAL NOTE

NASA TN D-4092

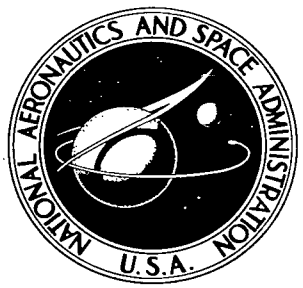

NASA TN D-4092

AERODYNAMIC CHARACTERISTICS OF A LARGE-SCALE V/STOL TRANSPORT MODEL WITH LIFT AND LIFT-CRUISE FANS

by Leo P. Hall, David H. Hickey, and Jerry V. Kirk

Ames Research Center
Moffett Field, Calif.

NATIONAL AERONAUTICS AND SPACE ADMINISTRATION • WASHINGTON, D. C. • AUGUST 1967

AERODYNAMIC CHARACTERISTICS OF A LARGE-SCALE V/STOL TRANSPORT MODEL WITH LIFT AND LIFT-CRUISE FANS

By Leo P. Hall, David H. Hickey,
and Jerry V. Kirk

Ames Research Center
Moffett Field, Calif.

NATIONAL AERONAUTICS AND SPACE ADMINISTRATION

For sale by the Clearinghouse for Federal Scientific and Technical Information
Springfield, Virginia 22151 – CFSTI price $3.00

AERODYNAMIC CHARACTERISTICS OF A LARGE-SCALE V/STOL TRANSPORT MODEL WITH LIFT AND LIFT-CRUISE FANS

By Leo P. Hall, David H. Hickey,
and Jerry V. Kirk

Ames Research Center

SUMMARY

A wind-tunnel investigation was conducted to determine the aerodynamic characteristics of two configurations of a V/STOL transport model powered by tip-turbine-driven fans. The VTOL propulsion system for the first configuration was a combination of lift fans and rotating cruise fans, and for the second configuration was tandem mounted lift fans. Both configurations used a high mounted wing with an aspect ratio of 5.8, swept back 35° at the quarter chord line, and a taper ratio of 0.3.

The results showed a large increase in lift with forward speed for both configurations in spite of the unloading of the wing induced by front fan operation. Longitudinal characteristics for both configurations with the fans operating appear to be similar to the characteristics of conventional aircraft; however, both configurations suffer directional instability over at least part of the speed range.

INTRODUCTION

The Ames Research Center is studying the large-scale low-speed aerodynamic characteristics of V/STOL transport configurations powered by lift fans, cruise fans, or combinations of both. The purpose of the present investigation, conducted in the 40- by 80-foot wind tunnel, was to determine the aerodynamic characteristics of two configurations: The first had lift fans mounted ahead of the wing and rotating cruise fans mounted aft of the wing; the second configuration had tandem mounted lift fans faired into the wing. The lift-propulsion system consisted of four 3-foot-diameter tip-driven fans powered by one gas generator.

General aerodynamic characteristics presented show the effects of fan operation on model variables and the effects of forward speed on fan operation. Some of the model variables investigated include the effects of exit-vane deflection, flap deflection, front lift fan location, and rotating cruise fan angle. Results for both configurations, obtained over the fan-powered speed range, are analyzed to show the effect of interference between the fan flow and airframe flow field.

NOTATION

A	fan exit area, sq ft, or wing aspect ratio
b	wing span, ft
c	wing chord parallel to plane of symmetry
$\bar{c}$	mean aerodynamic chord, $\frac{2}{S}\int_0^{b/2} c^2\,dy$
C_D	drag coefficient, $\frac{D}{qS}$
C_l	rolling-moment coefficient, $\frac{l}{qSb}$
C_L	lift coefficient, $\frac{L}{qS}$
C_m	pitching-moment coefficient, $\frac{M}{qS\bar{c}}$
C_n	yawing-moment coefficient, $\frac{N}{qSb}$
C_Y	side-force coefficient, $\frac{Y}{qS}$
D	drag, lb
D_f	diameter of the fan, ft
i_D	cruise duct angle, angle-of-thrust axis to free stream, deg
i_t	horizontal-tail incidence angle, deg
l	rolling moment, ft-lb
L	total lift on model, lb
M	pitching moment, ft-lb
MC	moment center
N	yawing moment, ft-lb
p_l	local static pressure, lb/sq ft
p_s	free-stream static pressure, lb/sq ft
P	pressure coefficient, $\frac{p_l - p_s}{q}$

P_o standard atmospheric pressure, 2116 lb/sq ft

q free-stream dynamic pressure, lb/sq ft

R fan radius, ft

RPM corrected fan rotational speed, $\frac{\text{fan speed}}{\sqrt{\theta}}$

S wing area, sq ft

T complete ducted fan thrust in the lift direction with $\alpha = 0^o$ and $\beta_v = 0^o$, $\rho A v_j^2$, lb

V air velocity, ft/sec

V_o free-stream air velocity, knots or ft/sec

x distance from the leading edge, ft

y spanwise distance perpendicular to the plane of symmetry, ft

Y side force, lb

α angle of attack of the wing chord plane, deg

β angle of sideslip, deg

β_v fan exit-vane deflection angle from the fan axis, deg

δ relative static pressure, $\frac{p_s}{P_o}$

δ_f trailing-edge flap deflection measured normal to the hinge line, deg

θ ratio of ambient temperature to standard temperature (519^o R)

ϵ average downwash at the horizontal tail, deg

η fraction of wing semispan, $\frac{2y}{b}$

μ tip-speed ratio, $\frac{V}{\omega R}$

ρ density, lb-sec^2/ft^4

ω fan rotational speed, radians/sec

Subscripts

j fan exit

s static conditions

T tare

u uncorrected

w wing

MODEL AND APPARATUS

The model is shown installed in the test section of the Ames 40- by 80-Foot Wind Tunnel in figure 1. Figure 1(a) is a photograph of the lift-cruise fan configuration (direct lift fan forward and rotating cruise fan aft). Figure 1(b) is a photograph of the tandem lift fan configuration. Pertinent dimensions of the two configurations are given in figures 2(a) and 2(b).

Wing Geometry

The high-mounted wing had an aspect ratio of 5.8 and a taper ratio of 0.3, and was swept back 35° at the quarter-chord line. An NACA 65-412 airfoil section was basic for the wing. Fairings covered the gap between the fan and the wing on the tandem lift fan configuration.

Details of the 22-percent-chord single-slotted flap are shown in figure 2(c). The flap on the configuration with the rotating cruise fans and direct lift fans extended from 15.9 to 63.6 percent semispan. The flap on the configuration with the tandem lift fans extended from 41.6 to 63.6 percent semispan. Flap deflections of 0° and 45° were tested.

Fuselage

The fuselage was slab sided with rounded corners. Overall it was 6.5 feet high, 5.8 feet wide, and 44.0 feet long. The fans were driven by a G.E. J85-5 gas generator mounted on top of the fuselage.

Tail

The geometry and location of the all movable horizontal tail are shown in figure 2(b). The tail was pivoted about the quarter chord and had a range from -13° to +23° incidence. For the tests indicated "tail off" only the horizontal tail was removed.

Propulsion System

For these studies, the four 3-foot-diameter G.E. X-376 tip-turbine-driven fans were powered by one G.E. J85-5 engine. The engine exhaust was ported through a diverter valve into a plenum chamber and then ducted to the tip turbines of the individual fans. Fan locations and associated ducting arrangements could be varied in order to test the two front fans in the positions shown in figure 2(a).

For the tests with only two fans operating, the excess J-85 exhaust was ducted out a tail pipe in the thrust direction; the data were corrected for this thrust.

Fan installation.- Details of the rotating cruise fan pods are given in figure 2(c). The exit area was intended to produce the design pressure ratio across the fan at zero and low forward speeds. Symmetrical airfoil-shaped fairings, attached to the fan pods, covered the supporting structure. Details of the lift fan pods, used for the lift-cruise fan configuration, are also given in figure 2(c). The lift fan pods were 0.67 foot thick and had a 0.33-foot-radius inlet.

For the tandem lift fan configuration the fan pods were the same as previously described; however, the gaps between the fans and the wing were covered with fairings.

A cascade of fourteen 4.06-inch-chord exit vanes was mounted downstream of the lift fan pods. These vanes extended across the tip-turbine exhaust and were used both to direct the fan flow and as a lower surface wing closure ($\beta_v = 90^\circ$) for power-off testing. The vane airfoil sections had a maximum thickness of 10-percent chord at 20-percent chord and a maximum of 2.3-percent-chord camber of the mean line at 35-percent chord.

TESTING AND PROCEDURE

Longitudinal force and moment data were obtained through an angle-of-attack range from -2° to $+24^\circ$; lateral directional data were obtained through an angle-of-sideslip range of -10° to $+4^\circ$ at 0° angle of attack. Airspeed of the tests, corresponding to a maximum Reynolds number of 10.4 million, varied from 0 to 140 knots. Fan RPM was varied from 1800 to 4000. Some fan exit pressures and wing surface pressure distributions were also measured during the tests.

Tests With Constant Angle of Attack

At 0° angle of attack, fan speed and wind-tunnel velocity were varied independently. For the lift-cruise fan configuration, results were obtained for three front lift-fan locations, five rotating cruise fan angles, several exit vane angles, two flap deflections, tail on and tail off. Also, a limited amount of data was taken at 12° angle of attack. For the tandem lift fan

configuration results were obtained at several exit vane angles, two flap deflections, tail on and tail off. Some data were taken with the fairings removed from the tandem lift fan configuration.

Tests With Varying Angle of Attack

Fan RPM and tunnel forward speed were maintained essentially constant when angle of attack was varied. These tests were made at several values of fan RPM and tunnel airspeed. The model variables tested in this manner were the same as those mentioned above.

CORRECTIONS

Force and moment data obtained without the fans operating were corrected for the effect of wind-tunnel wall constraint as follows:

$$\alpha = \alpha_u + 0.486\ C_{L_u}$$

$$C_D = C_{D_u} + 0.0085\ C_{L_u}^2$$

$$C_m = C_{m_u} + 0.0169\ C_{L_u} \text{ (tail on only)}$$

Reference 1 defines a set of model-to-wind-tunnel sizing constraints that give only small wind-tunnel wall effects. According to those constraints there should be only small wind-tunnel wall effects for the subject model; therefore no wind-tunnel wall corrections were applied to the results obtained with the fans operating.

A correction of $C_{D_T} = 0.0016$ for the drag of the model support structure has been applied to all of the data.

RESULTS

Table I is an index to the figures. Results from the lift-cruise fan configuration are presented before those from the tandem lift fan configuration. (Unless otherwise noted, the lift fans are in the low aft position, fig. 2(a).) For each configuration the characteristics at constant angle of attack are presented first, then results with variable angle of attack, and last, results with variable angle of yaw.

Tip-speed ratio, μ, will be used as the independent parameter in the following data presentation. The relationship between tip-speed ratio and the more general parameter, free-stream to fan-velocity ratio, is shown in figure 3.

Lift-Cruise Fan Configuration

Fan characteristics.- The effect of test and configuration variables on fan performance at zero airspeed is shown by the results in figure 4. Figure 4(a) shows the total forces and moments on the complete lift-cruise fan configuration at various cruise fan angles, with and without the lift fans running. The effect of exit-vane angle deflection on forces and moments contributed by the left front fan operating at 3600 RPM is presented in figure 4(b). Figure 5 presents the variation of average fan thrust with airspeed for the left front fan as measured with an equal-area momentum rake.

Aerodynamic characteristics with constant angle of attack.- Figures 6 through 16 show the effect of fan and model configuration variables on longitudinal and lateral-directional characteristics.

The variation with tip-speed ratio of the ratio of lift at forward speed to the static lift and the ratio of moment to static lift for trim drag (D = 0) for the two front fans operating in each of the three alternate positions is presented in figure 6(a). Similar data for the lift-cruise fan configuration with the horizontal tail off are presented in figure 6(b), and for the complete lift-cruise fan configuration in figure 6(c). The static lift used in figure 6 is for a cruise duct angle of 90° and $\beta_V = 0^{\circ}$.

Results in figures 7 through 11 show the longitudinal characteristics as a function of tip-speed ratio for the model variables tested. Figures 7 through 9 show characteristics with only the two front fans operating in three positions; figure 7 presents data for the high aft position, figure 8 presents data for the high forward position, and figure 9 presents data for the low aft position. A limited amount of data at 12° angle of attack is also included. Figure 10 shows the longitudinal characteristics with just the rotating cruise fans operating. Figure 11 shows the longitudinal characteristics for the complete lift-cruise fan configuration with several exit-vane angles and rotating cruise fan angles. Included in figure 11 are the data with the horizontal tail off.

Results in figures 12 and 13, showing the effect of varying fan rotational speed at several cruise fan angles and forward speeds, demonstrate the adequacy of tip-speed ratio as a parameter.

Figure 14 shows the effect of front lift fan location on spanwise wing loading when only the front lift fans are operating. Tabulated on this figure are the wing lift coefficients from integrated pressure distributions.

Figure 15 shows the trim effectiveness of the horizontal tail with power off and lift fans sealed; figure 16 shows the average downwash at the horizontal tail for different cruise fan duct angles and forward speeds as computed from tail-on and tail-off data.

Variation of aerodynamic characteristics with angle of attack.- Data in figures 17 through 24 show the variation of longitudinal characteristics with angle of attack. The data for speeds up to 30 knots are presented as forces and moments while the results for higher speeds are in coefficient form.

Figure 17 presents the longitudinal characteristics for the basic model with all fans removed. Figure 18 presents similar data for the three alternate lift fan locations (power off) with the rotating cruise fans removed. Figure 19 presents power-off data for the complete lift-cruise fan configuration. Figure 20 presents the longitudinal characteristics at low forward speed with four fans operating, and figure 21 presents similar data at higher forward speeds. Figure 22 presents the longitudinal characteristics for the model in the cruise configuration with a cruise fan angle of 0° and flaps up. Figures 23 and 24 show the variation of longitudinal characteristics with angle of attack for the front lift fans operating in the three alternate positions with the rotating cruise fans removed.

Aerodynamic characteristics with variable angle of sideslip.- Figure 25 presents the effect of sideslip angle on the longitudinal and lateral-directional characteristics for the complete lift-cruise fan configuration. The data obtained were for two tip-speed ratios and three rotating cruise fan angles.

Tandem Lift Fan Configuration

Fan characteristics.- Figure 26 presents the zero airspeed characteristics of the model with only the left front fan operating and with all four fans operating in the tandem lift fan configuration.

Aerodynamic characteristics with zero angle of attack.- Results presented in figures 27 through 34 show longitudinal characteristics at 0° angle of attack as a function of tip-speed ratio. The variation of the ratio of lift at forward speed to static lift and the ratio of moment to static lift for trim drag is shown in figure 27. Results for the rear fans operating and front fans sealed are presented in figure 28 and those for the front fans operating and rear fans sealed, in figure 29. Figures 30 and 31 show the longitudinal characteristics for the complete tandem lift fan configuration, with flaps at 45° and 0°, respectively. The longitudinal characteristics with the horizontal tail and fairings removed are shown in figures 32 and 33. For analysis of these data, moments are presented for two moment centers (see fig. 2(b)).

Figures 34 and 35 present the trim effectiveness of the horizontal tail and average downwash at the horizontal tail for the complete tandem lift fan configuration.

Aerodynamic characteristics with variable angles of attack.- Data in figures 36 through 38 show the variation of longitudinal characteristics with angle of attack. Figure 36 presents the power-off longitudinal characteristics showing the effect of flap deflection, horizontal tail, and fairings. Figure 37 presents the longitudinal characteristics for the complete tandem lift fan configuration at various tip-speed ratios. The low speed data are presented as forces and moments while the results at higher speed are in coefficient form. Figure 38 presents similar longitudinal characteristics with the fairings removed.

Aerodynamic characteristics with variable angle of sideslip.- Figures 39 and 40 present the effect of sideslip angle on longitudinal and lateral-directional characteristics for the complete tandem lift fan configuration. Figure 39 presents the low speed data as forces and moments. Figure 40 presents the higher speed data in coefficient form.

DISCUSSION

Combination Lift Fans and Rotating Cruise Fans

Fan performance.- Comparison of the left front fan thrust (figs. 4(b) and 26) with the two-fan thrust (fig. 4(a)) and the four lift fans (fig. 26) indicates that the left front lift fan thrust is 86 percent of the right fan thrust and of the rear lift fans. This poor performance of the left front lift fan is probably caused by leakage from the turbine into the fan flow. The measured static lift fan thrust, for both front lift fans, is 80 percent of the cruise fan thrust (calculated for $i_D = 90^o$). This decrement is believed due to inlet losses, exit-louver losses, and the previously noted leakage.

Aerodynamic characteristics.- In order to determine and minimize unloading of the wing induced by fan operation, the two front fans were tested in three positions before the complete configuration was tested. The spanwise wing loading for these three front fan positions shows that fan operation did cause negative wing lift over part of the tip-speed ratio range in all fan locations, and in the worst fan location (high aft), caused negative wing lift at all airspeeds. With fan power off, wing lift was positive because of lift due to camber. In spite of the unloading of the wing due to fan operation, the ratio of total lift to fan static thrust as a function of tip-speed ratio for trim drag (fig. 6(a)) shows an increase of lift with forward speed for each of the three front fan locations. This surprising result is discussed more completely in reference 2. The low fan position just forward of the wing leading edge has the largest lift-to-thrust ratio over the whole speed range; consequently, the complete lift-cruise fan configuration was tested with the lift fans in this low aft position.

The variations of the ratio of total lift at forward speed to static lift with tip-speed ratio, figure 6, summarize the data in figures 7 through 9 and figure 11. Figures 6(b) and (c) show a marked increase in lift ratio with tip-speed ratio for the complete lift-cruise fan configuration; however, a large portion of this lift is due to wing lift. At high tip-speed ratios the lift-to-static-thrust ratio without the wing lift is less than 1, indicating that when the complete lift-cruise fan configuration is assembled, induced lift due to the operation of lift fans and cruise fans is not sufficient to balance the lift lost by vectoring the lift fan flow or rotating the cruise fans.

The variation of longitudinal characteristics with angle of attack at several airspeeds and cruise duct angles (figs. 17-24) shows that within the

angle-of-attack range tested, the model has a basic pitch-up problem typical of a high horizontal-tail location. Lift-cruise fan operation did not significantly affect this problem.

The variation of lateral-directional characteristics with angle of sideslip (fig. 25) for the complete lift-cruise fan configuration shows the variation of side force and rolling moment with sideslip to be linear and stable. The variation of yawing moment with sideslip is neither linear nor stable.

Tandem Lift Fan Configuration

Fan performance.- As mentioned in the discussion of the lift-cruise fan configuration, the static performance of the left front lift fan (fig. 26) was less than would be anticipated from the data with all four fans operating. If the difference between the two-fan data (fig. 4) and the left front lift fan data is used as the thrust of the other fans, the total lift fan performance can be predicted quite closely.

Aerodynamic characteristics.- The variation with tip-speed ratio of the ratio of lift at forward speed to static lift for zero drag (fig. 27) summarizes the data in figures 28 through 33. This summary shows that with only the rear fans operating, there is a large amount of positive induced lift, whereas with only the front fans operating, there is a negative induced lift. With all four fans operating lift was approximately midway between that for the other two situations. The effect of the fairings between the lift fans and the wing is also shown on this figure. These results show slightly less induced lift with the fairings than without. As in reference 3 there was no evidence of lift loss with increasing forward speed for any of the flap or exit-vane conditions studied when all four fans were operating.

Power-off longitudinal characteristics for the tandem lift fan configuration (fig. 36) had a severe pitch-up, perhaps caused by both the horizontal-tail location and the wing planform. Lift fan operation caused little change in lift-curve slope or static margin. The pitching-moment variation with airspeed, discussed more fully in reference 2, was less for this configuration than for an equivalent fan-in-wing model.

The lateral-directional characteristics with angle of sideslip (figs. 39 and 40) show side force and rolling moment to be large and a function of airspeed but stable. The variation of yawing moment with sideslip is unstable only at low speeds.

Ames Research Center
National Aeronautics and Space Administration
Moffett Field, Calif., 94035, April 13, 1967
721-03-00-06-00-21

REFERENCES

1. Cook, Woodrow L.; and Hickey, David H.: Comparison of Wind-Tunnel and Flight-Test Aerodynamic Data in the Transition-Flight Speed Range for Five V/STOL Aircraft. NASA SP-116, 1966.

2. Hickey, David H.; Kirk, Jerry V.; and Hall, Leo P.: Aerodynamic Characteristics of a V/STOL Transport Model With Lift and Lift-Cruise Fan Power Plants. NASA SP-116, 1966.

3. Hickey, David H.; and Hall, Leo P.: Aerodynamic Characteristics of a Large-Scale Model With Two High Disk-Loading Fans Mounted in the Wing. NASA TN D-1650, 1963.

TABLE I.- LIST OF FIGURES

Figure	α, deg	β, deg	β_V, deg	μ	Configuration: δ_F, deg	Configuration: i_D, deg	Configuration: Tail	Remarks
Lift-cruise fan configuration								
3	0	0	0	Variable	45	Off	0	Relationship of μ to V_o/V_j
4(a)			0	0				Lift fan performance
4(b)			Variable	0				
5			-10 to 30	Variable				
6(a)			Set to trim drag		0		Off	Lift and moment for trim drag
6(b)					45	30,60,75	Off	
6(c)					45	30,45,60,75	0,15	
7(a)			-10 to 50		0	Off	Off	Front fans operating only
7(b)	12							
8(a)	0							
8(b)	0							
8(c)	12							
9(a)	0							
9(b)	12							
10(a)	0		Sealed and removed		0,45	0,45,60	0	Cruise fans operating only
10(b)								
10(c)								
11(a)			-10 to 40		45	75		Complete configuration
11(b)			-10 to 40			60		
11(c)			-10 to 50			45	15	
11(d)						30	0	
11(e)						75	Off	
11(f)						60	Off	
11(g)			-10 to 40			30	Off	
12(a)			0			75	0	Effect of varying fan speed, complete configuration
12(b)			0			60	0	
12(c)			10,38			45	7,15	
12(d)			0			30	0	
13(a)						75	Off	
13(b)						60		
13(c)						30		
14(a)				0.06,0.09,0.12,	0	Off		Spanwise wing loading
14(b)				0.18,0.24,0.30				
14(c)								
15			90	∞	45	60	Variable	Trim effectiveness
16			0	Variable	45	30,60,75	~	Average downwash power off
17	Variable		Off	∞	0,45	Off	0	
18			90		0	Off	Off	
19			90		45	0,45,60,75	0,15	
20			0,9	0.06,0.10		75	20	Complete configuration
21(a)			25,30	0.13,0.16		75	20	
21(b)			15,30	0.15,0.18,0.21		60	14,20	
21(c)			10,38,40	0.18,0.24,0.30		30	6,7,15	
21(d)			30,40	0.28,0.34,0.40		30	0	
22			Off	0.40,0.43	0	0	0	
23			3,2	0.08,0.09,0.10		Off	Off	Front fans operating only
24(a)			7,17,32	0.13,0.19,0.25				
24(b)			8,17,32	0.12,0.18,0.24				
24(c)			11,20,31	0.14,0.21,0.26				
25(a)	0	Variable	10,25,30	0.134,0.184	45	45,60,75	15,20	Lateral-directional data
25(b)	0	Variable	10,25,30	0.134,0.184	45	45,60,75	15,20	Lateral-directional data
Tandem lift fan configuration								
26	0	0	0	0	45	Off	0	Static fan characteristics
27			To trim drag	Variable	0,45		0,Off	Lift and moment for trim drag
28			-10 to 40		0		Off	Rear fans operating only
29			-10 to 50		0		Off	Front fans operating only
30(a)			-10 to 40		45		0	Complete configuration
30(b)			-10 to 40		45			
31(a)			-10 to 60		0			
31(b)			-10 to 60					
32(a)			-10 to 50				Off	
32(b)								
33(a)					45			Fairings off
33(b)								Fairings off
34			15,35,40	0.13,0.24,0.32			Variable	Trim effectiveness
35			0	Variable	0		~	Average downwash power off
36	Variable		90	∞	0,45		0,Off	
37(a)			0,10,20	0.09	45		15	Complete configuration
37(b)			5 to 36	0.13,0.19			-8,23	
37(c)			25 to 50	0.24,0.31			-8,0	
38			14,24,37	0.13,0.19,0.25			Off	Fairings off
39(a)	0	Variable	3,10,15	0.06,0.09,0.13			0,15,23	Lateral-directional data
39(b)			3,10,15	0.06,0.09,0.13			0,15,23	
40(a)			26,35,50,90	0.18,0.25,0.30,∞			0,8	
40(b)			26,35,50,90	0.18,0.25,0.30,∞			0,8	

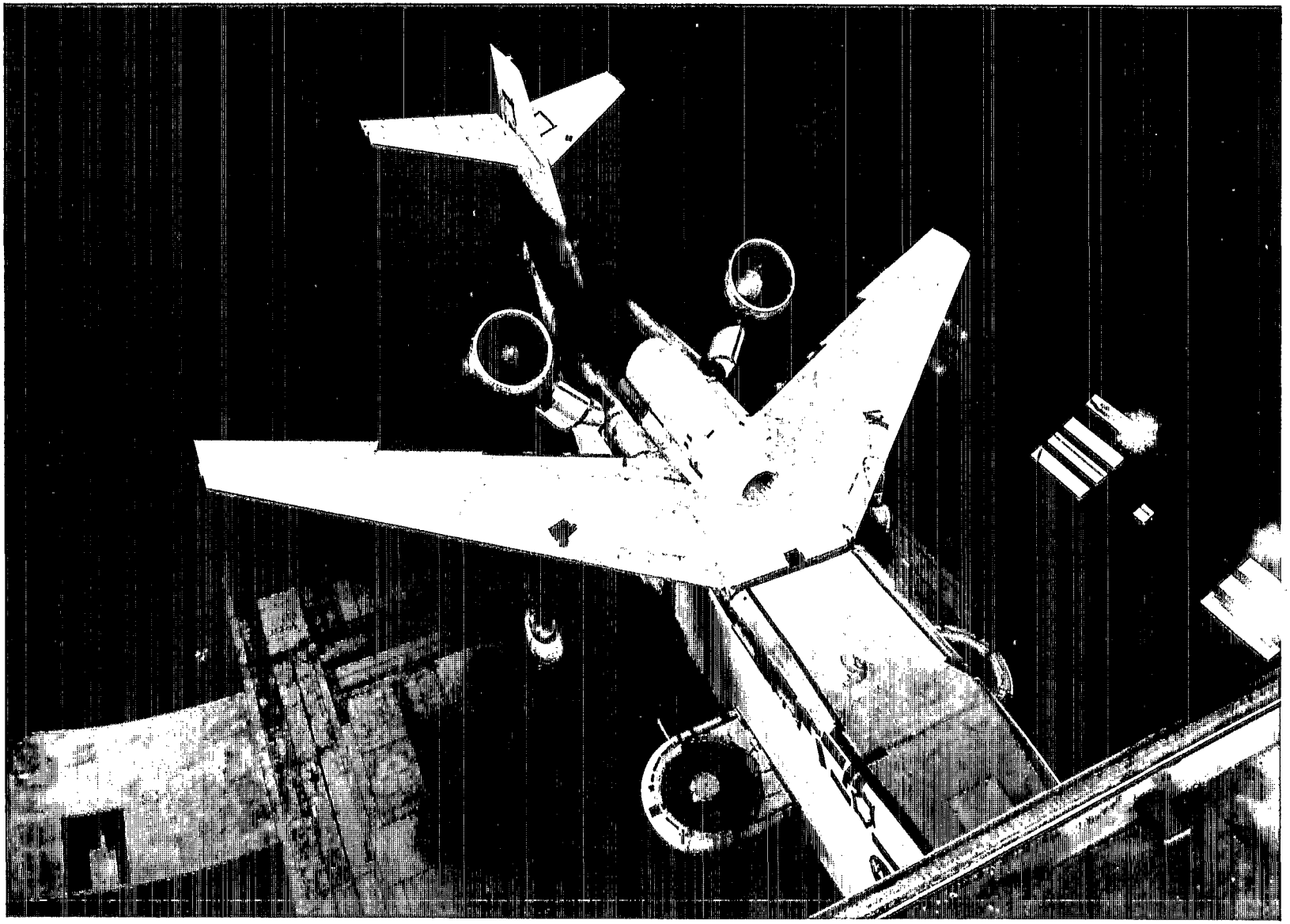

(a) Lift-cruise fan configuration.

A-35554

Figure 1.- Model mounted in Ames 40- by 80-Foot Wind Tunnel.

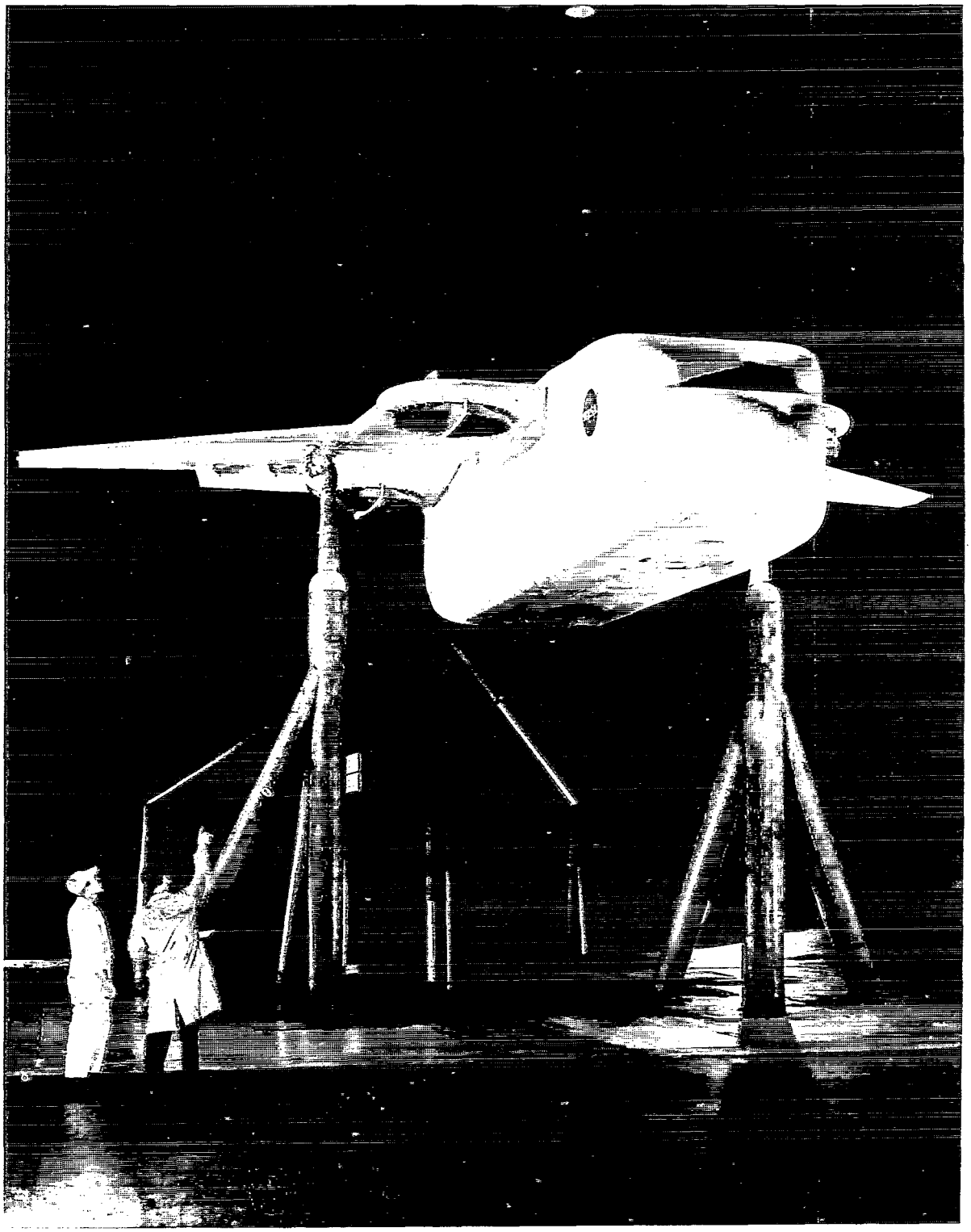

A-35376

(b) Tandem lift fan configuration.

Figure 1.- Concluded.

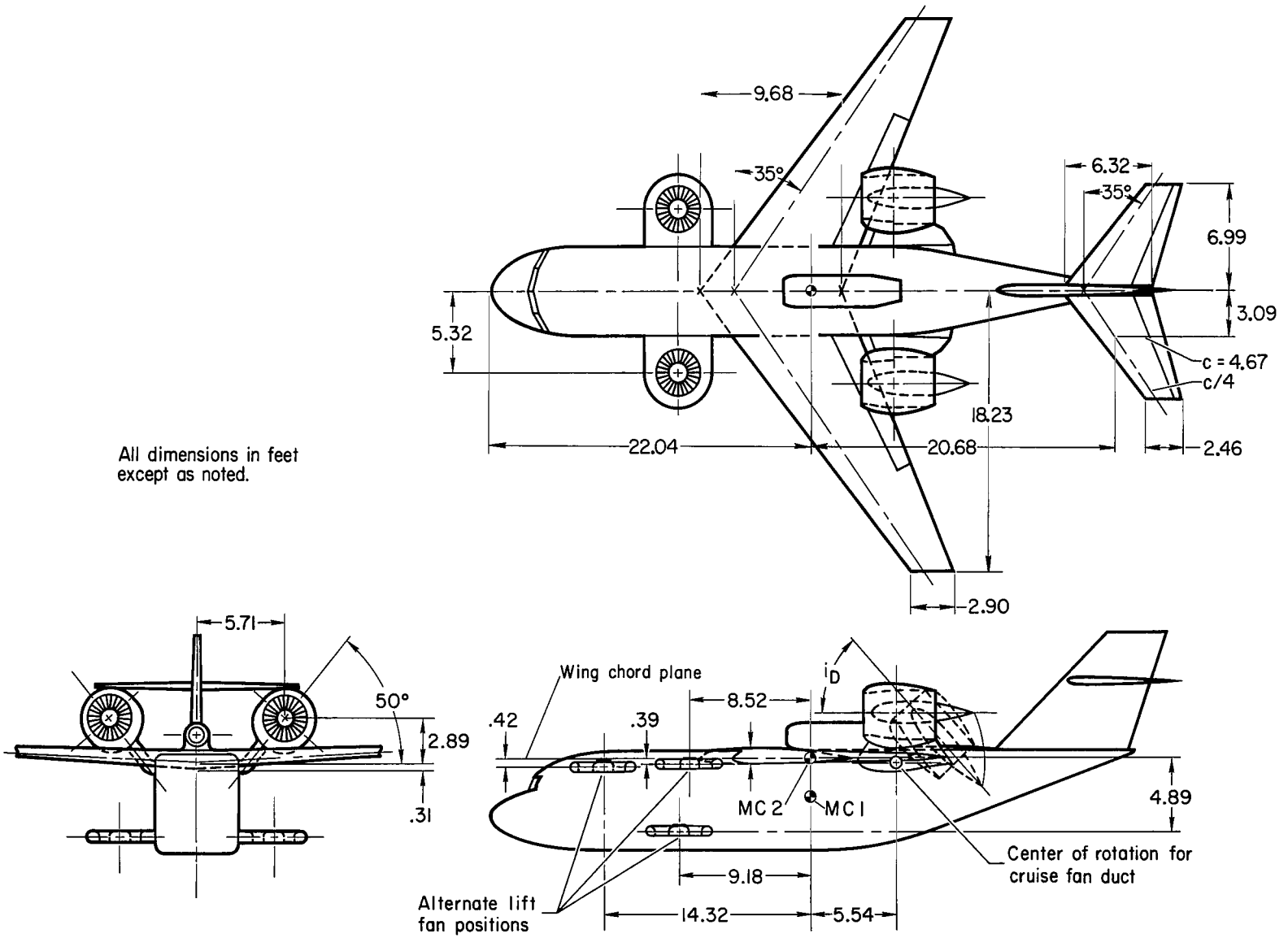

(a) Lift-cruise fan configuration.

Figure 2.- Geometric details of the V/STOL transport model.

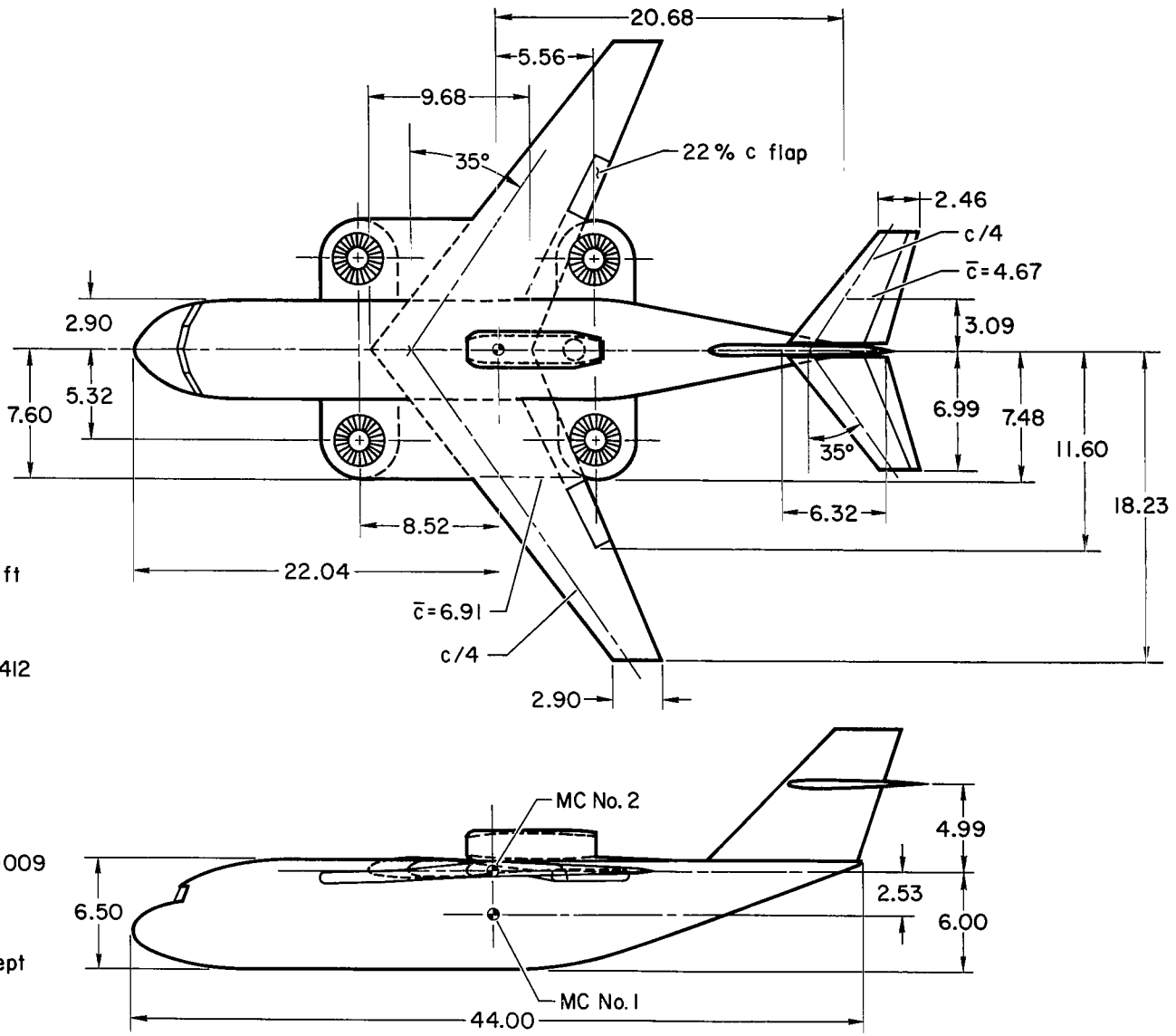

Basic wing

Area	229.5 sq ft
Aspect ratio	5.8
Taper ratio	0.3
Airfoil section	NACA 65-412

Horizontal tail

Area	61.4 sq ft
Aspect ratio	3.2
Taper ratio	0.4
Airfoil section	NACA 64-009
$\bar{V}$	0.8

All dimentions in feet except as noted

(b) Tandem lift fan configuration.

Figure 2.- Continued.

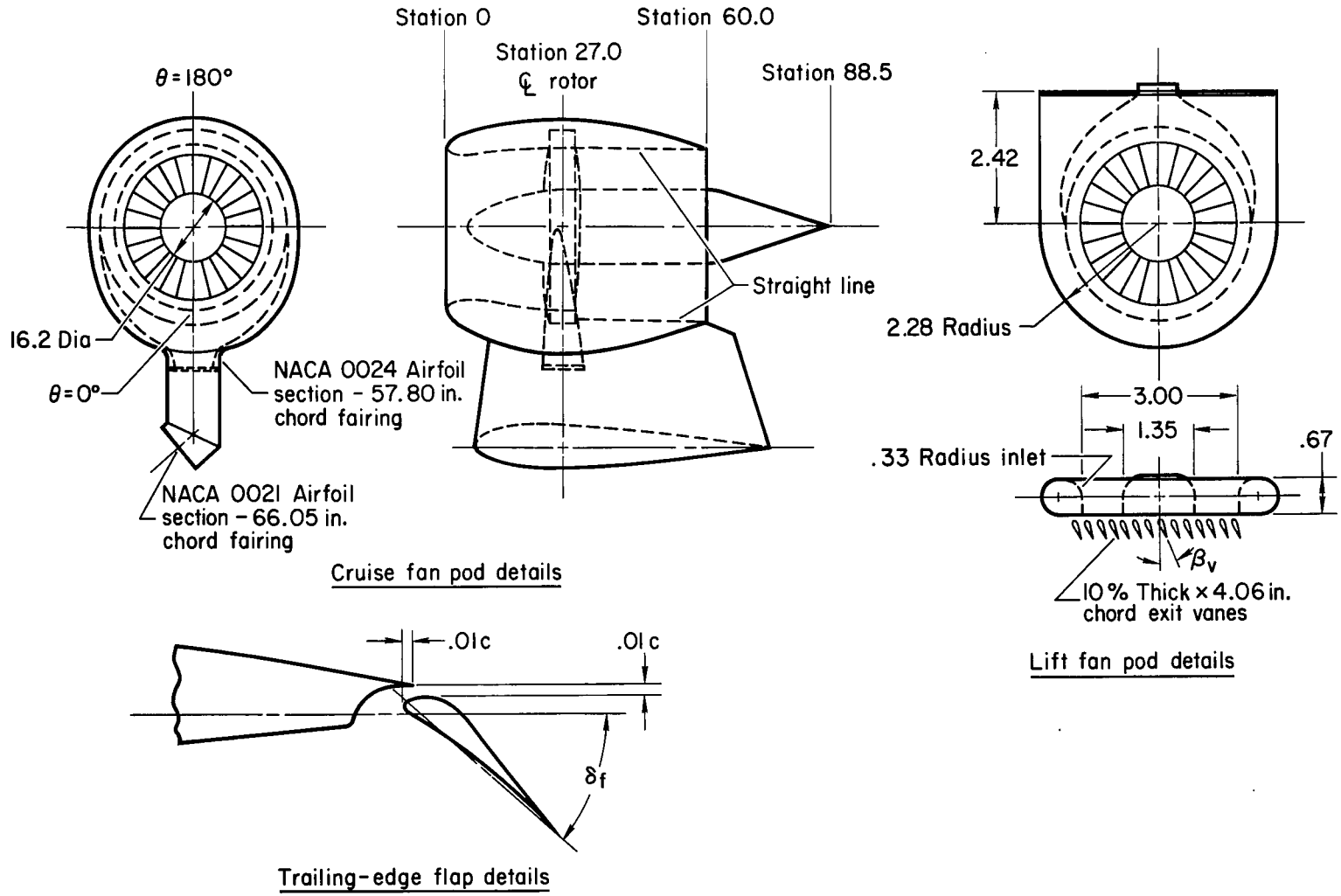

(c) Details of the cruise fan pod, lift fan pod, and trailing-edge flap.

Figure 2.- Concluded.

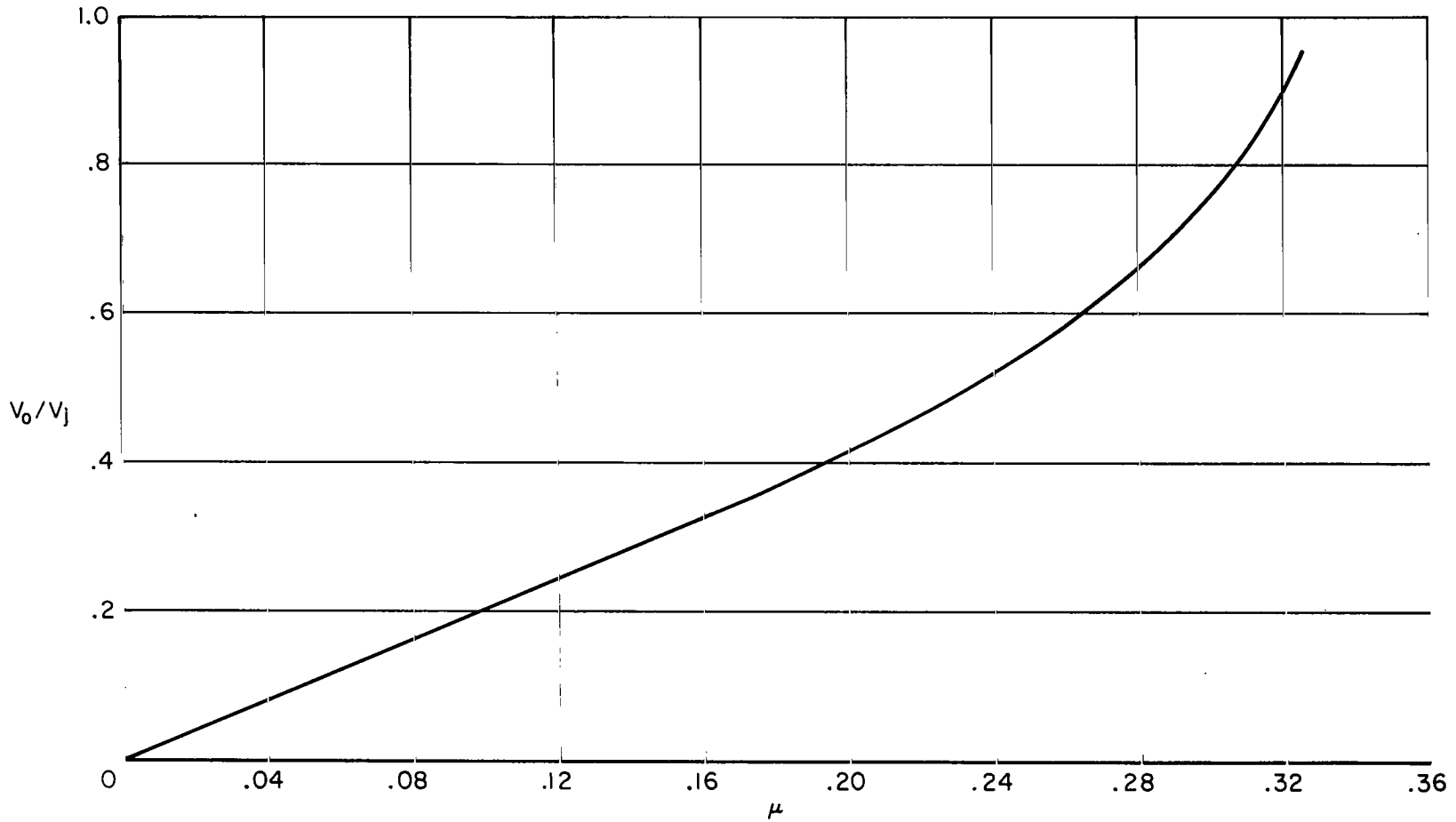

Figure 3.- The average variation of velocity ratio with tip-speed ratio for the lift fan; $\beta_V = 0$.

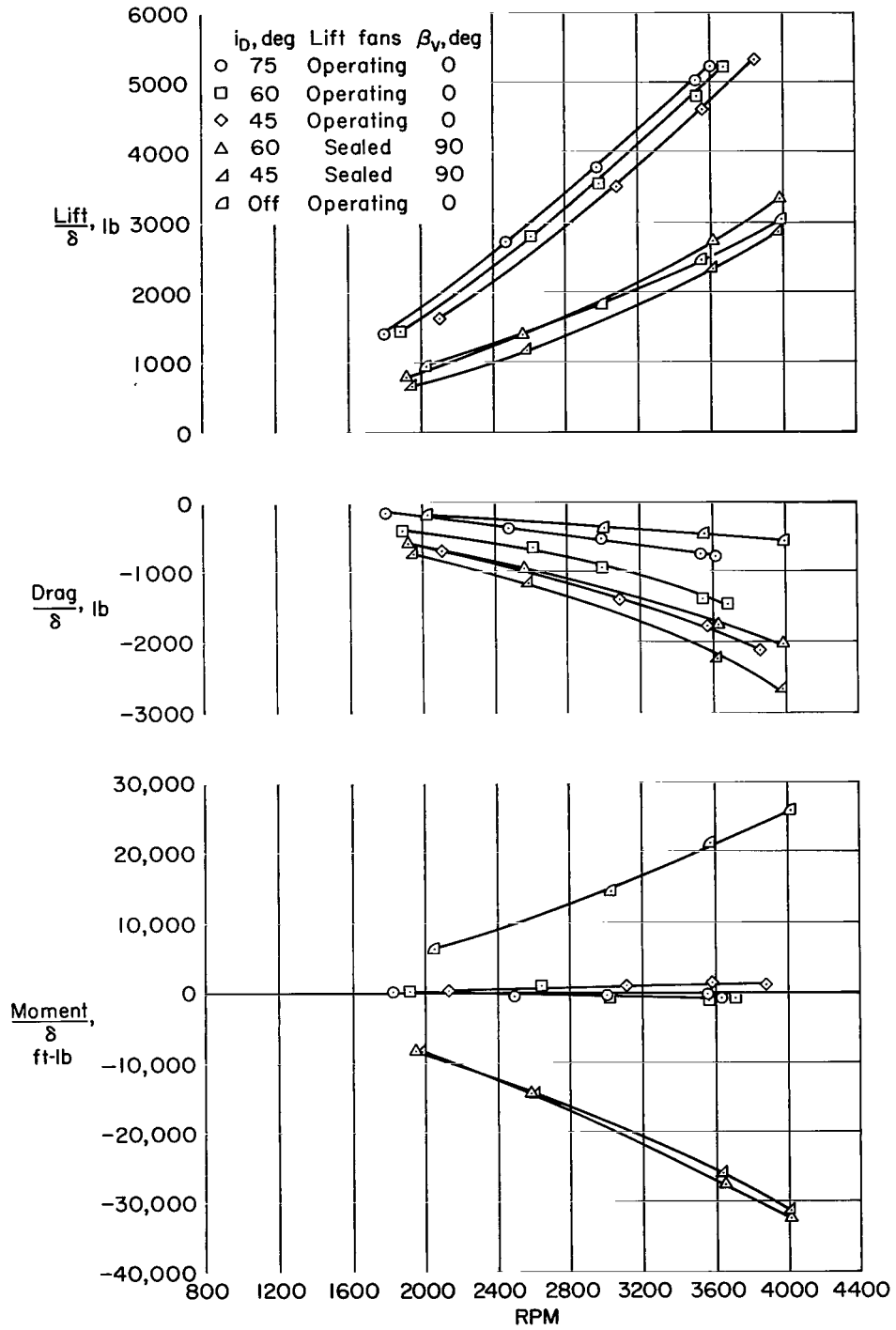

(a) Variation with RPM.

Figure 4.- Zero airspeed characteristics for the lift-cruise fan configuration; tail on, $i_t = 0^o$, $\delta_f = 45^o$.

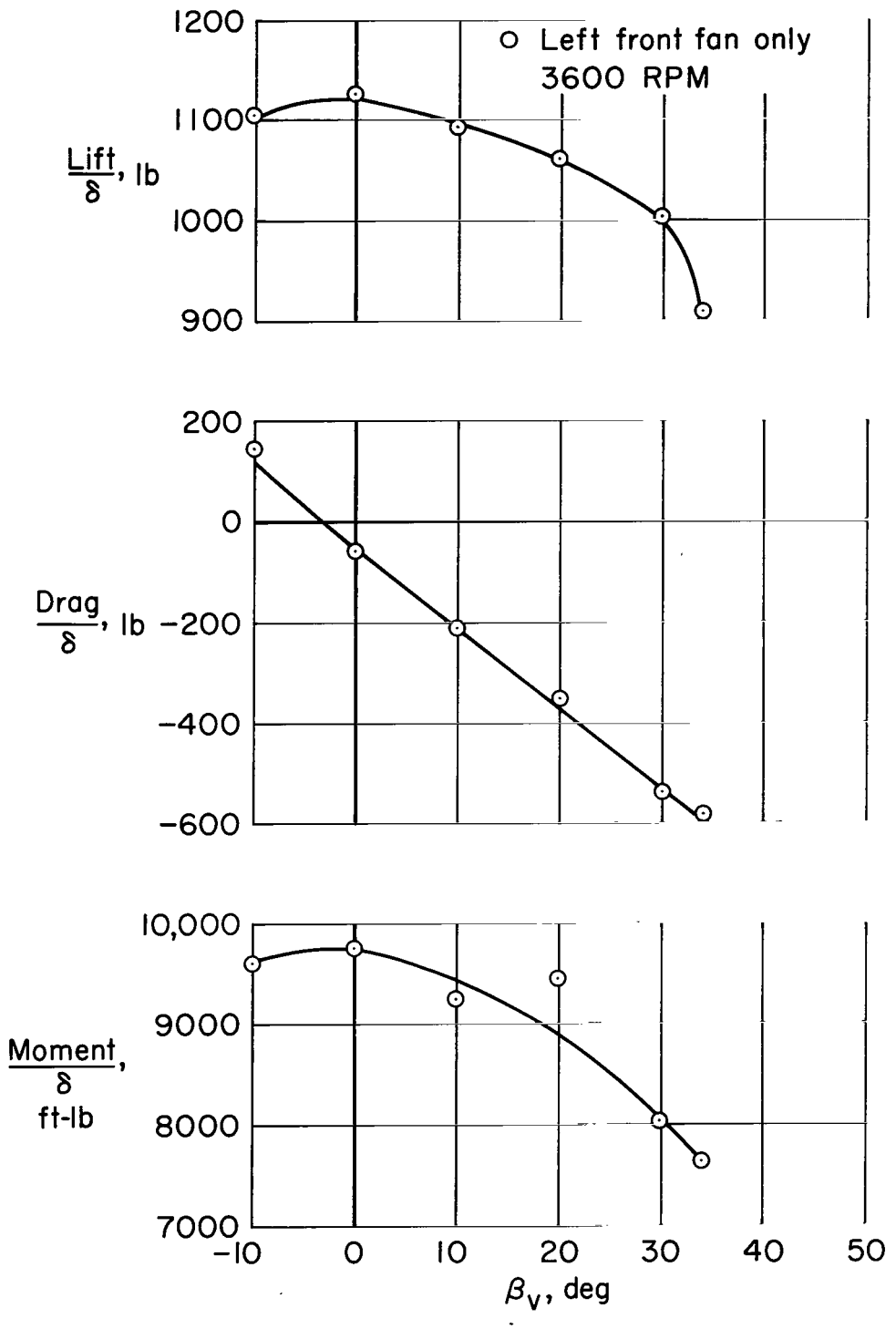

(b) Variation with exit vanes.

Figure 4.- Concluded.

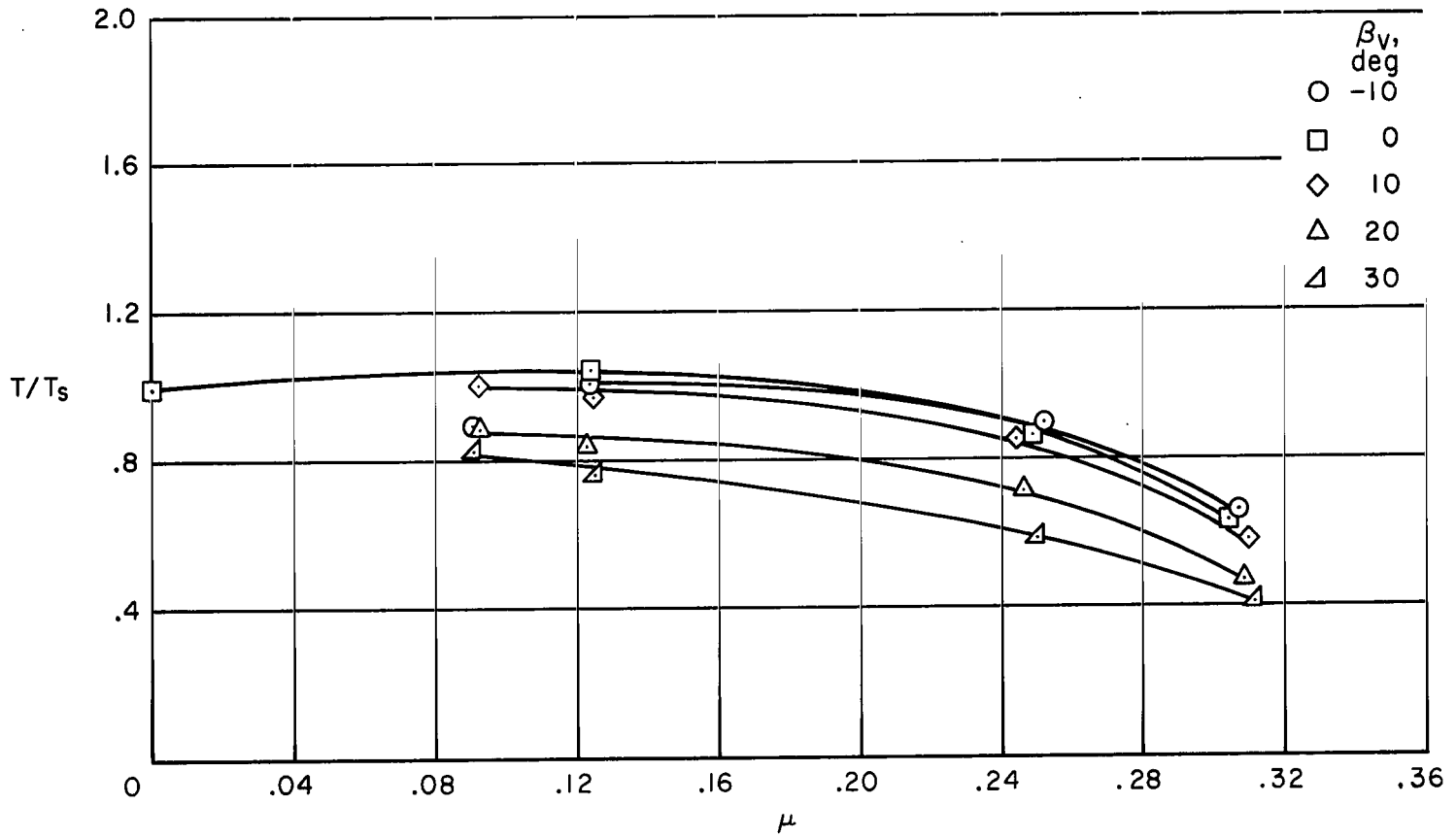

Figure 5.- The effect of forward speed on average fan thrust as measured by exit pressures; left front fan operating only.

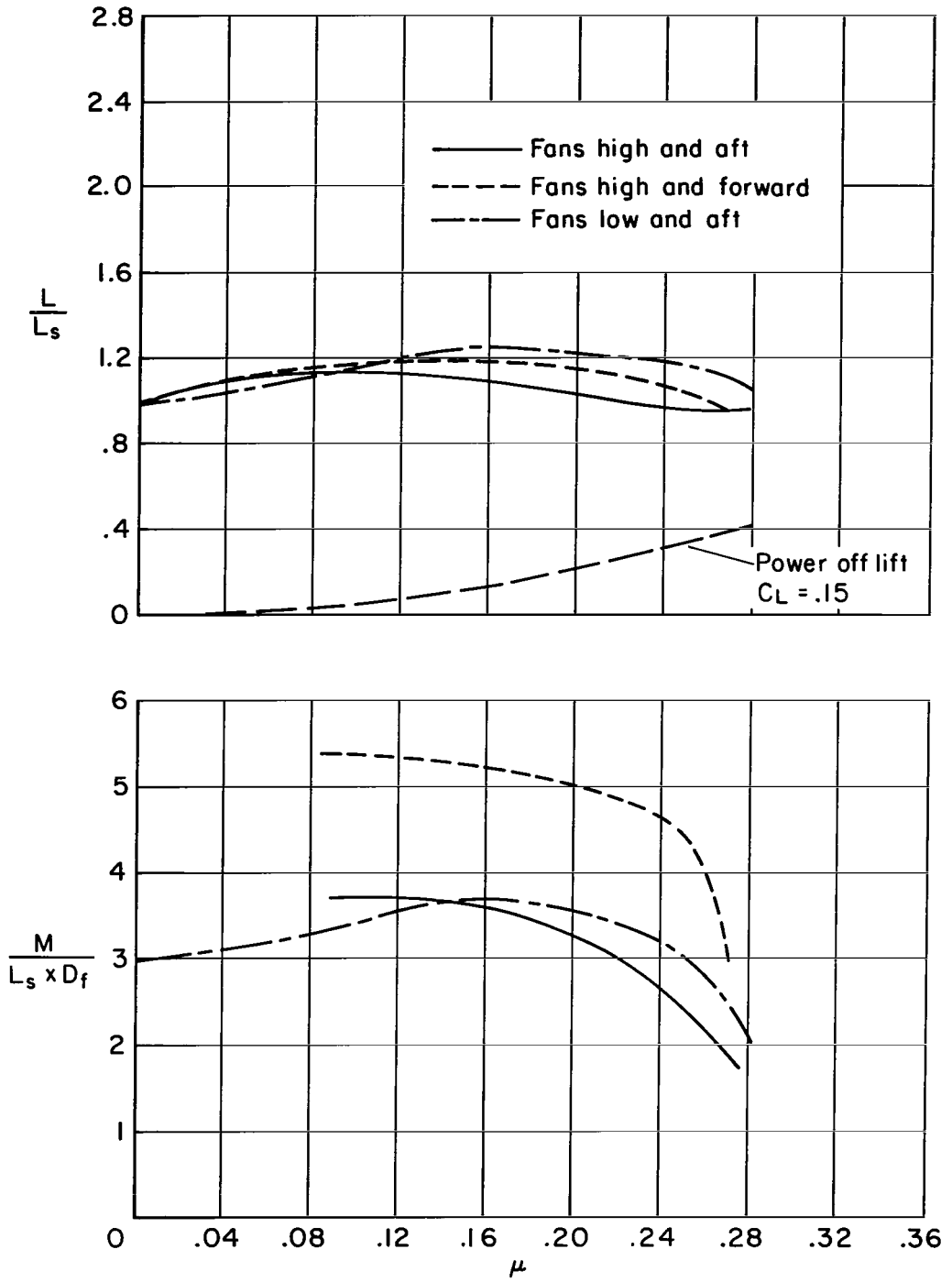

(a) Two front fans operating, horizontal tail off, flaps up, rear fans removed.

Figure 6.- The effect of forward speed and fan RPM (tip-speed ratio) on total lift and moment for trim drag.

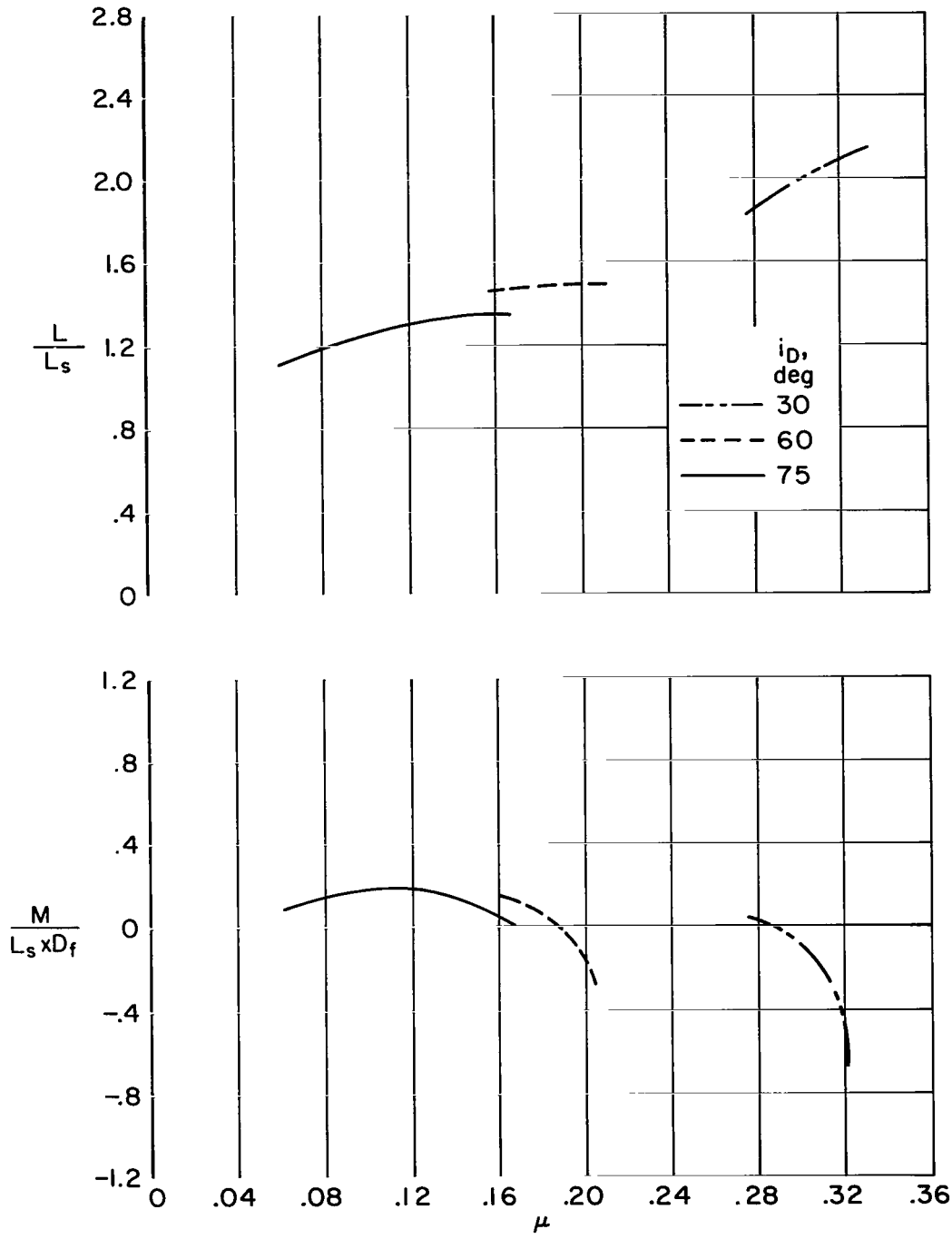

(b) Four fans running, horizontal tail off, $\delta_f = 45^o$.

Figure 6.- Continued.

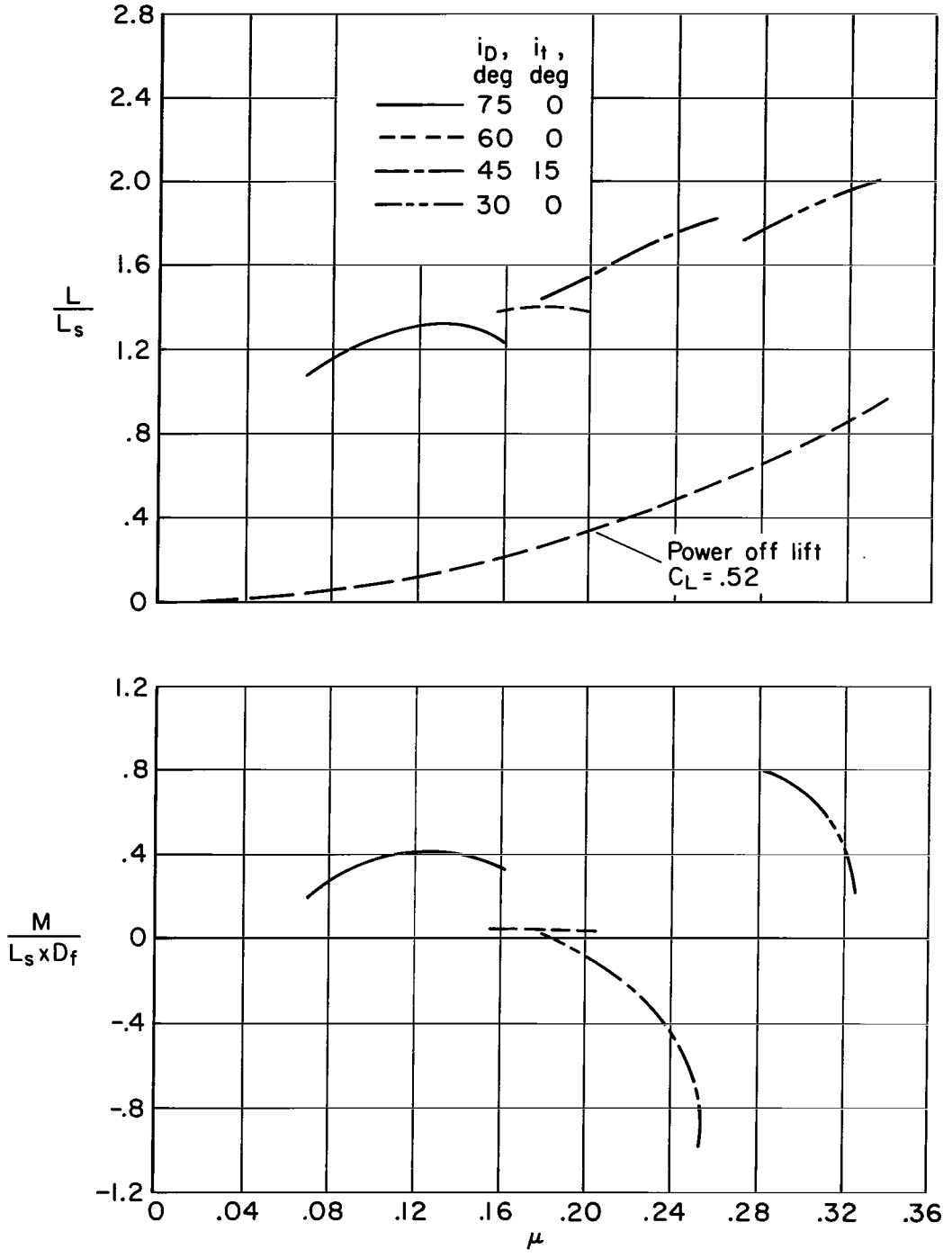

(c) Four fans running, horizontal tail on, $\delta_f = 45^\circ$.

Figure 6.- Concluded.

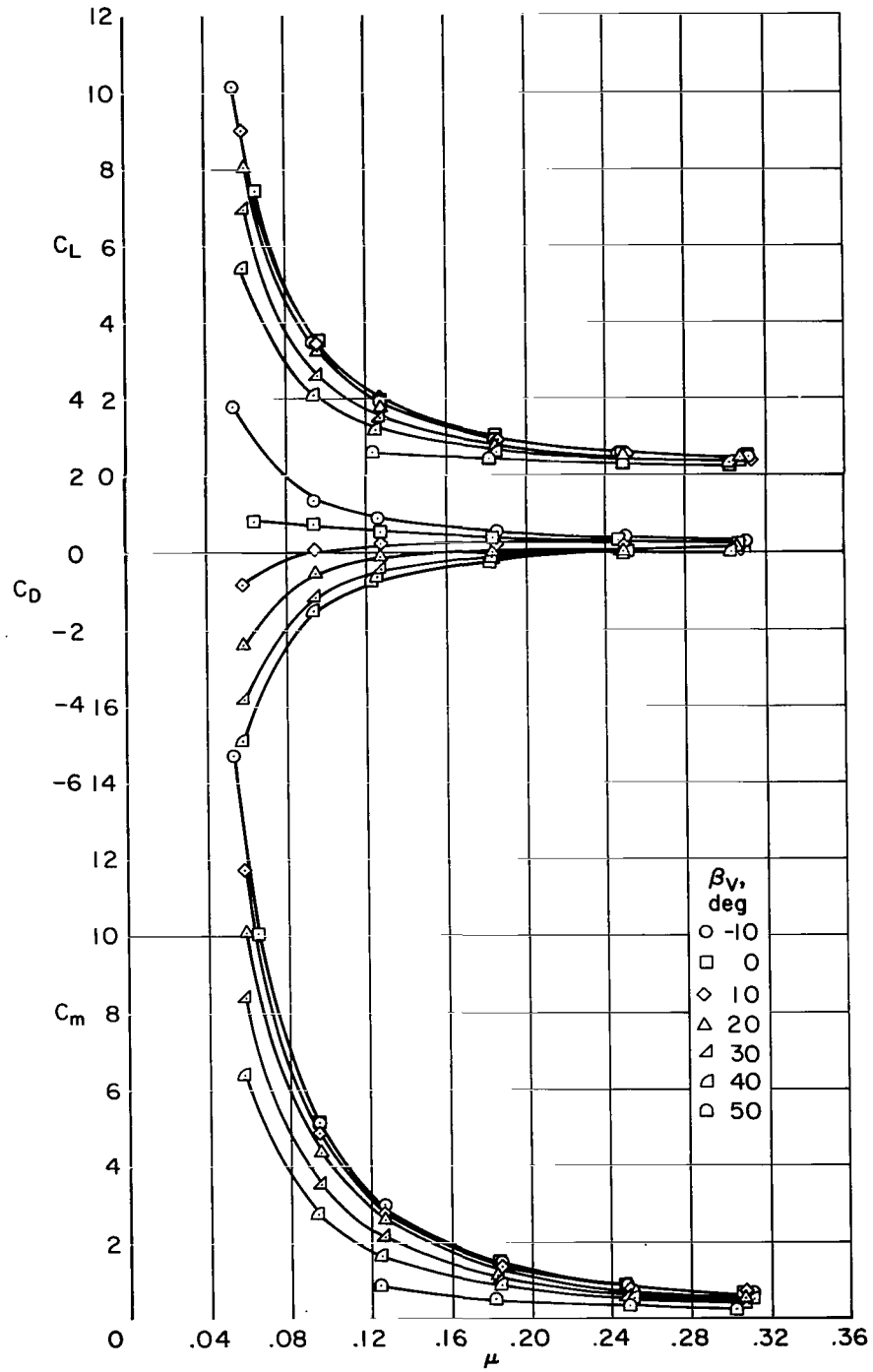

(a) $\alpha = 0^\circ$

Figure 7.- The effect of tip-speed ratio on the longitudinal characteristics with the two front fans operating in the high-aft position, rear fans removed, tail off, flaps up.

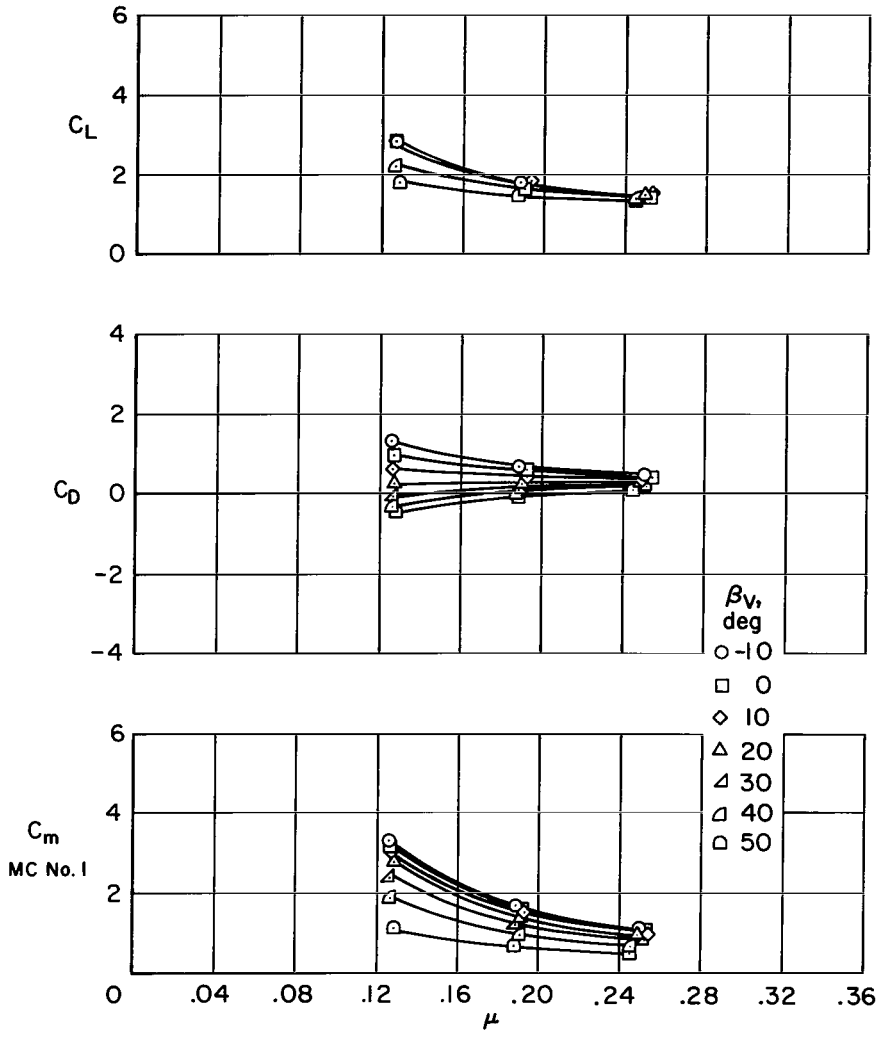

(b) $\alpha = 12^{\circ}$

Figure 7.- Concluded.

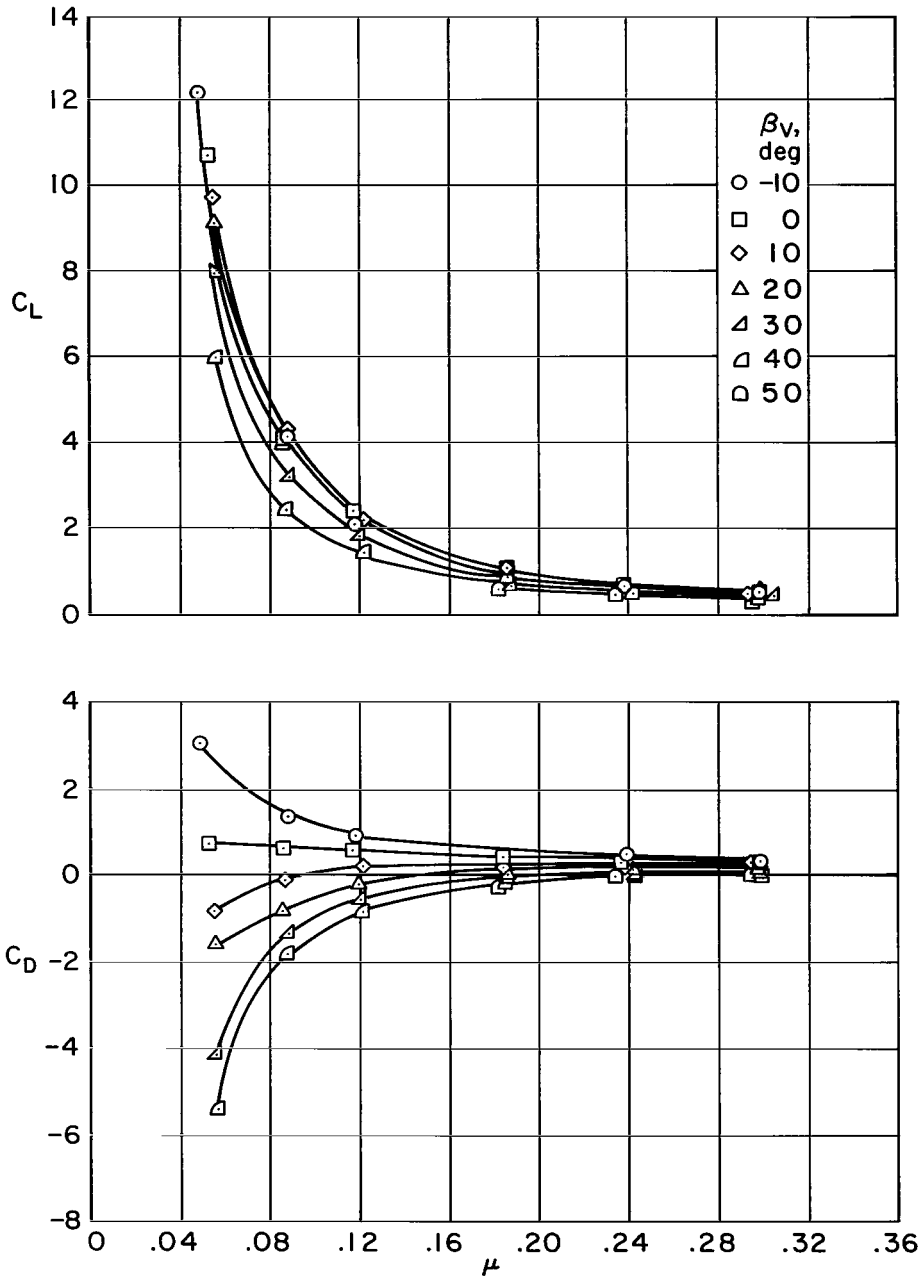

(a) Lift and drag coefficients, $\alpha = 0^{\circ}$.

Figure 8.- The effect of tip-speed ratio on the longitudinal characteristics with the two front fans operating in the high forward position, rear fans removed, tail off, flaps up.

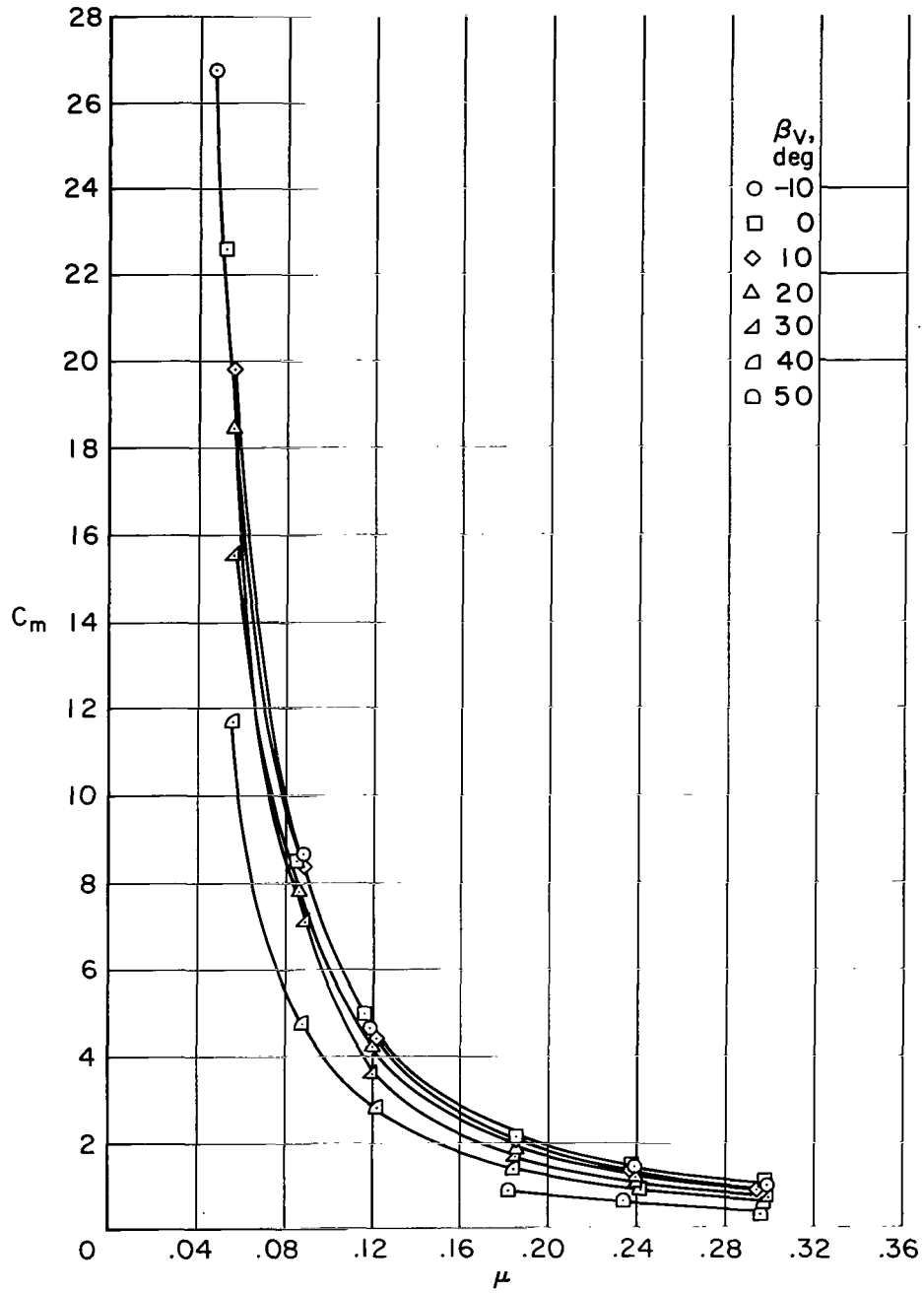

(b) Moment coefficient, $\alpha = 0^{\circ}$.

Figure 8.- Continued.

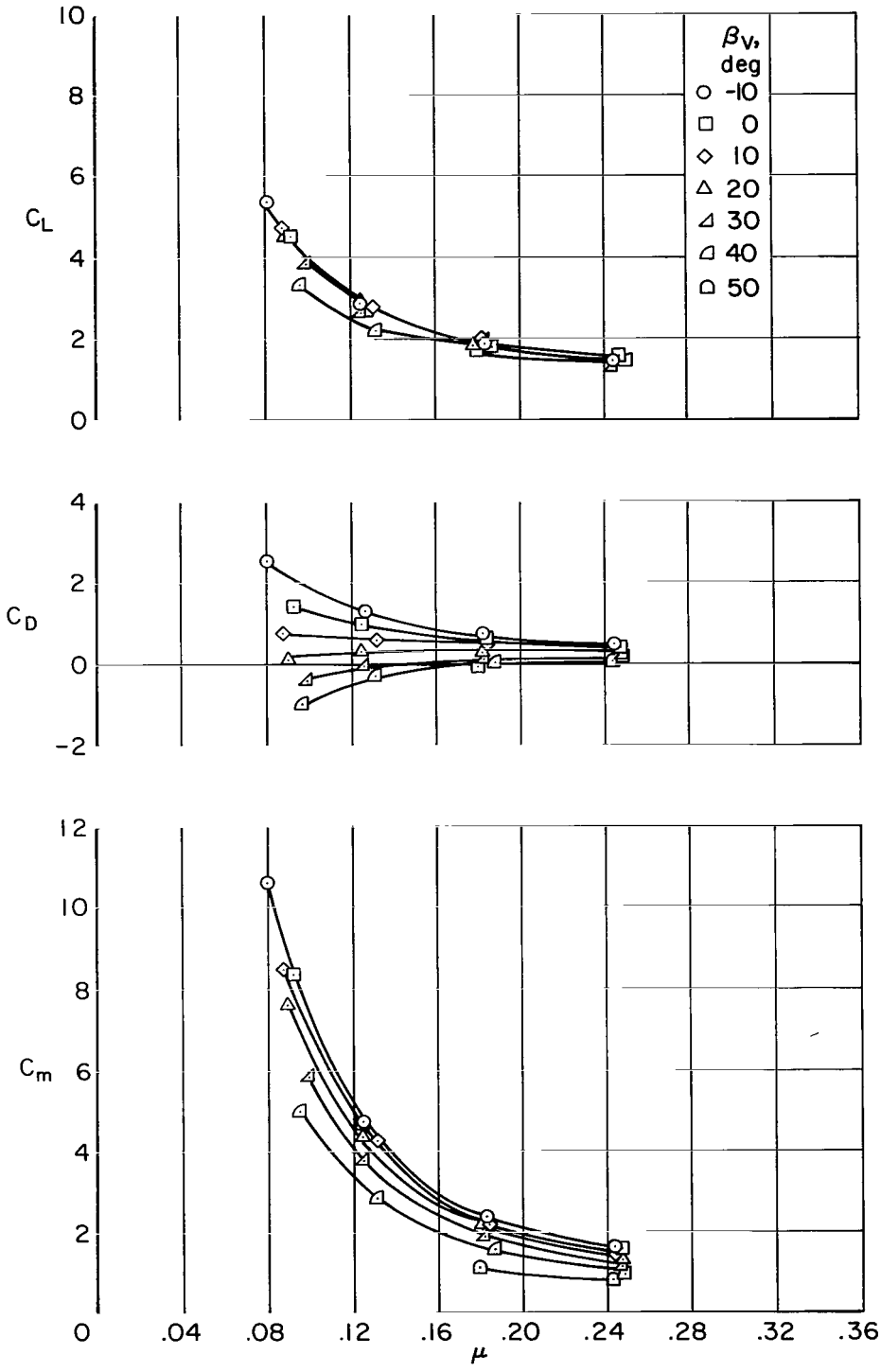

(c) Lift, drag, and moment coefficients, $\alpha = 12^{\circ}$.

Figure 8.- Concluded.

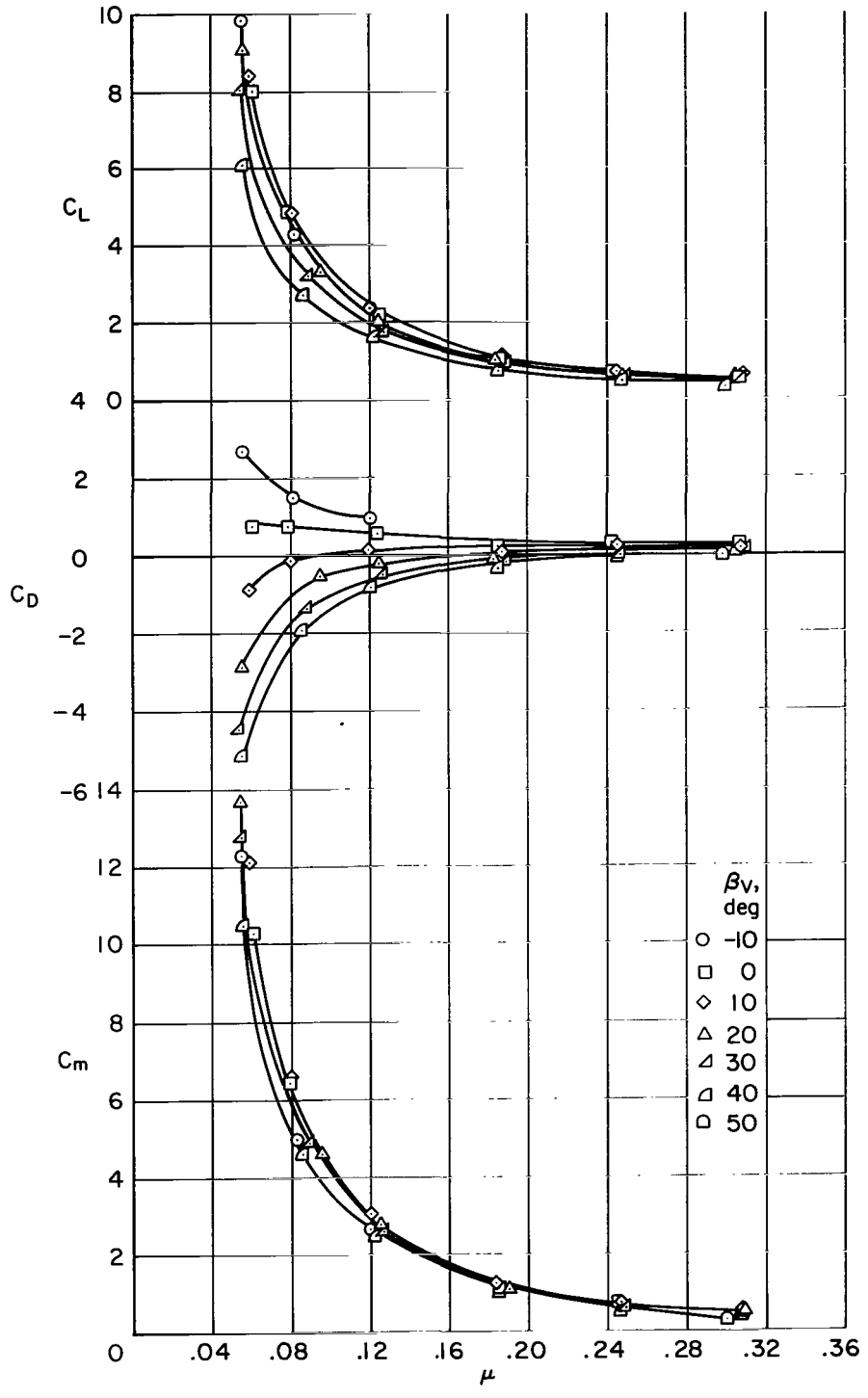

(a) $\alpha = 0^\circ$

Figure 9.- The effect of tip-speed ratio on the longitudinal characteristics with the two front fans operating in the low aft position, rear fans removed, tail off, flaps up.

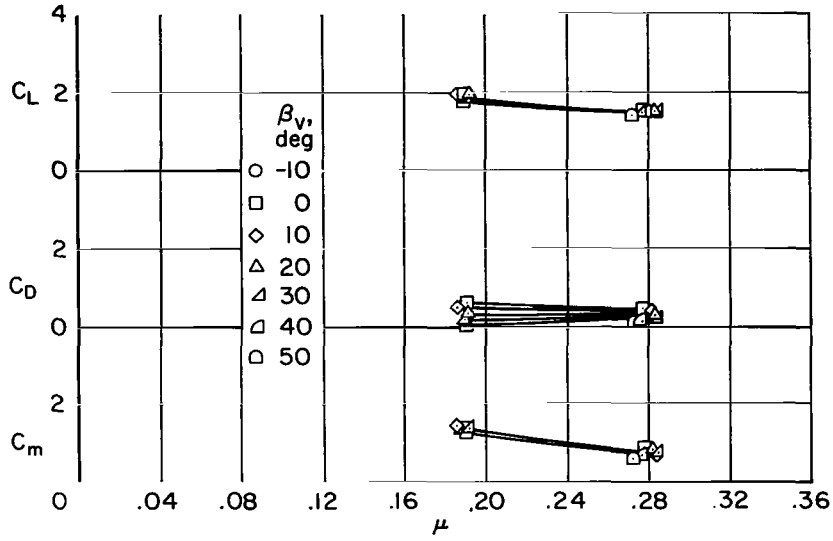

(b) $\alpha = 12^{\circ}$

Figure 9.- Concluded.

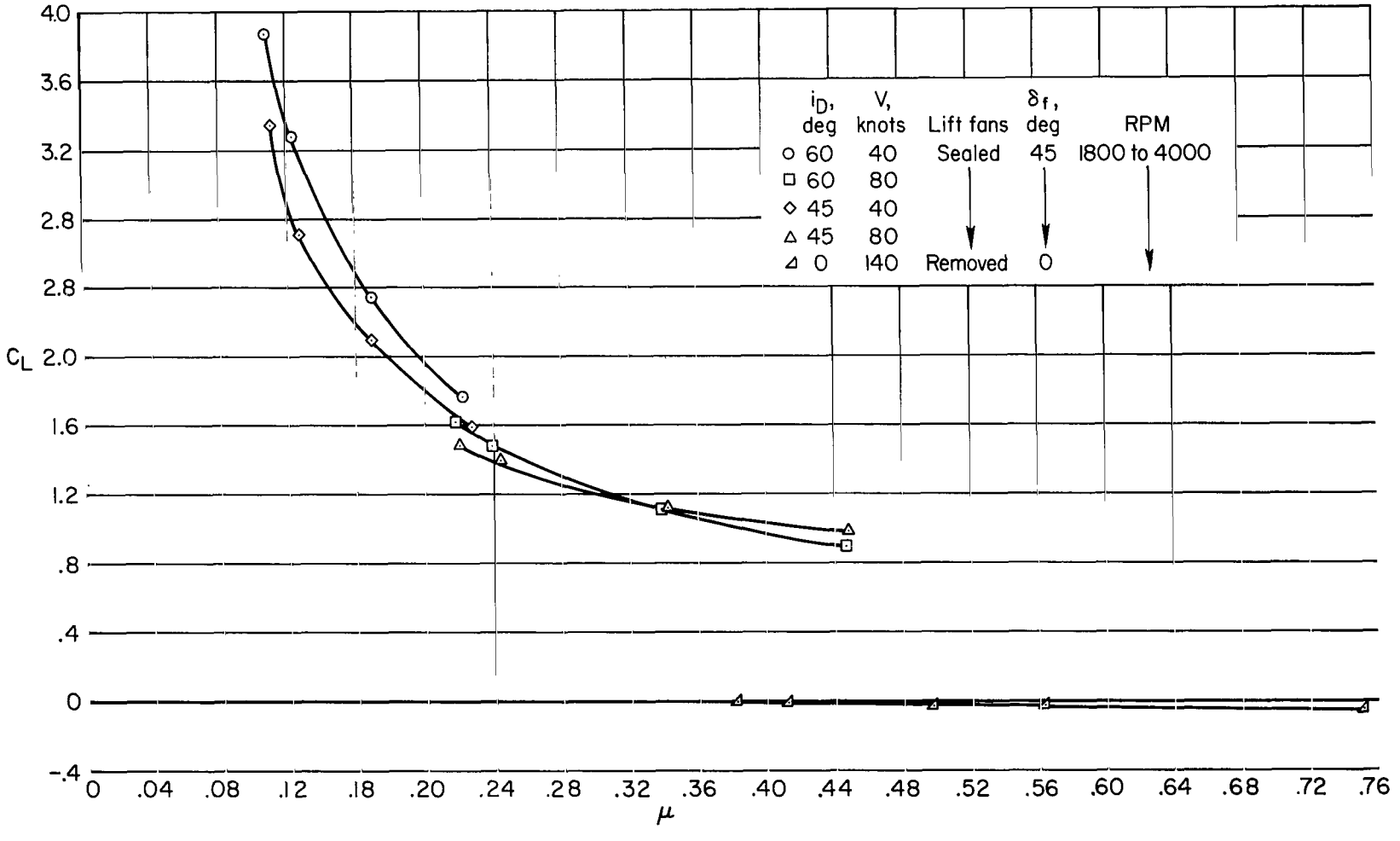

(a) Variation of lift.

Figure 10.- The effect of varying fan speed at several cruise fan angles and forward speeds; cruise fans operating only, tail on, $i_t = 0^\circ$, $\alpha = 0^\circ$.

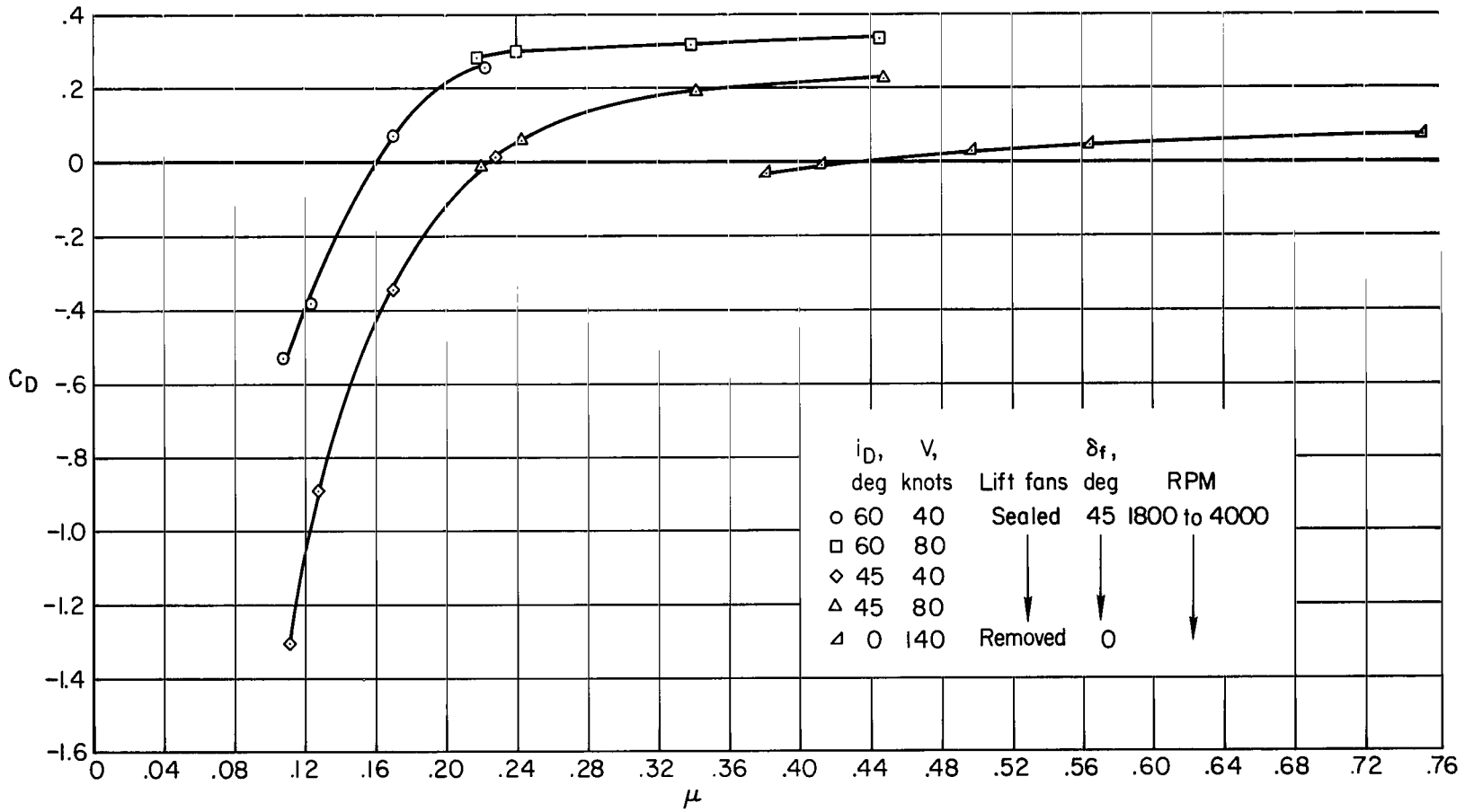

(b) Variation of drag.

Figure 10.- Continued.

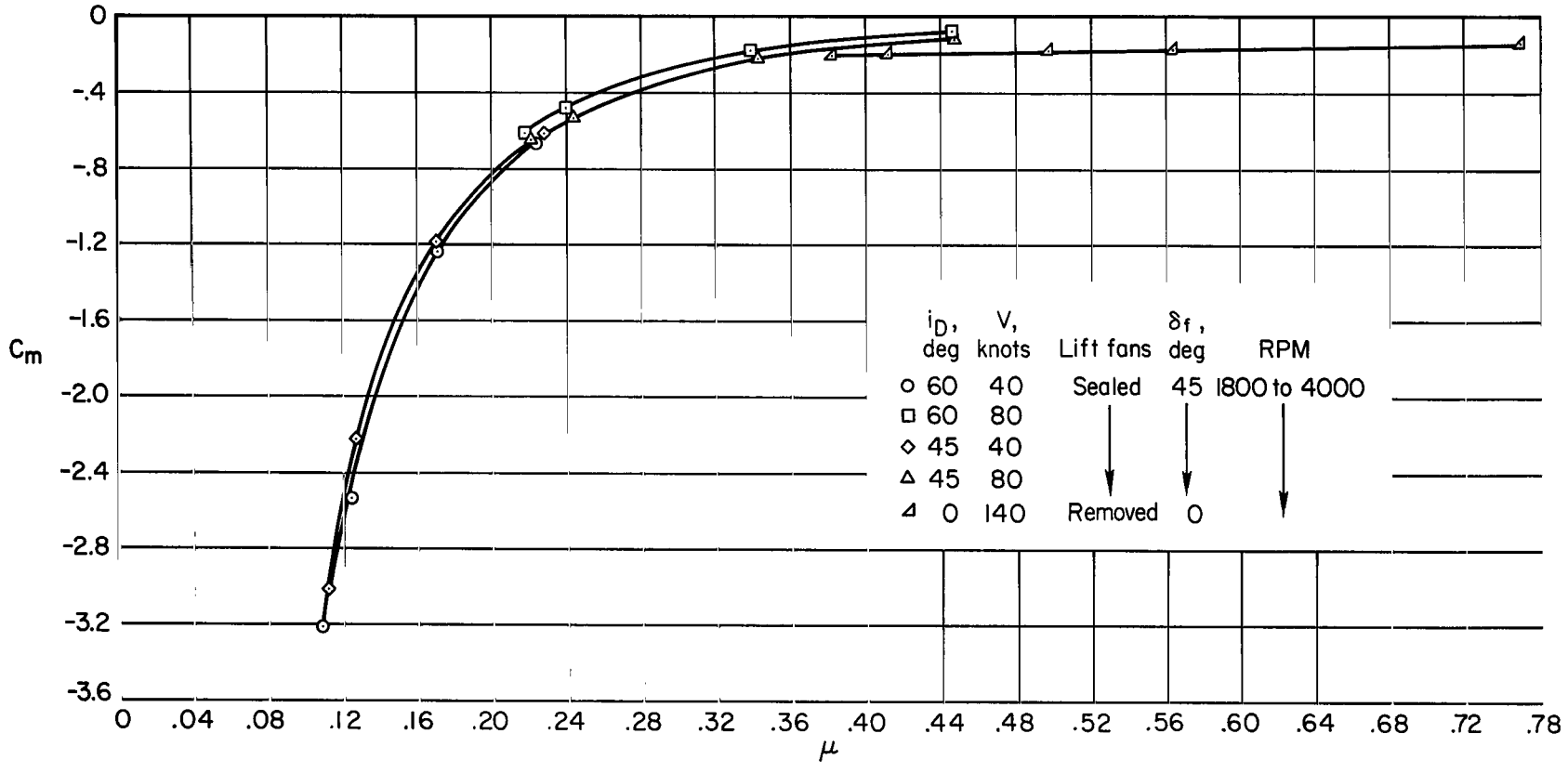

(c) Variation of moment.

Figure 10.- Concluded.

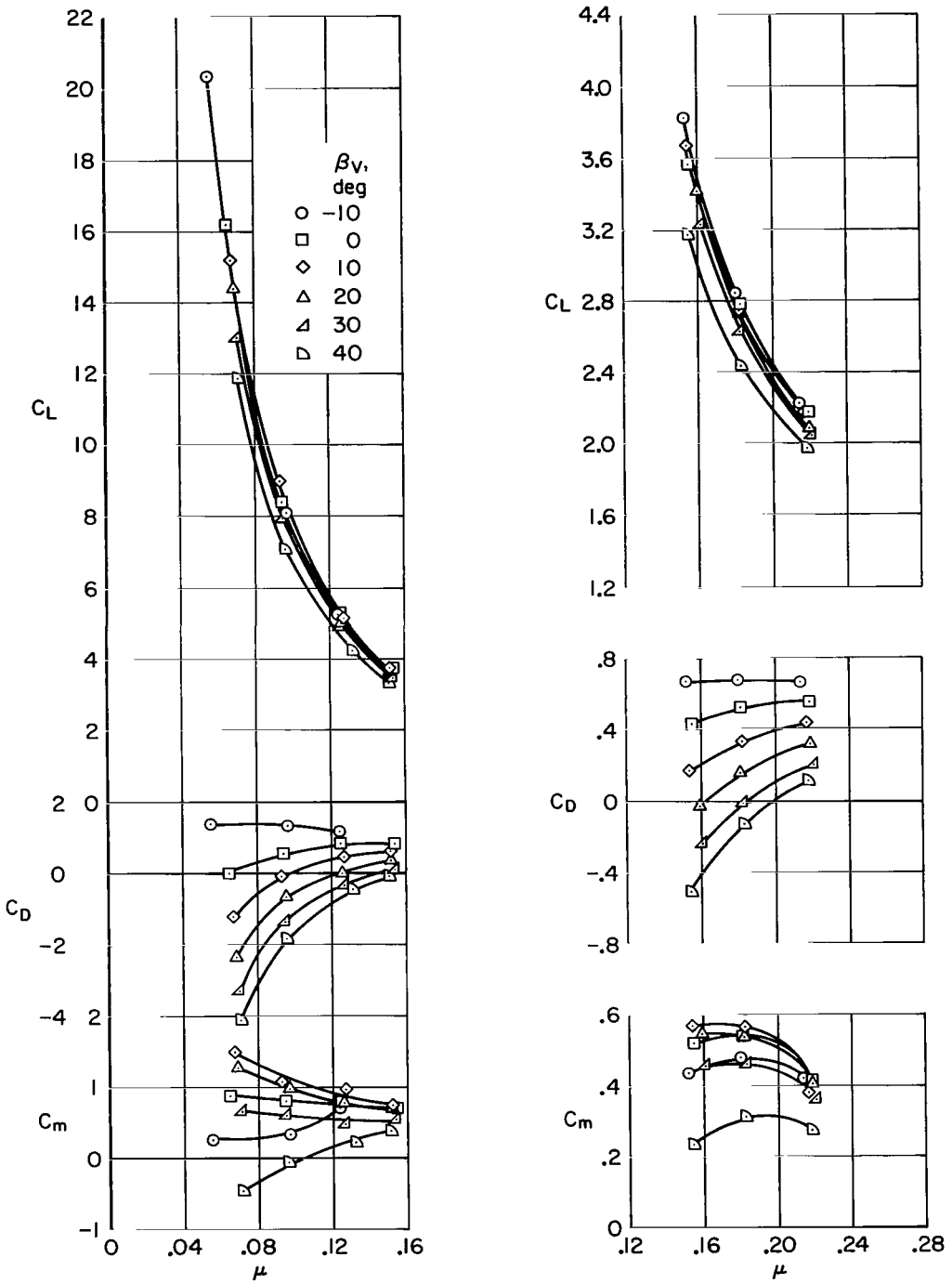

(a) $i_D = 75^\circ$, $i_t = 0^\circ$ (b) $i_D = 60^\circ$, $i_t = 0^\circ$

Figure 11.- The effect of tip-speed ratio on the longitudinal characteristics for the complete lift-cruise fan configuration; $\delta_f = 45^\circ$.

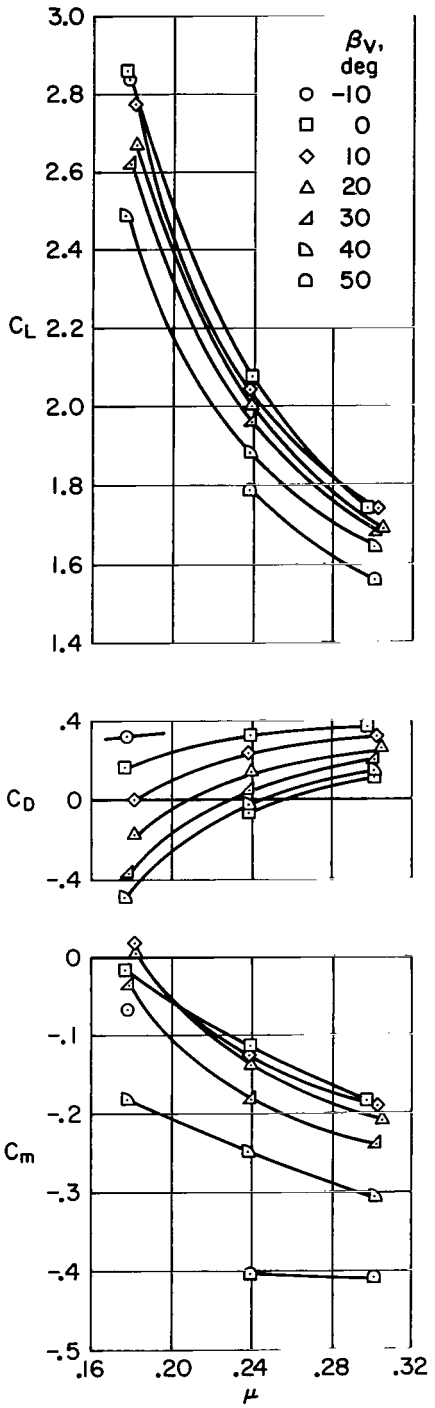

(c) $i_D = 45^\circ$, $i_t = 15^\circ$

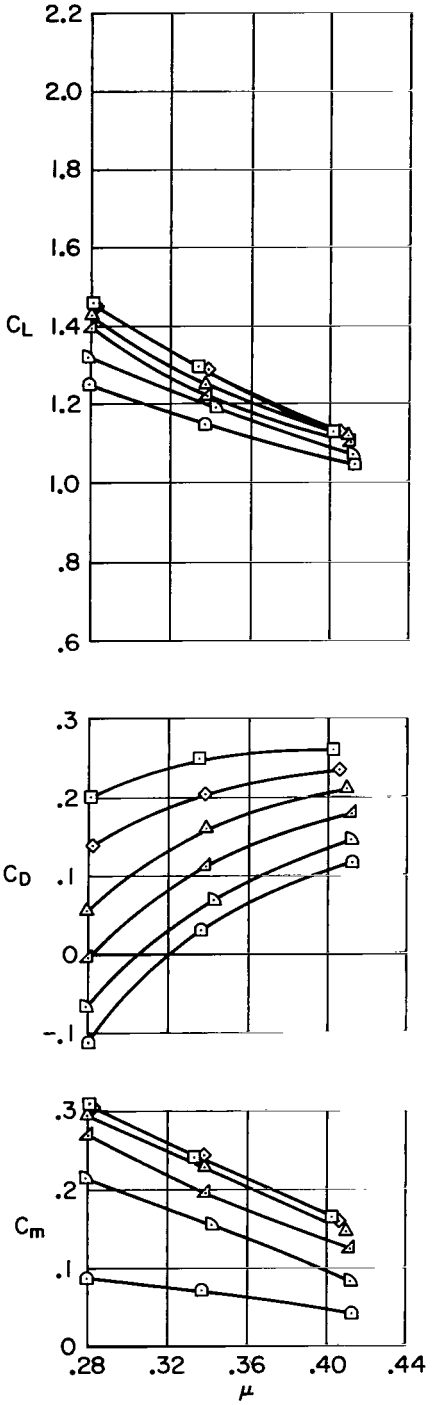

(d) $i_D = 30^\circ$, $i_t = 0^\circ$

Figure 11.- Continued.

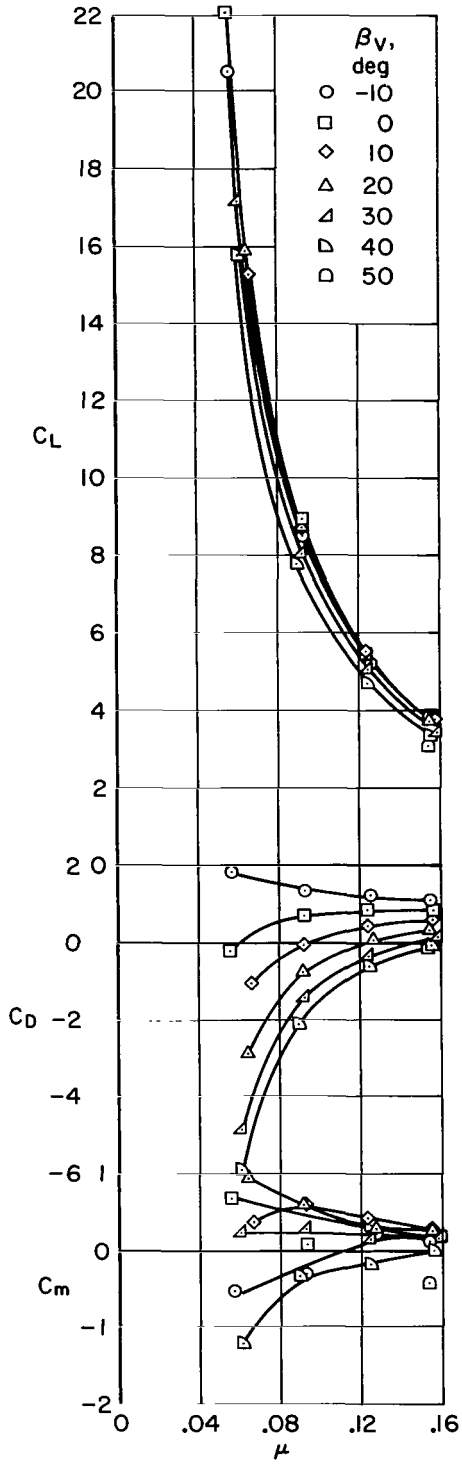

(e) $i_D = 75^\circ$, tail off.

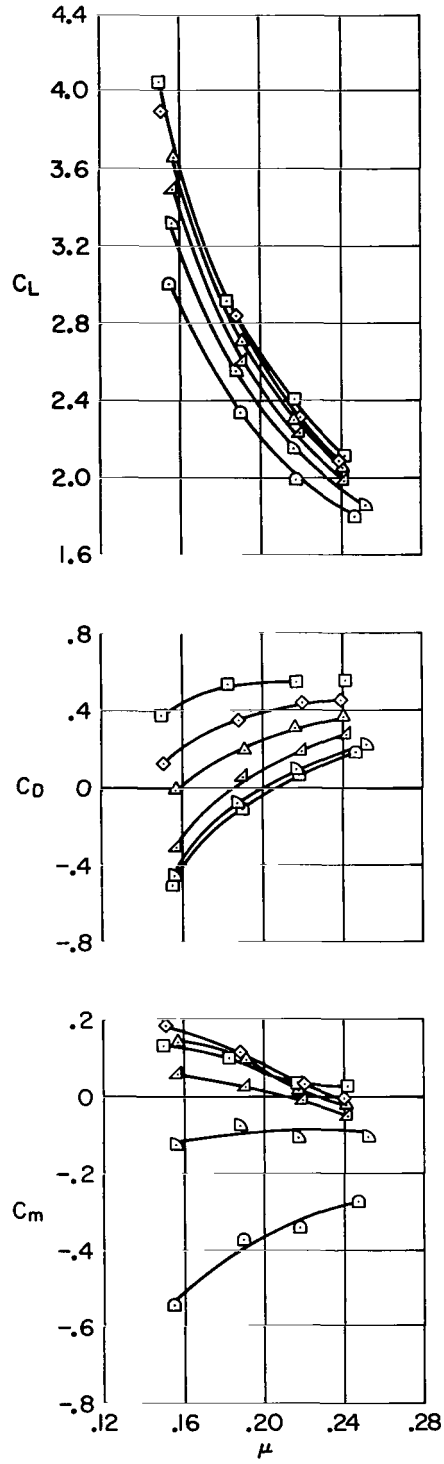

(f) $i_D = 60^\circ$, tail off.

Figure 11.- Continued.

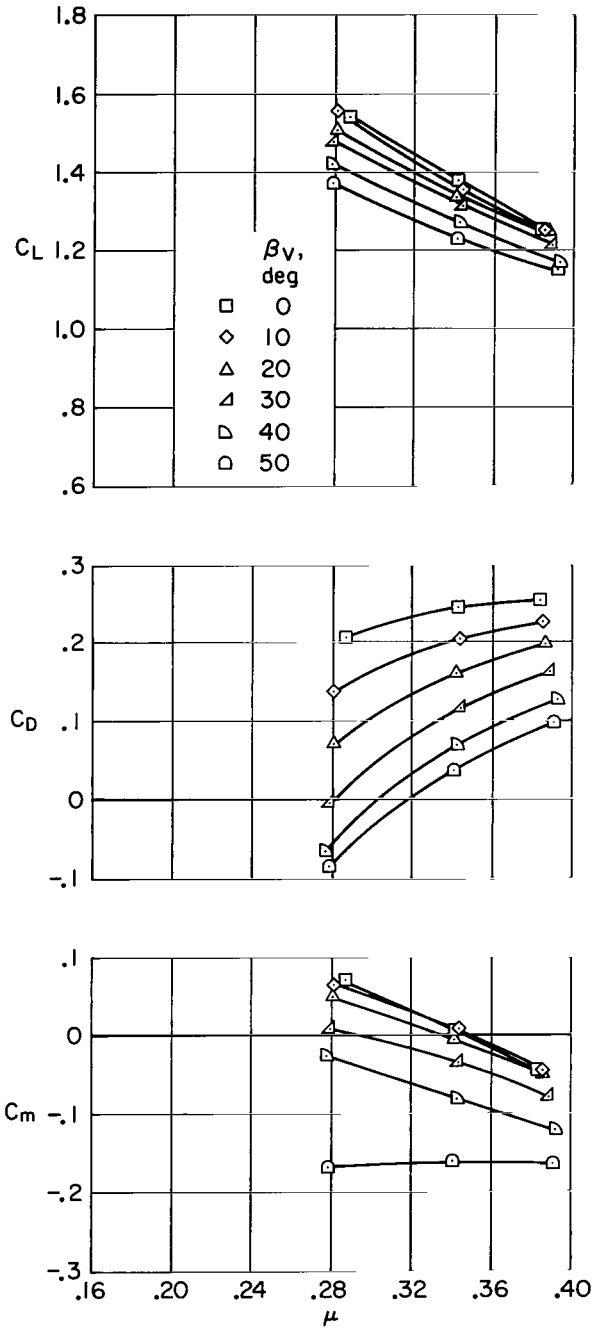

(g) $i_D = 30^\circ$, tail off.

Figure 11.- Concluded.

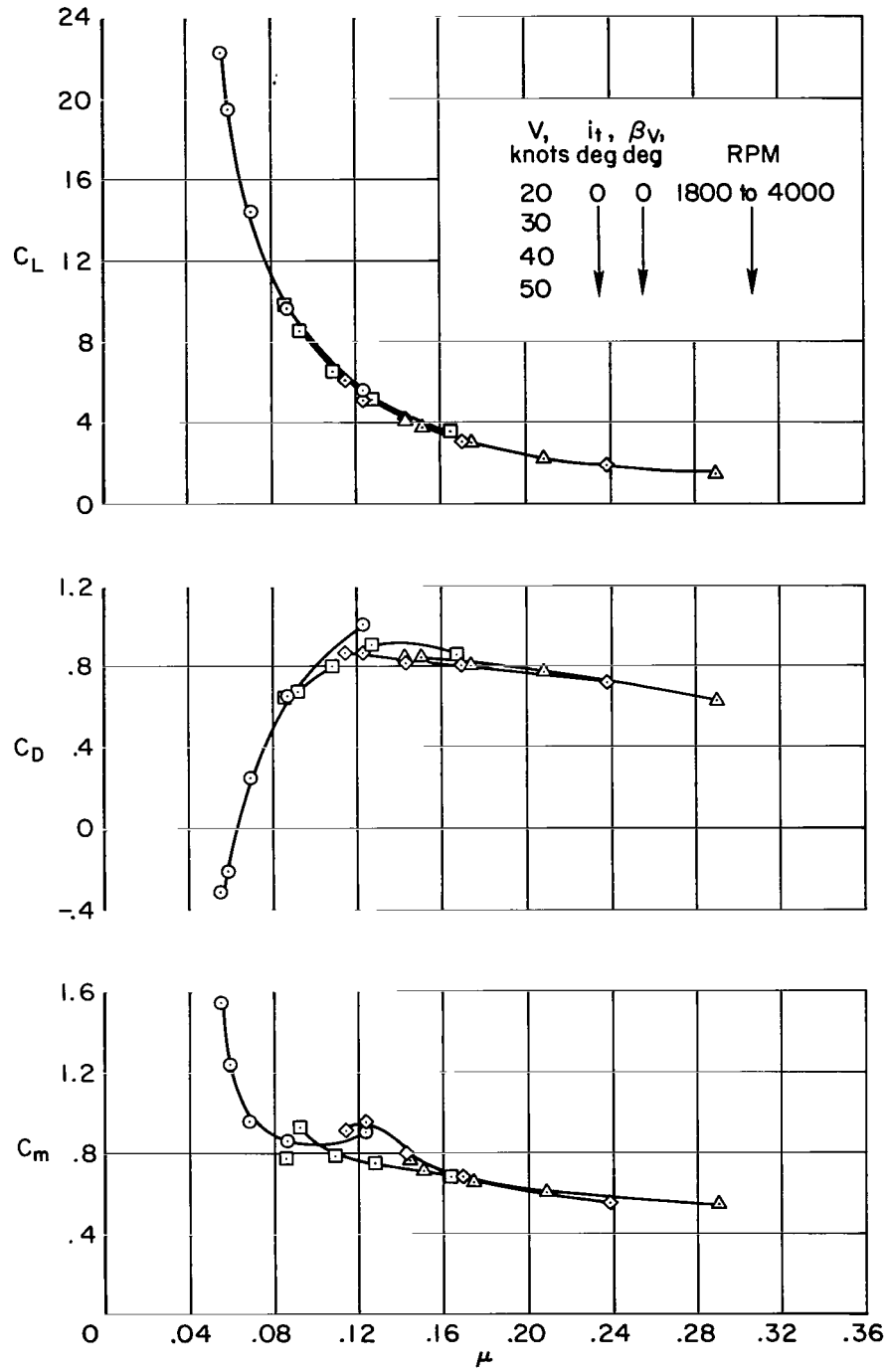

(a) $i_D = 75^\circ$

Figure 12.- The effect of varying fan speed at several cruise fan angles and forward speeds for the complete lift-cruise fan configuration; horizontal tail on, $\alpha = 0^\circ$, $\delta_f = 45^\circ$.

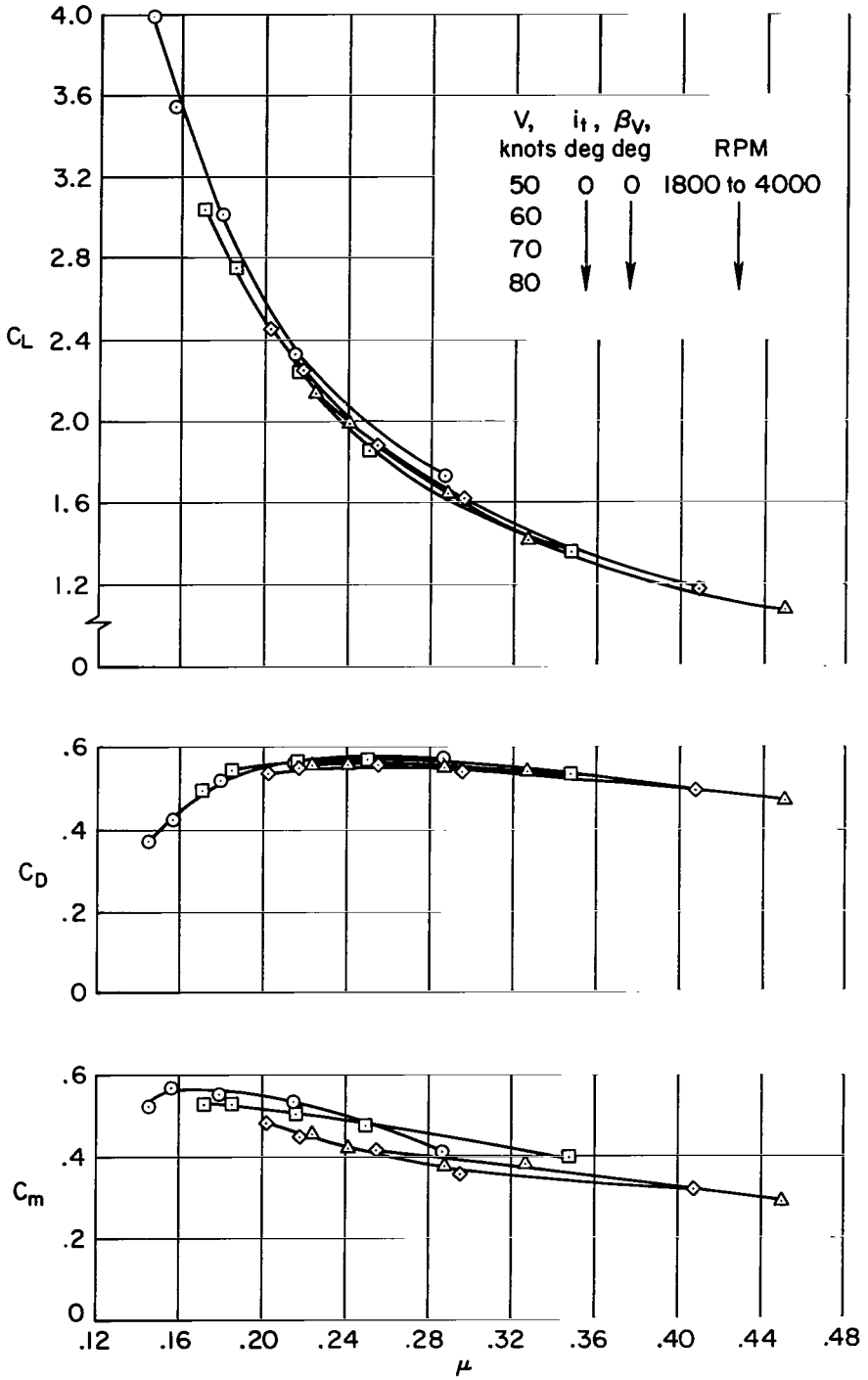

(b) $i_D = 60^\circ$

Figure 12.- Continued.

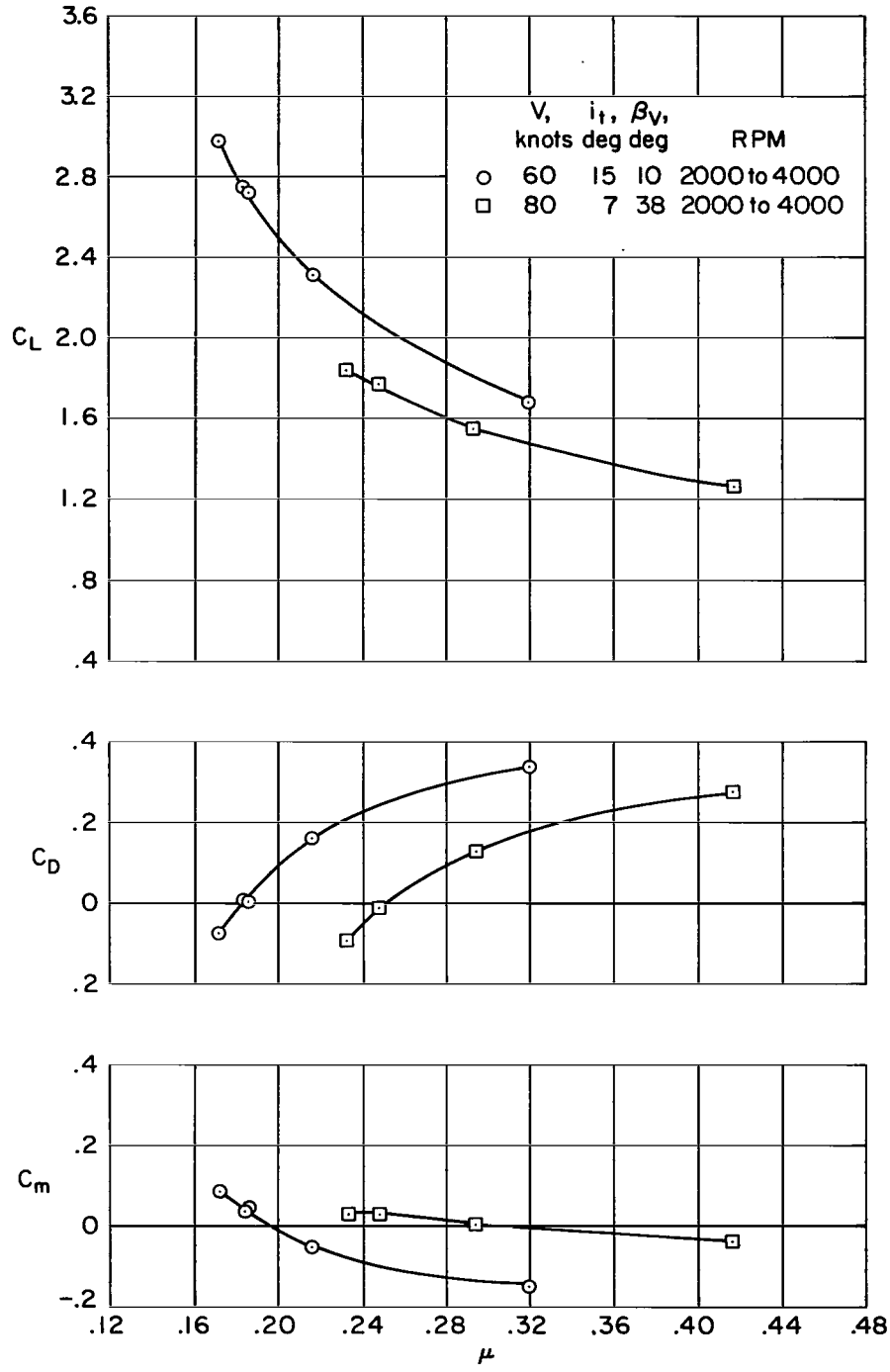

(c) $i_D = 45^\circ$

Figure 12.- Continued.

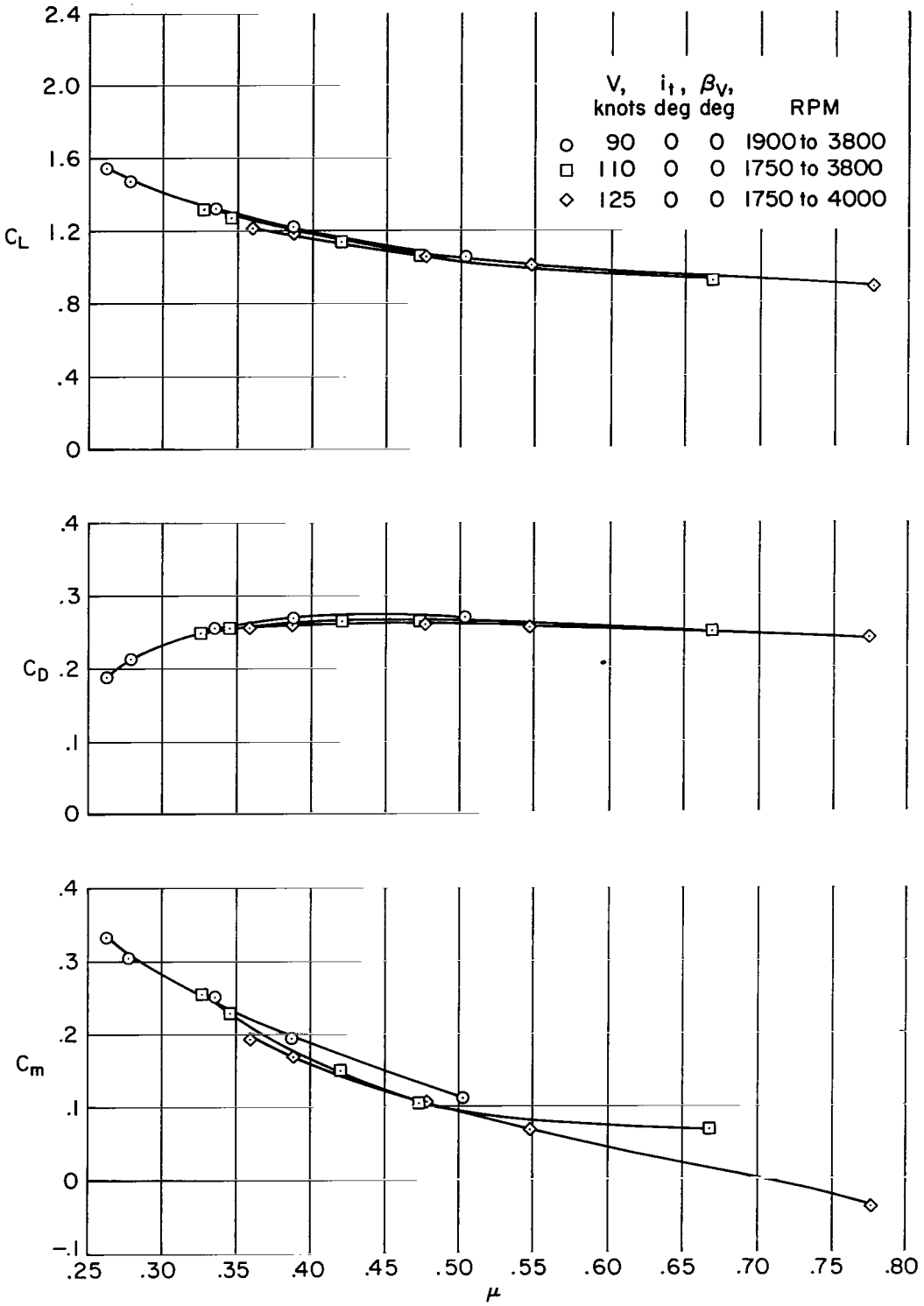

(d) $i_D = 30^\circ$

Figure 12.- Concluded.

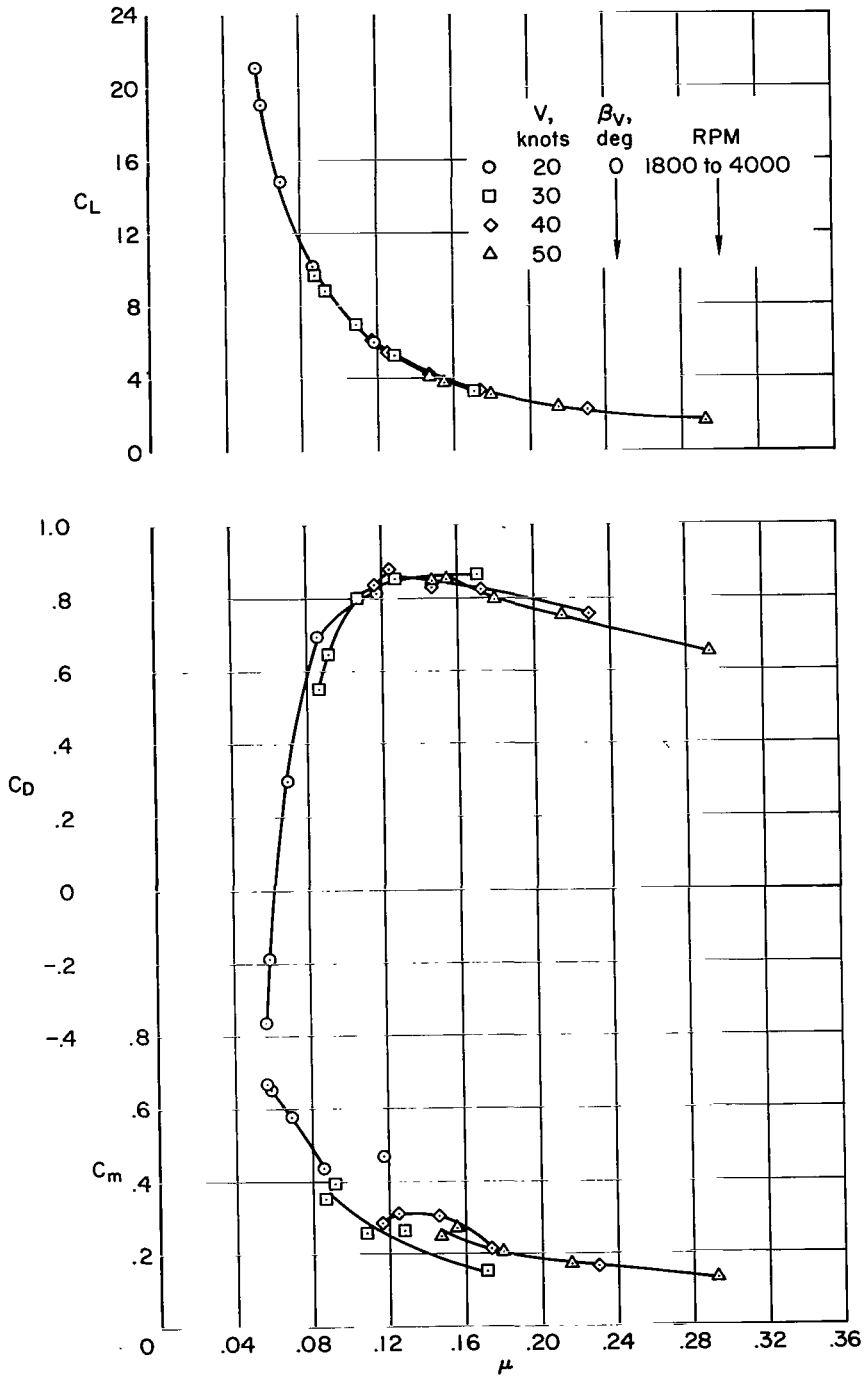

(a) $i_D = 75^\circ$

Figure 13.- The effect of varying fan speed at several cruise fan angles and forward speeds for the lift-cruise fan configuration; horizontal tail off, $\alpha = 0^\circ$, $\delta_f = 45^\circ$.

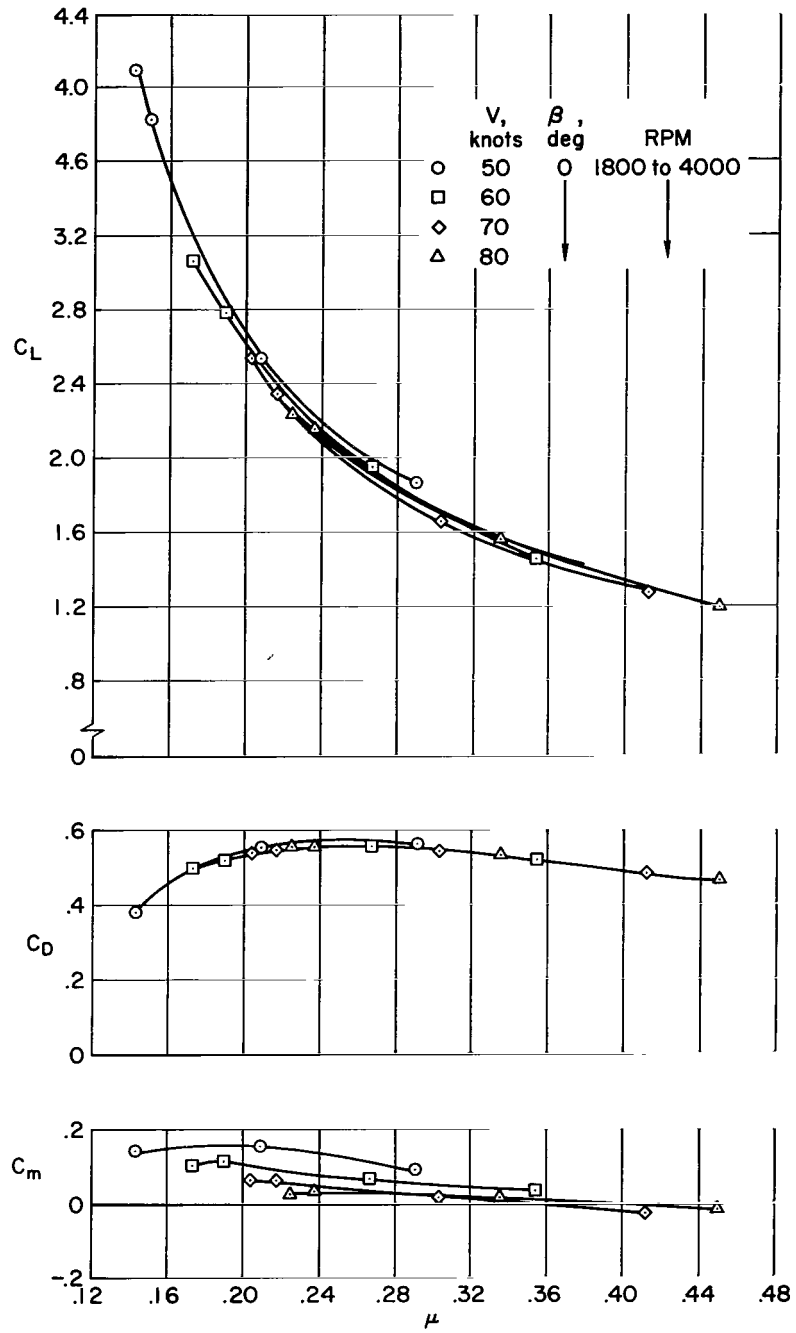

(b) $i_D = 60^\circ$

Figure 13.- Continued.

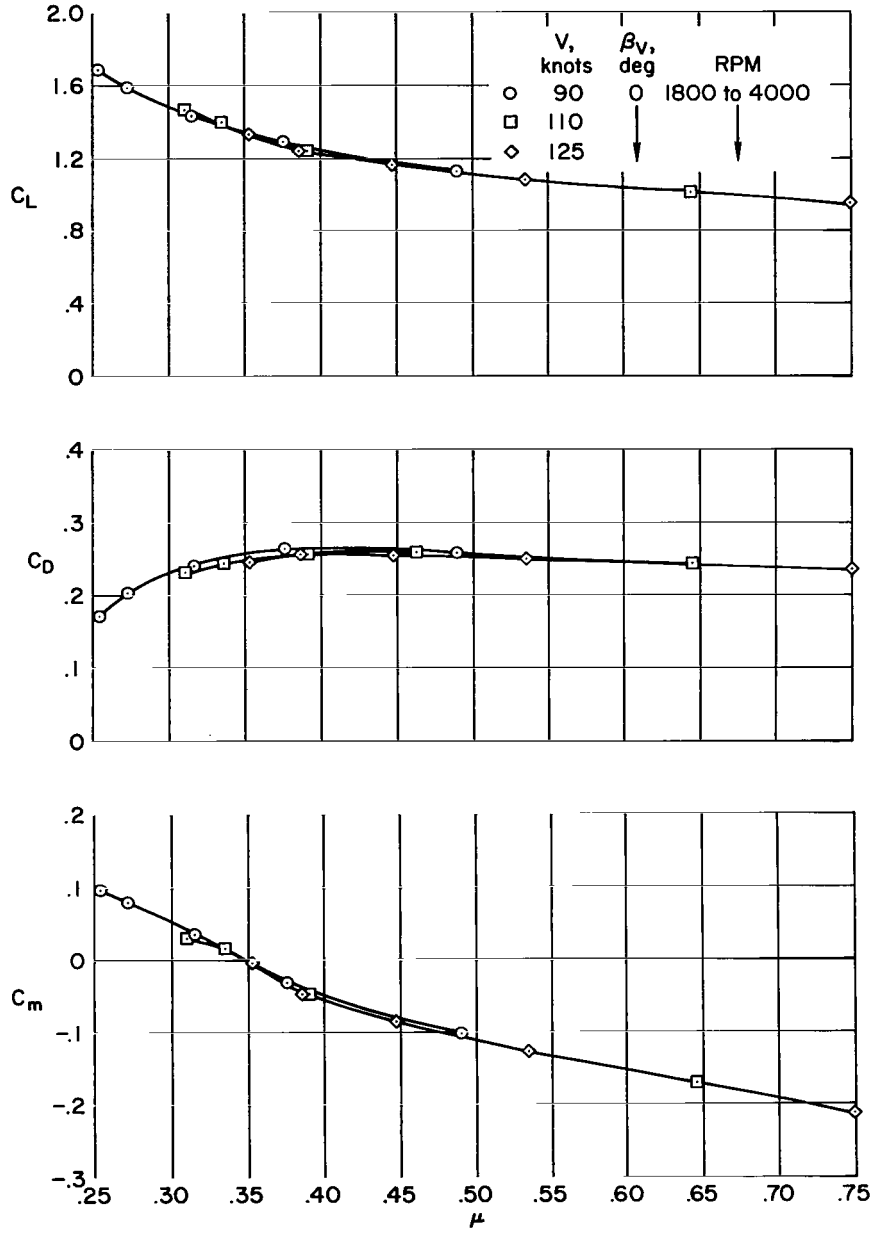

(c) $i_D = 30^\circ$

Figure 13.- Concluded.

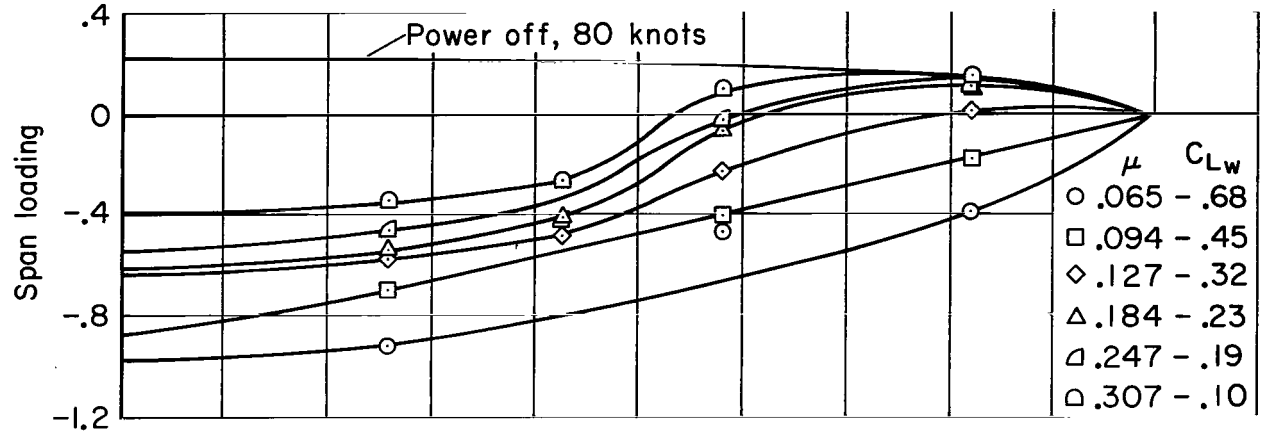

(a) Lift fans in the high aft position.

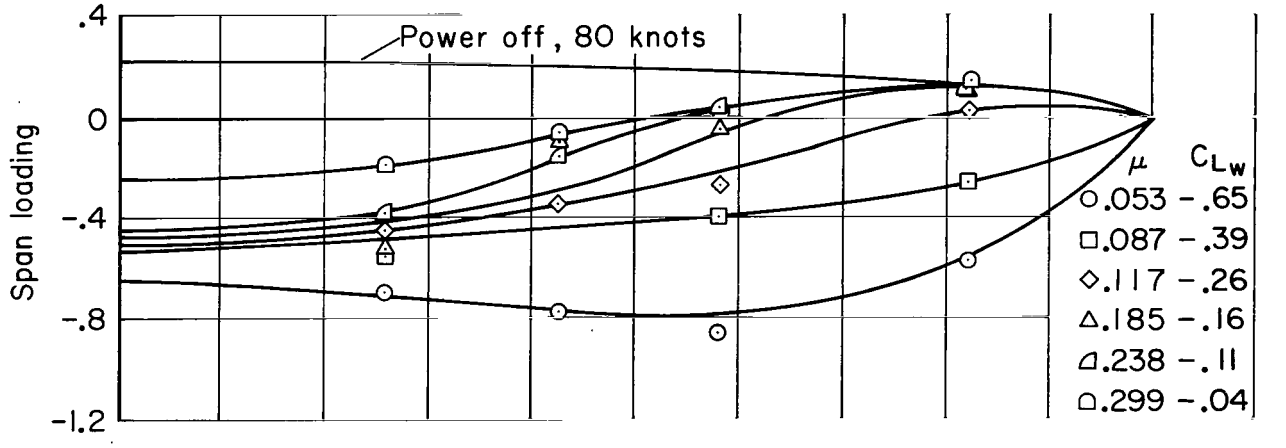

(b) Lift fans in the high forward position.

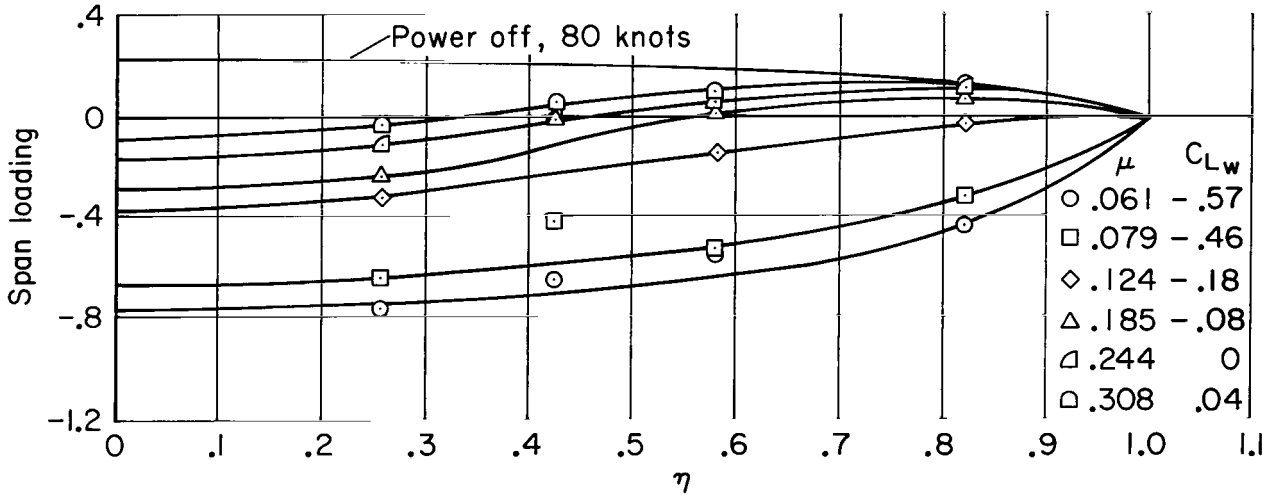

(c) Lift fans in the low aft position.

Figure 14.- The effect of front lift fan location on spanwise wing loading; front lift fans operating, rear fans removed, $\alpha = 0^{\circ}$, $\beta_v = 0^{\circ}$, $\delta_f = 0^{\circ}$.

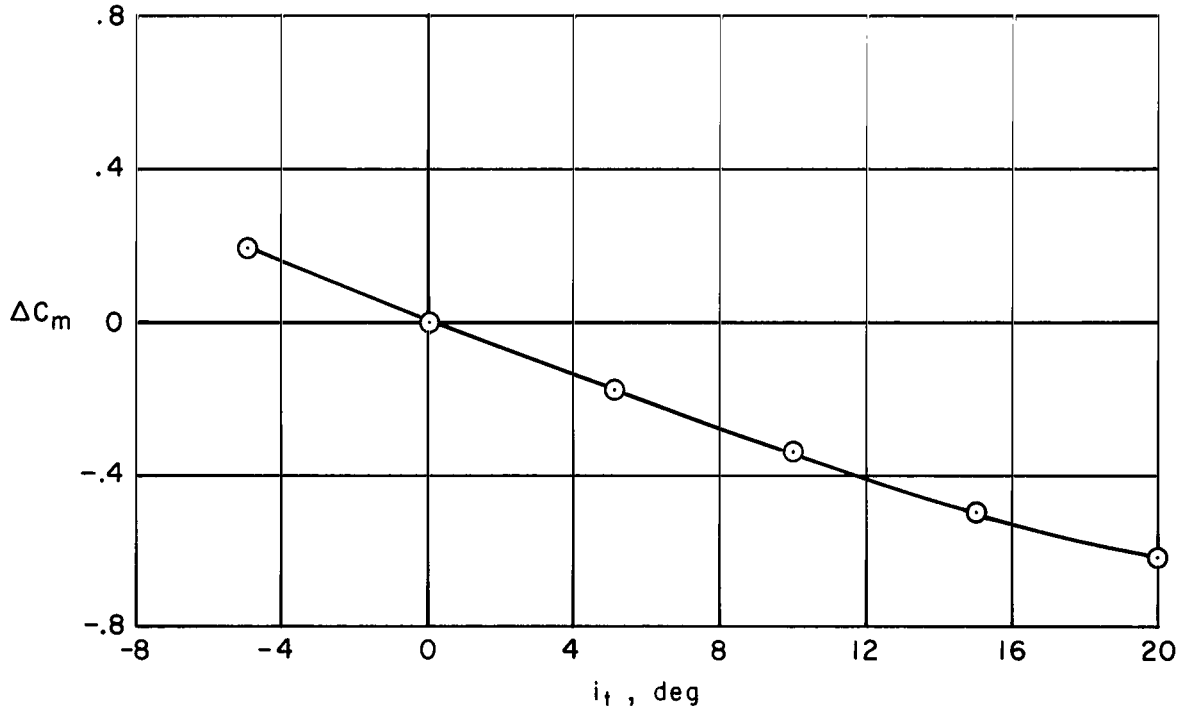

Figure 15.- The trim effectiveness of the horizontal tail with power off for the complete lift-cruise fan configuration; front lift fans sealed, $i_D = 60^\circ$, V = 80 knots, $\delta_f = 45^\circ$, $\alpha = 0^\circ$.

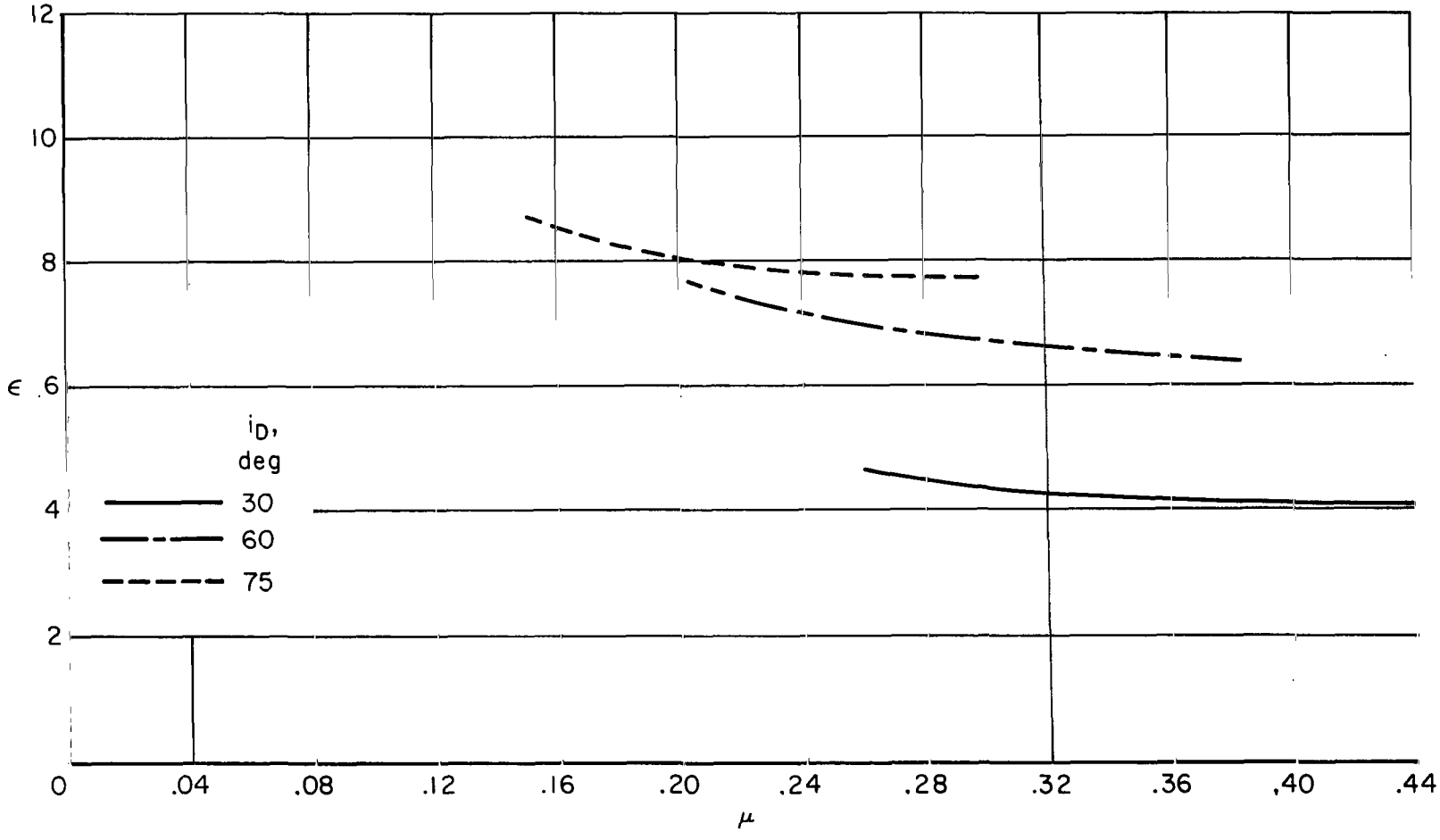

Figure 16.- The variation of average downwash at the horizontal tail for the complete lift-cruise fan configuration; $\delta_f = 45^\circ$, $\beta_v = 0^\circ$, $\alpha = 0^\circ$.

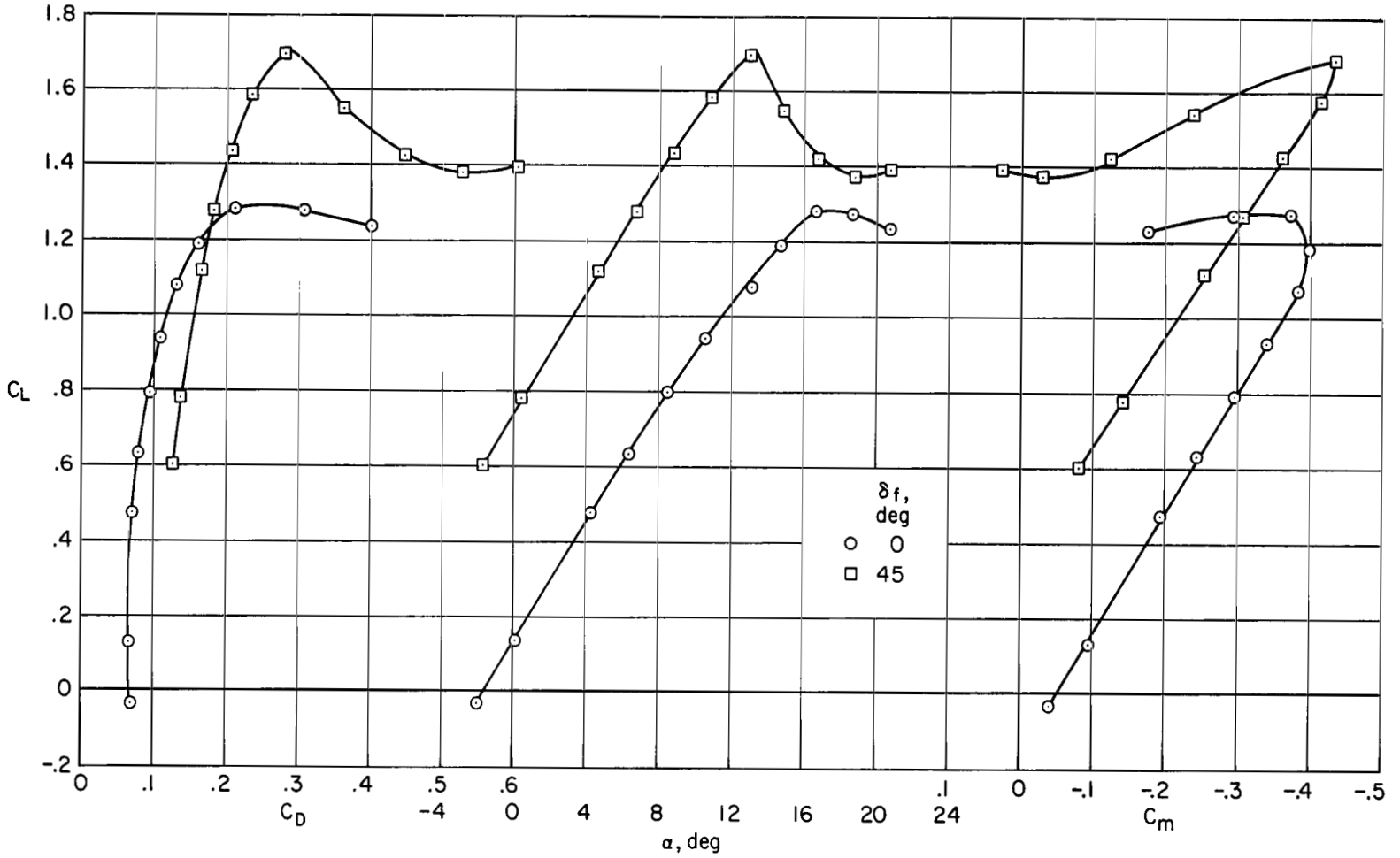

Figure 17.- Longitudinal characteristics with power off; all fans removed, tail on, $i_t = 0^\circ$, V = 80 knots.

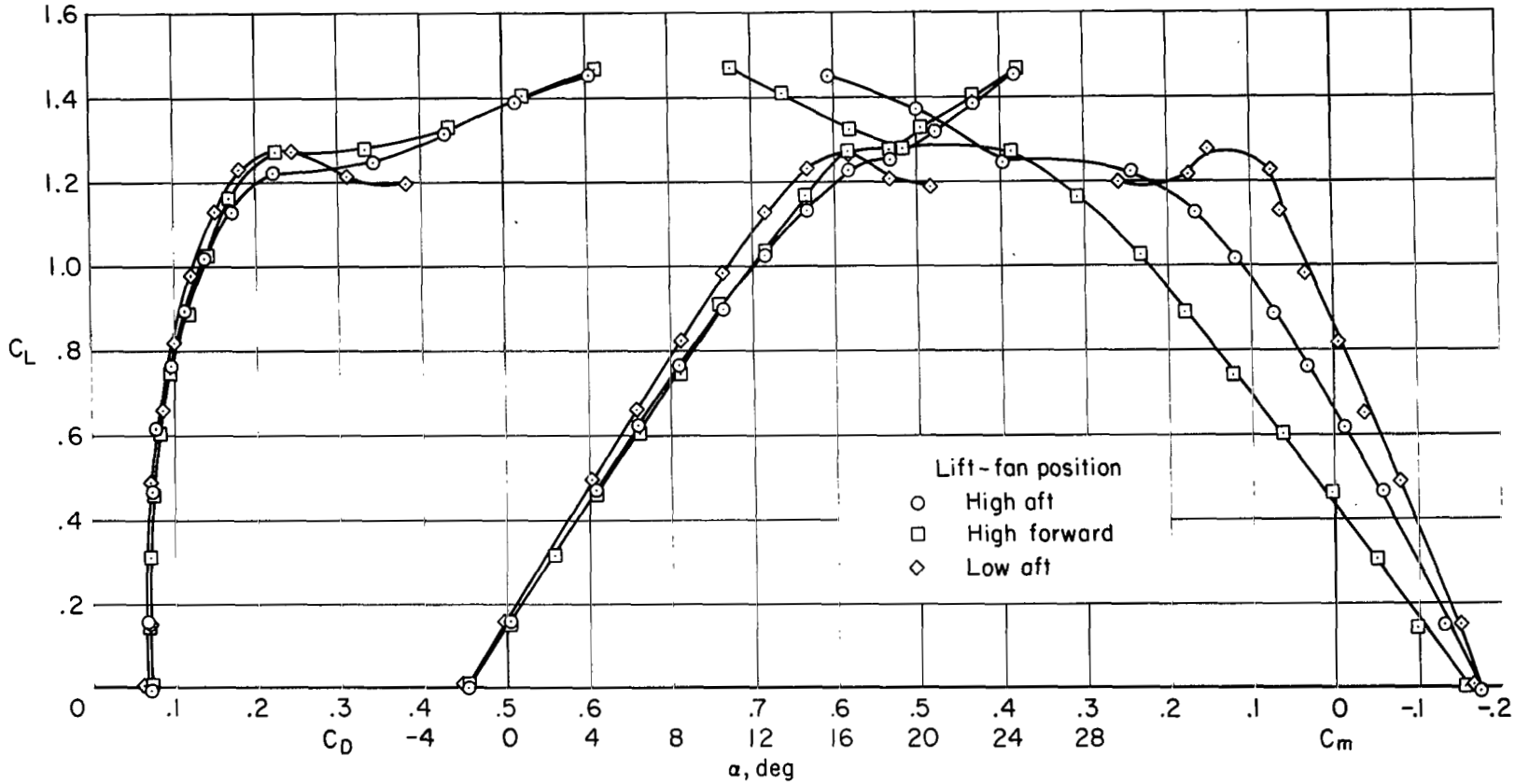

Figure 18.- Longitudinal characteristics with power off for the alternate lift-fan locations; cruise fans removed, tail off, $\delta_f = 0^\circ$, V = 80 knots.

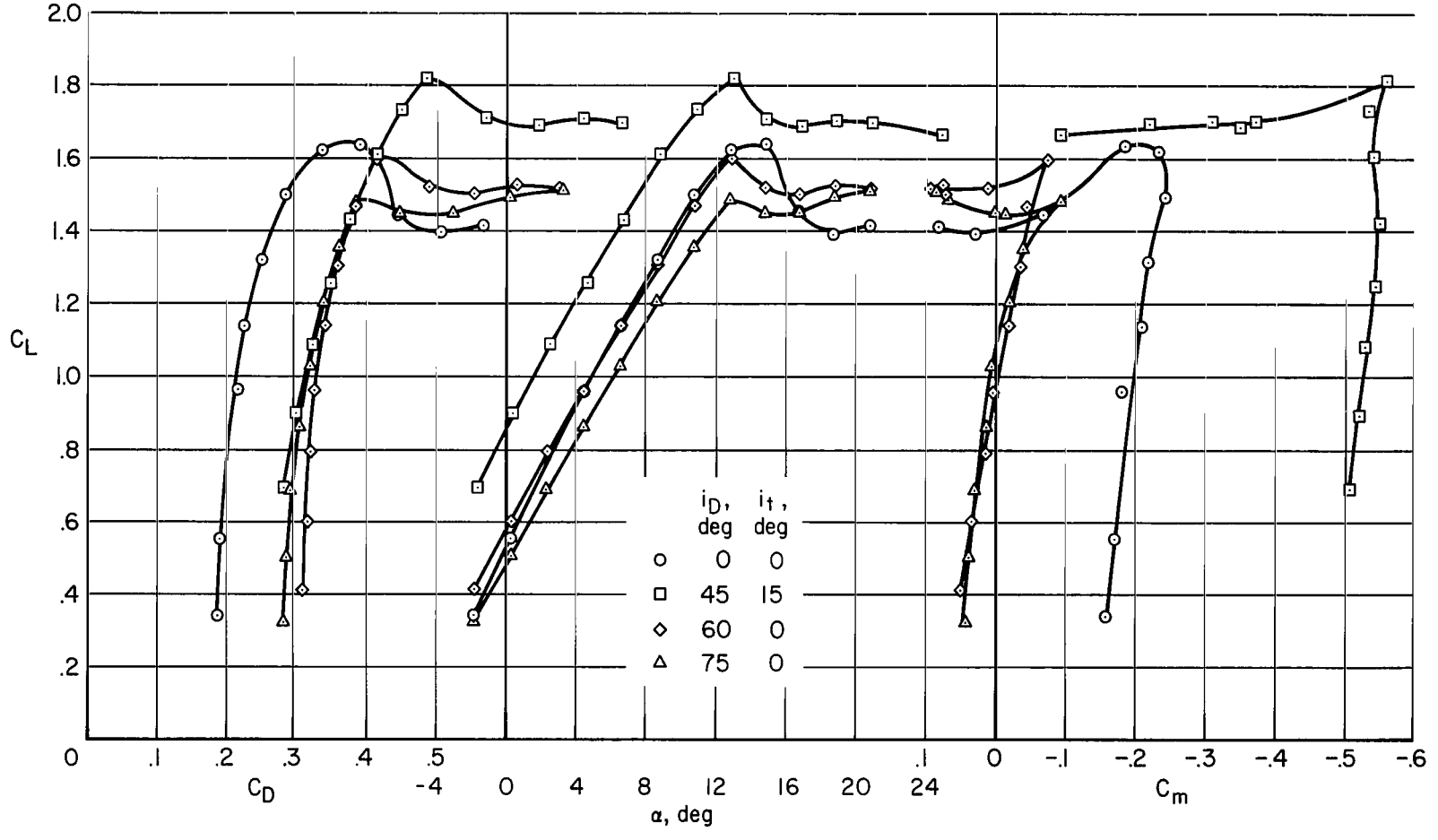

Figure 19.- Longitudinal characteristics with power off for the complete lift-cruise fan configuration; front lift fans sealed, rear cruise fans windmilling, tail on, $\delta_f = 45^\circ$, V = 80 knots.

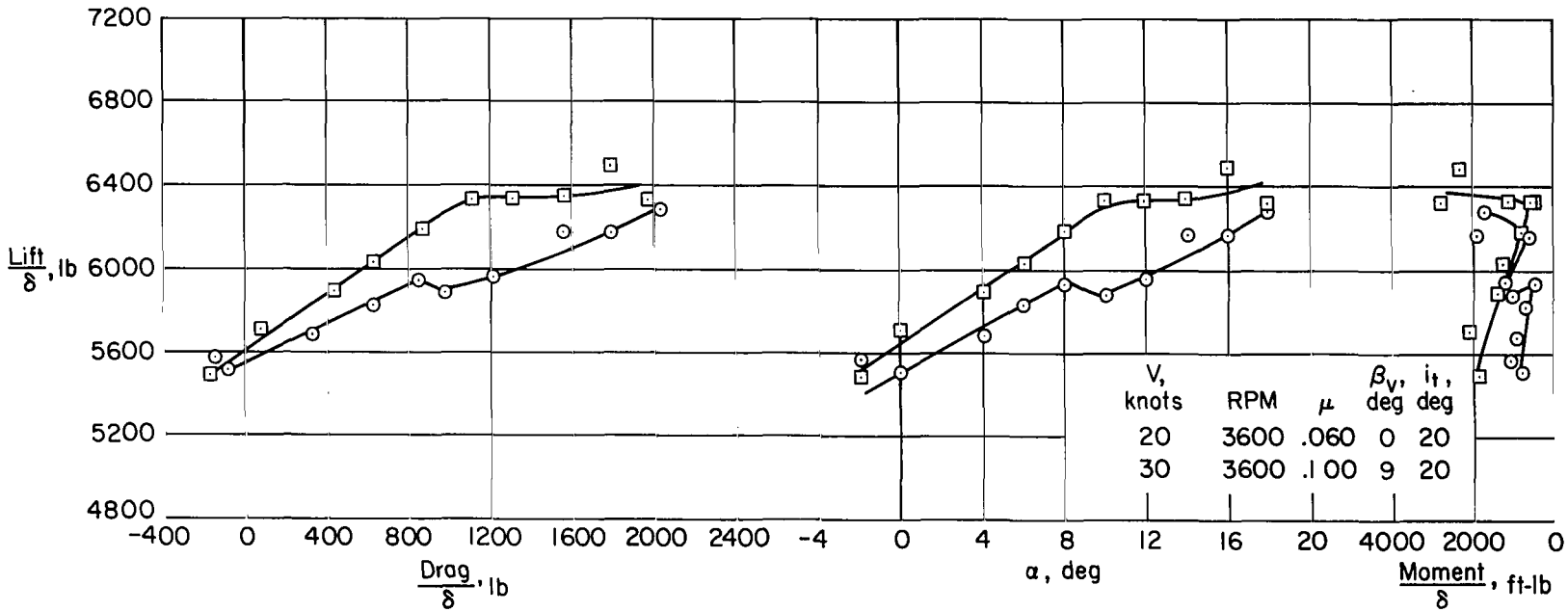

Figure 20.- Longitudinal characteristics for the complete lift-cruise fan configuration with four fans operating at low tip-speed ratios; tail on, $\delta_f = 45^\circ$, $i_D = 75^\circ$.

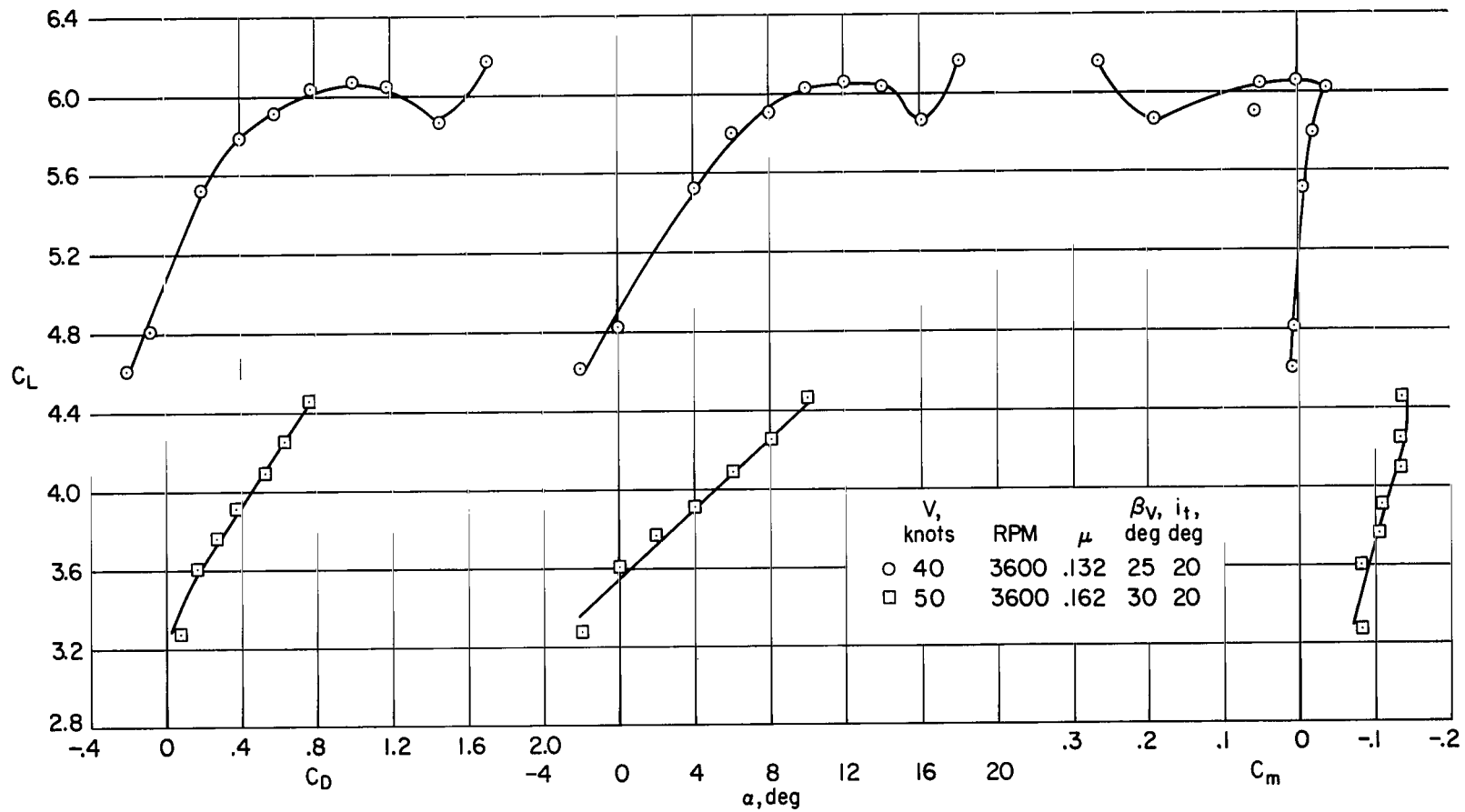

(a) $i_D = 75^\circ$

Figure 21.- Longitudinal characteristics for the complete lift-cruise fan configuration with four fans operating at various tip-speed ratios; tail on, $\delta_f = 45^\circ$.

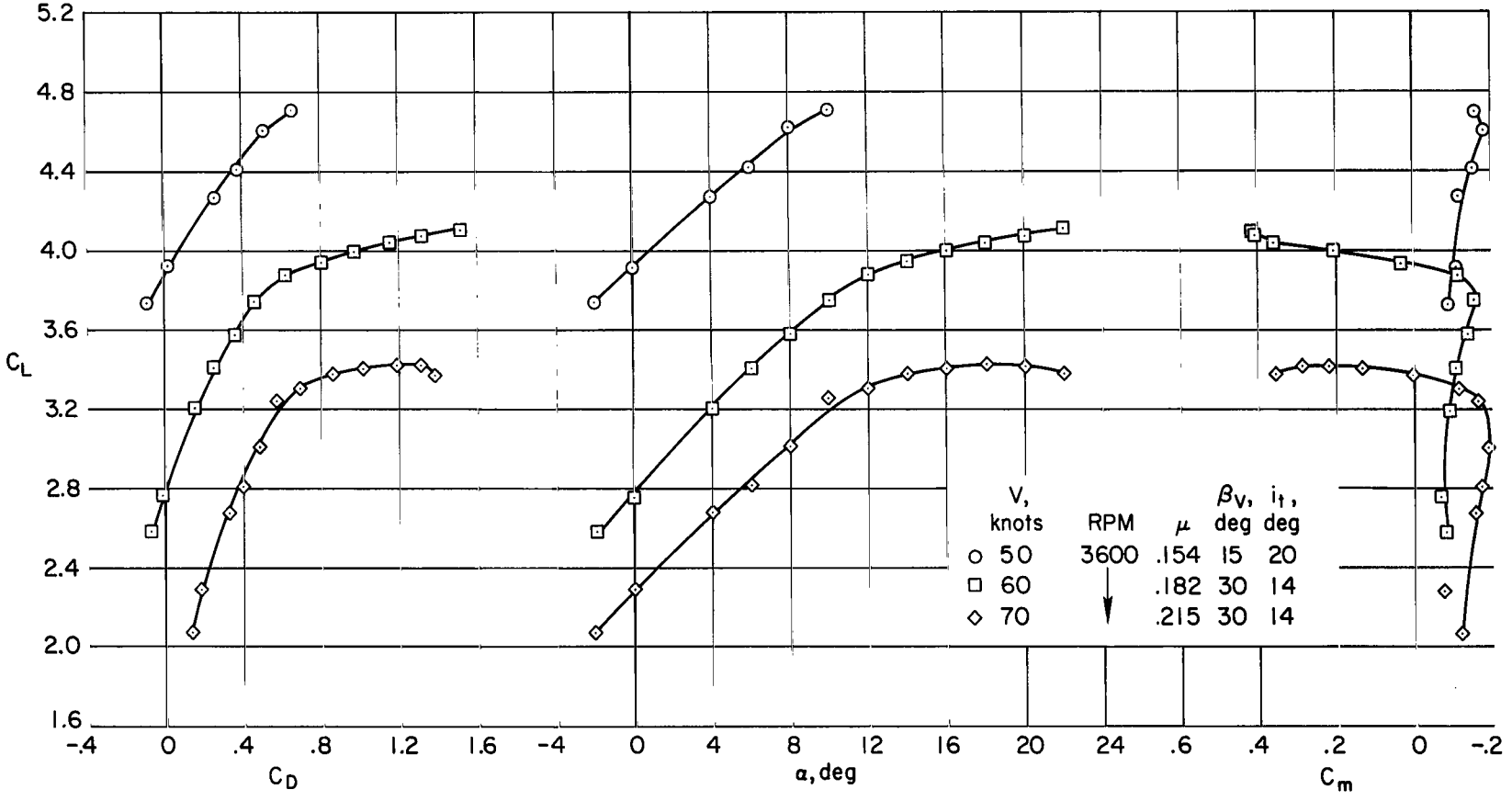

(b) $i_D = 60°$

Figure 21.- Continued.

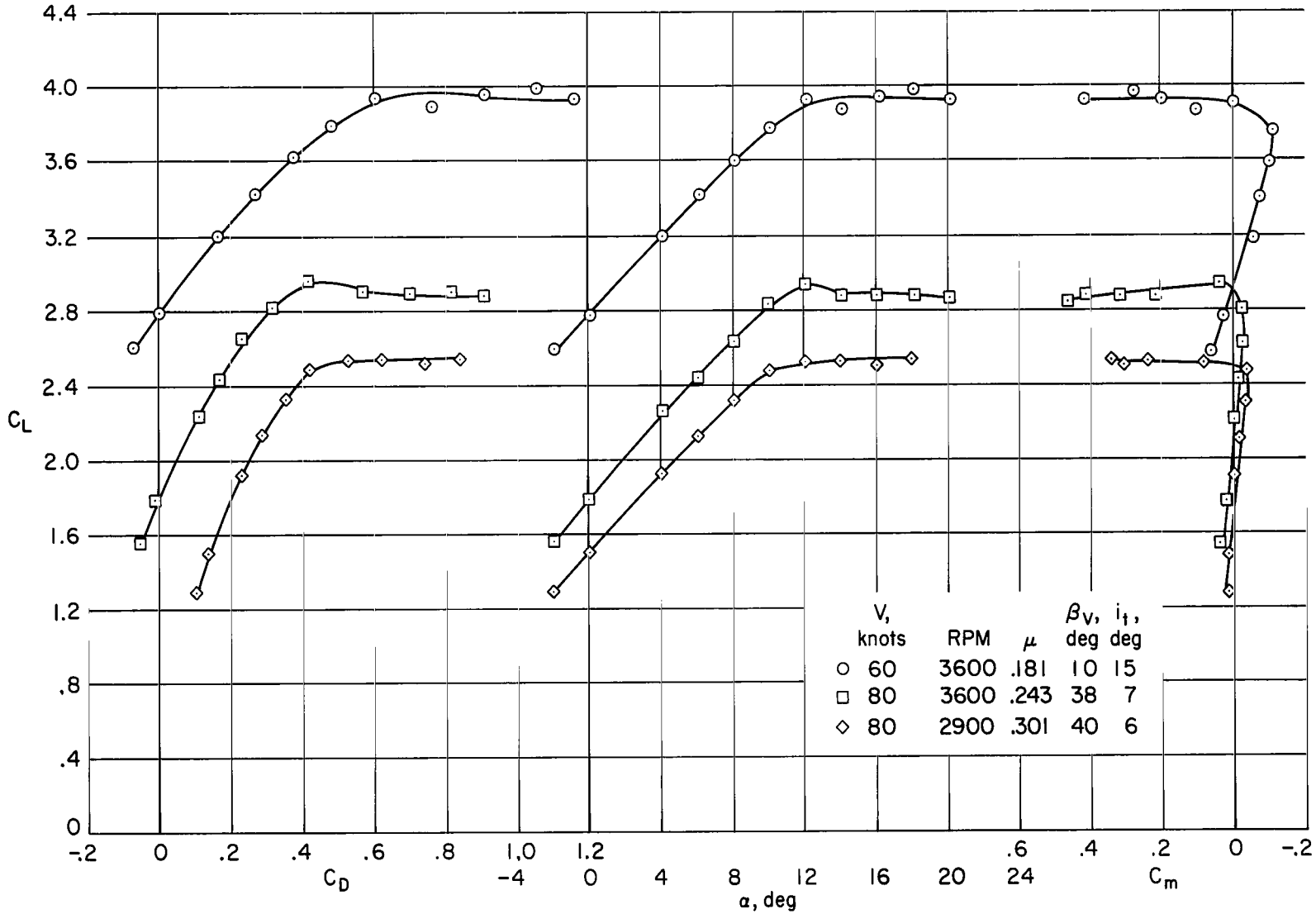

(c) $i_D = 30^\circ$

Figure 21.- Continued.

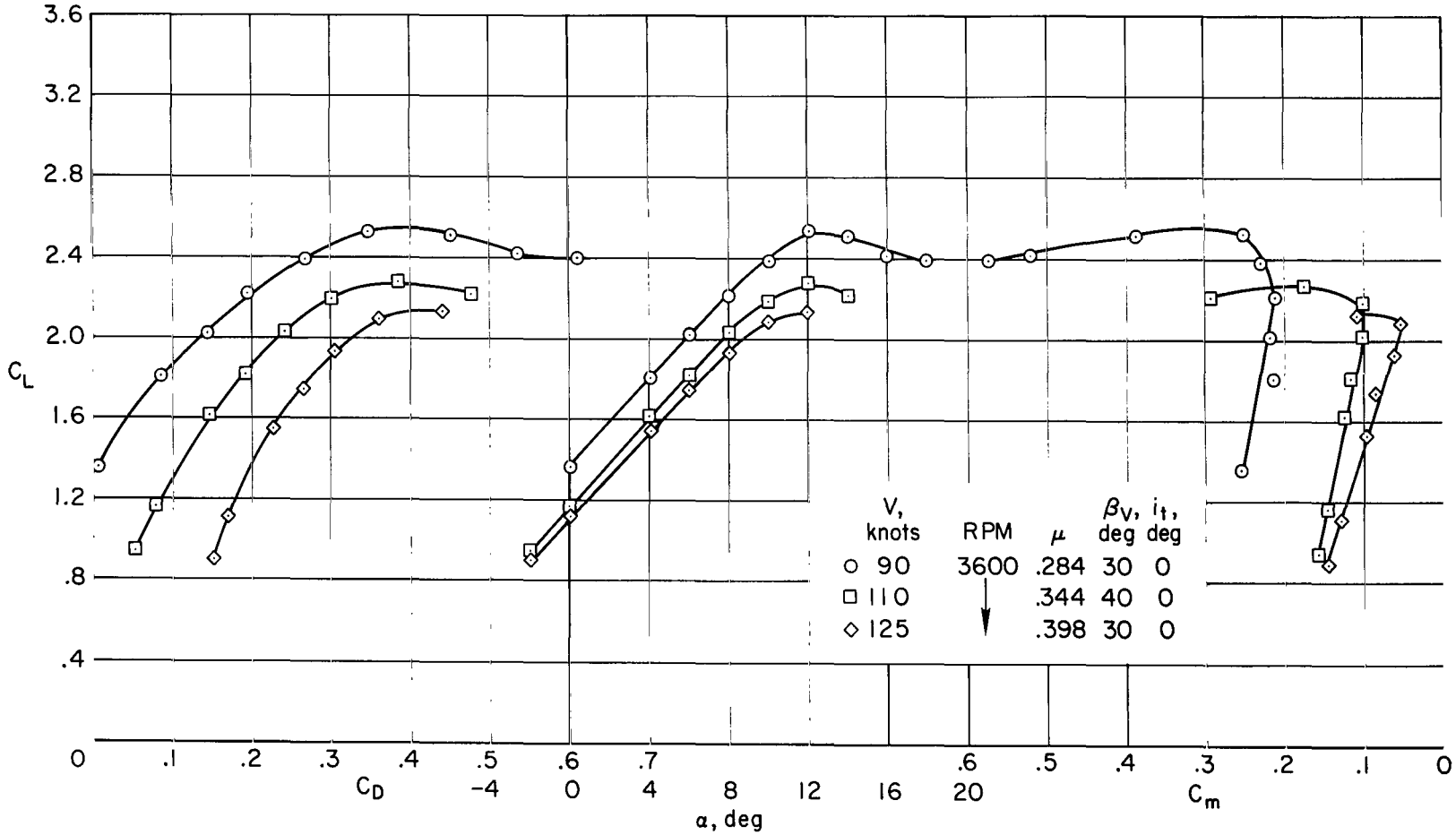

(d) $i_D = 30^\circ$

Figure 21.- Concluded.

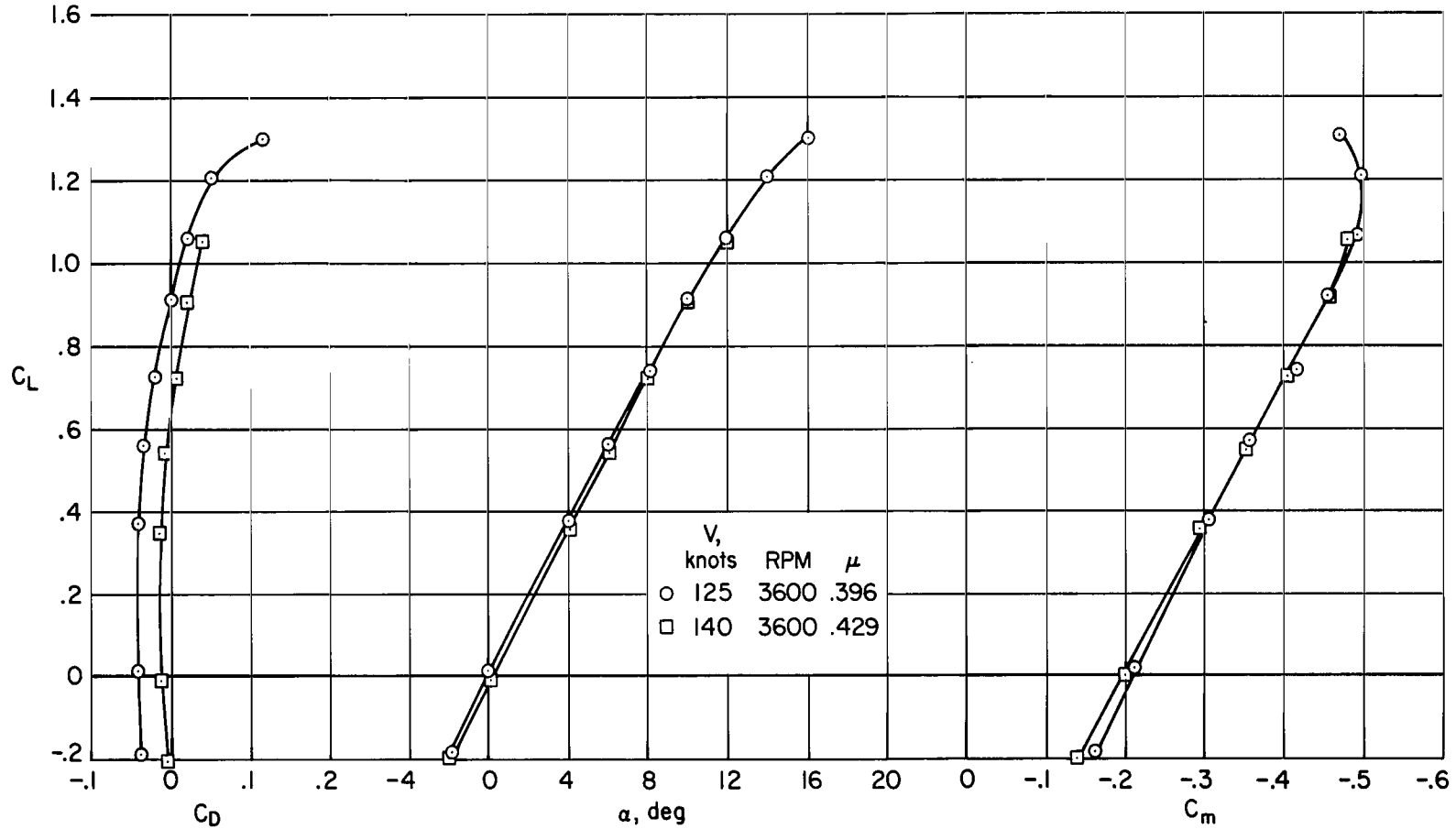

Figure 22.- Longitudinal characteristics with two cruise fans operating at high tip-speed ratios; front lift fans removed, rear cruise fans at $i_D = 0^\circ$, tail on, $i_t = 0^\circ$, $\delta_f = 0^\circ$.

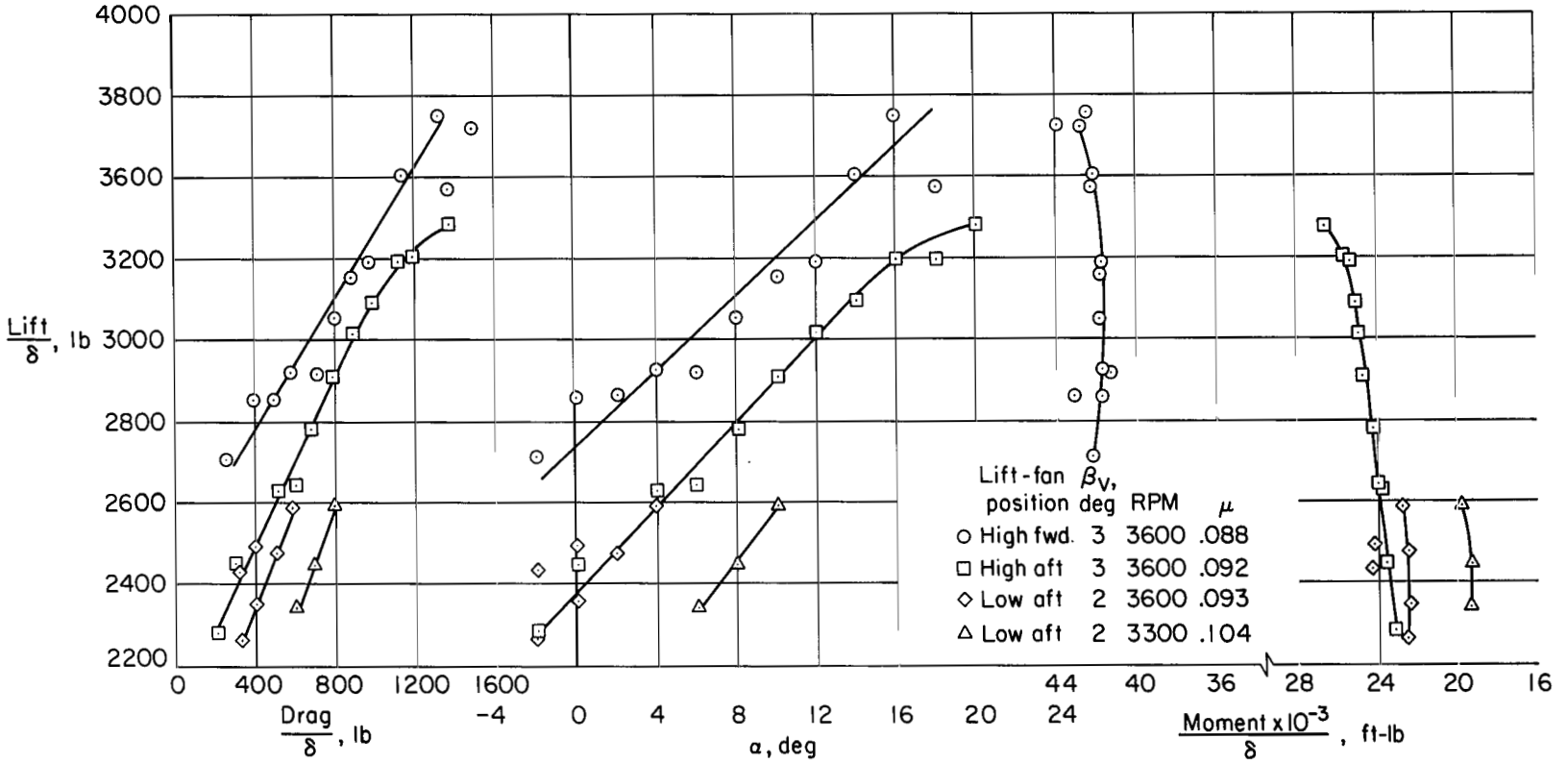

Figure 23.- The effect of front fan location on longitudinal characteristics with the two front lift fans operating at low tip-speed ratios; rear cruise fans removed, tail off, $\delta_f = 0^\circ$, V = 30 knots.

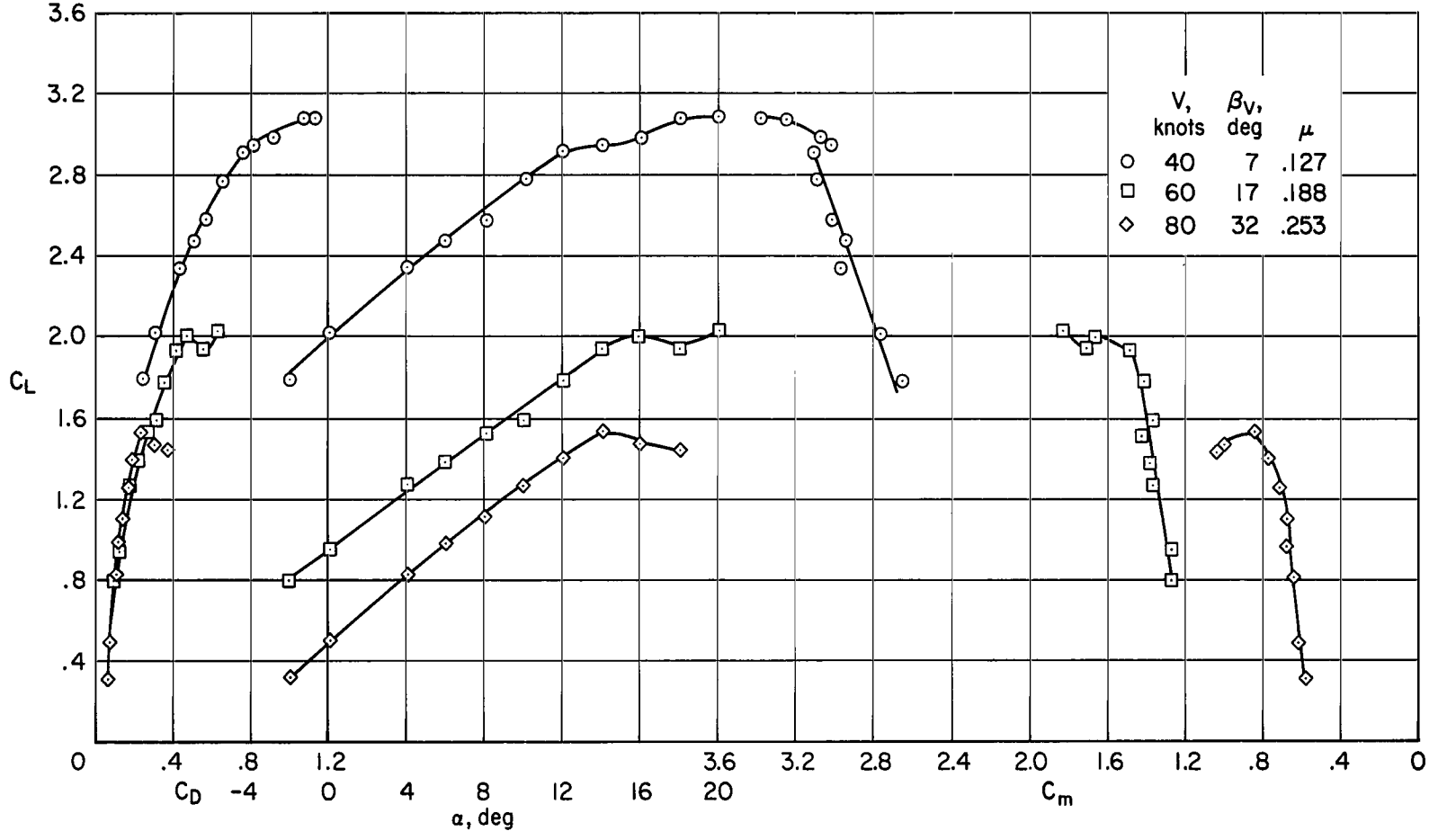

(a) Front lift fans in the high aft position.

Figure 24.- The effect of front fan location on longitudinal characteristics with the two front lift fans operating at various tip-speed ratios; rear cruise fans removed, tail off, $\delta_f = 0^\circ$.

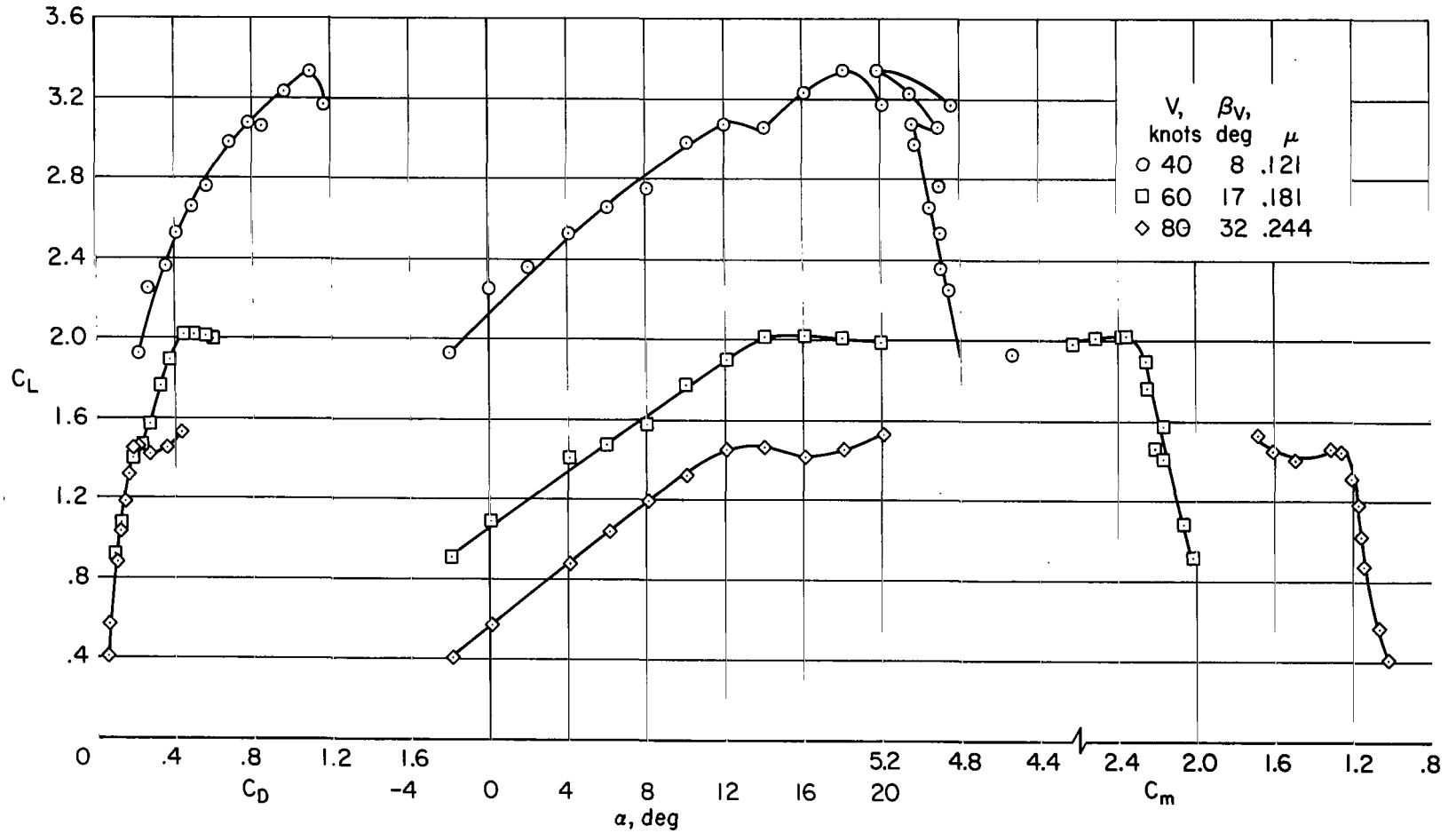

(b) Front lift fans in the high forward position.

Figure 24.- Continued.

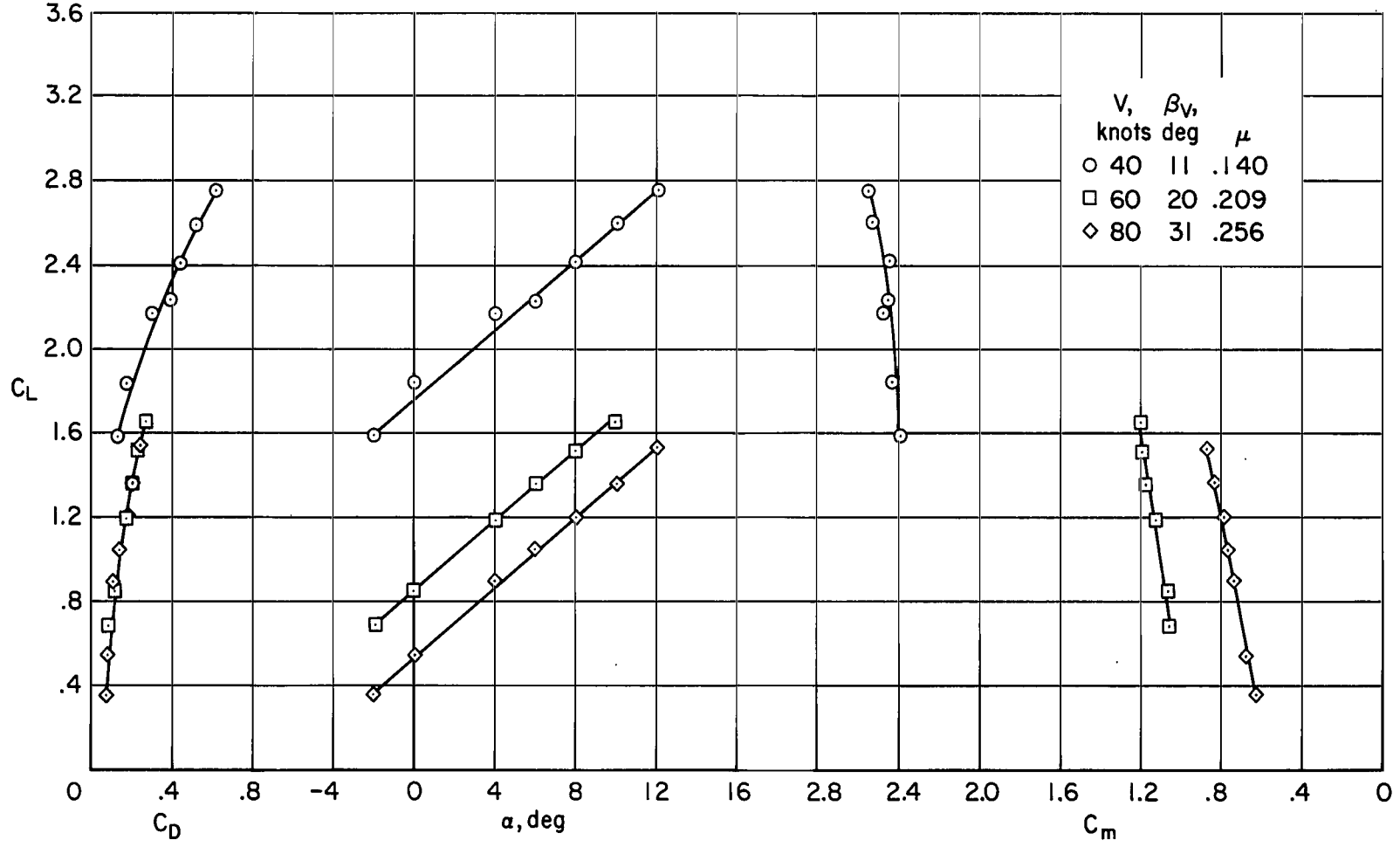

(c) Front lift fans in the low aft position.

Figure 24.- Concluded.

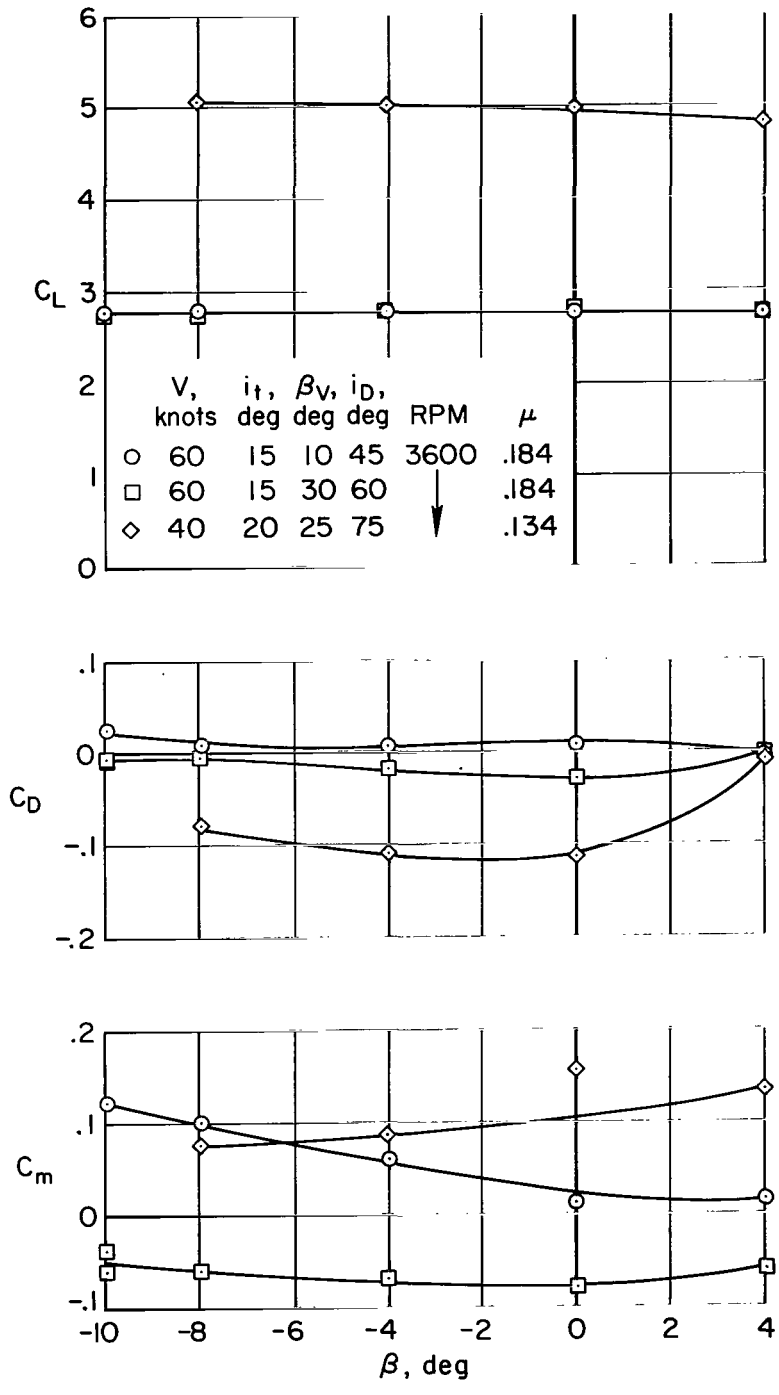

(a) Longitudinal characteristics.

Figure 25.- The effect of sideslip angle on the longitudinal and lateral characteristics for the complete lift-cruise fan configuration; tail on, $\delta_f = 45^\circ$, $\alpha = 0^\circ$.

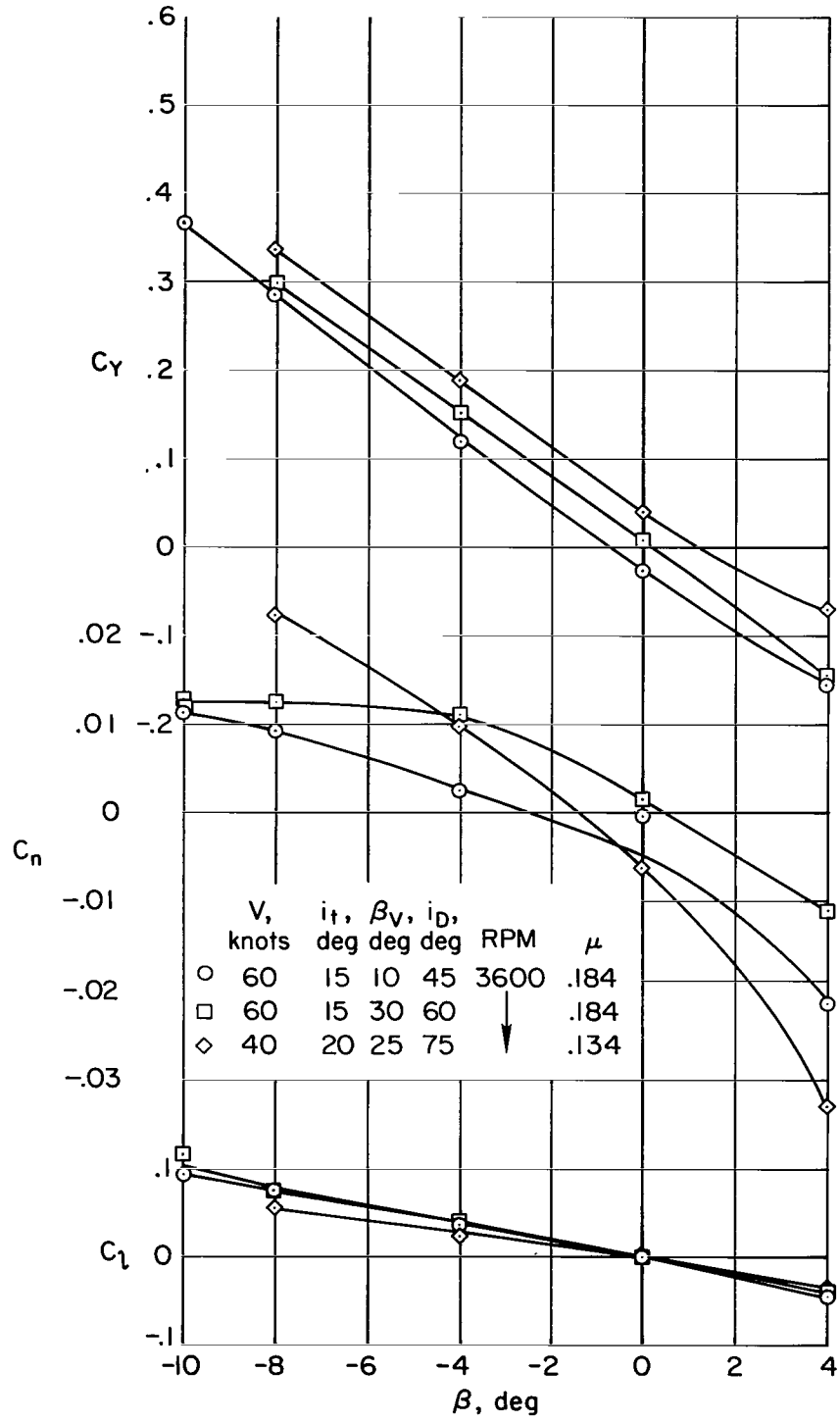

(b) Lateral characteristics.

Figure 25.- Concluded.

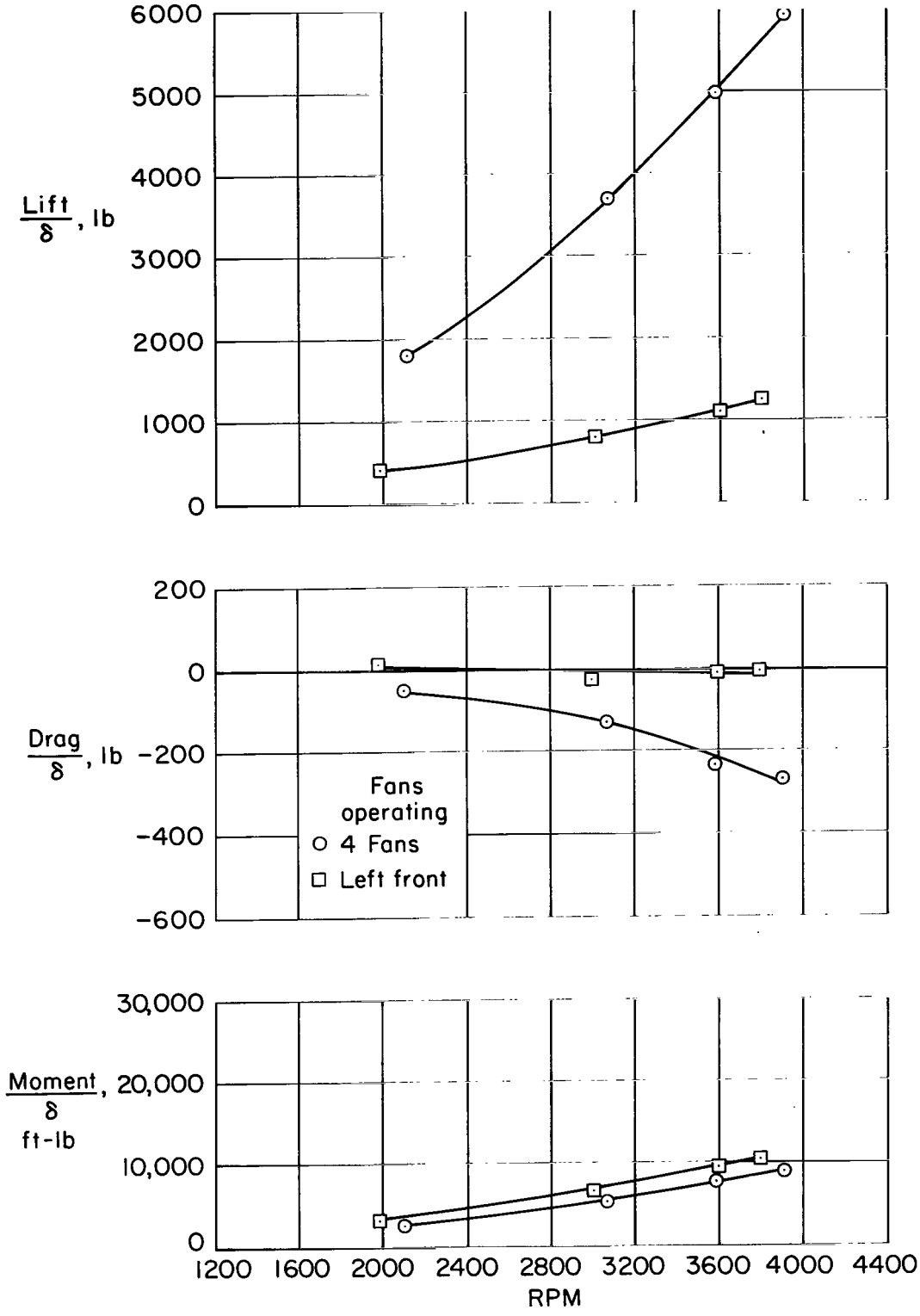

Figure 26.- Zero airspeed characteristics for the tandem lift fan configuration; tail on, $i_t = 0^\circ$, $\delta_f = 45^\circ$, $\beta_V = 0^\circ$, $\alpha = 0^\circ$.

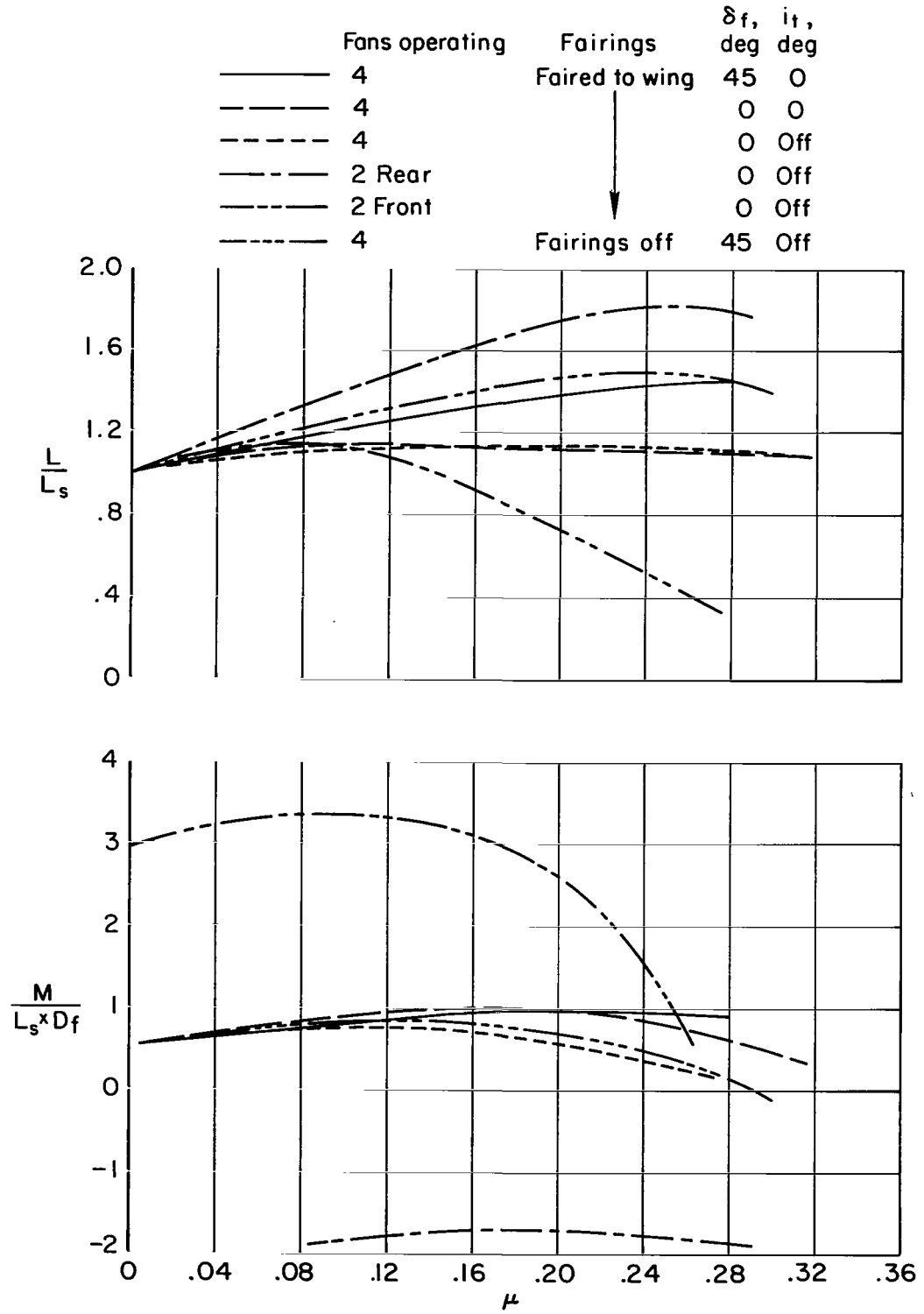

Figure 27.- The effect of forward speed and fan RPM (tip-speed ratio) on total lift and moment for trim drag; tandem lift fan configuration, $\alpha = 0^{\circ}$.

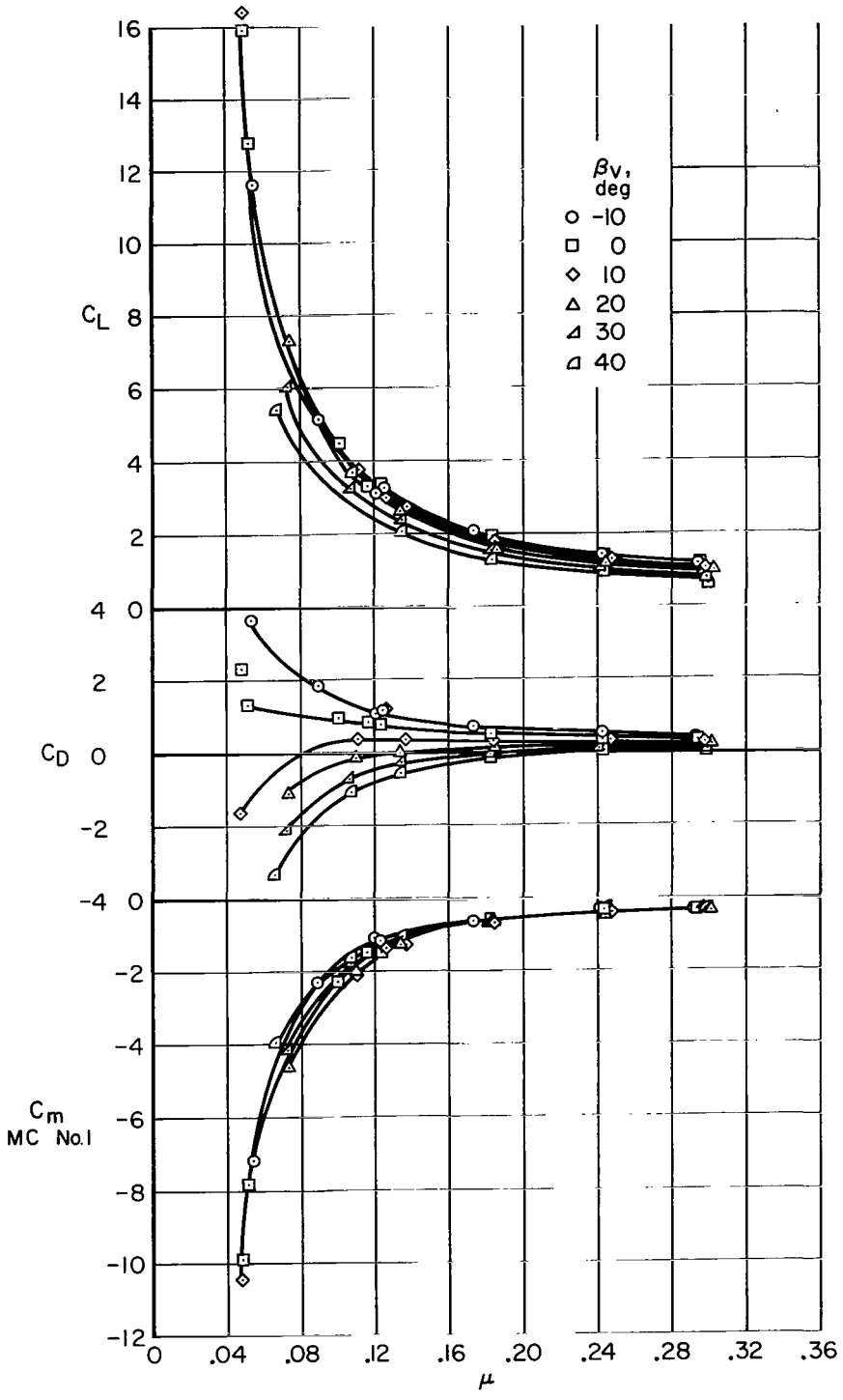

Figure 28.- The effect of tip-speed ratio on the longitudinal characteristics with the rear fans operating; front fans sealed; tandem lift fan configuration; tail off; $\delta_f = 0^\circ$; $\alpha = 0^\circ$.

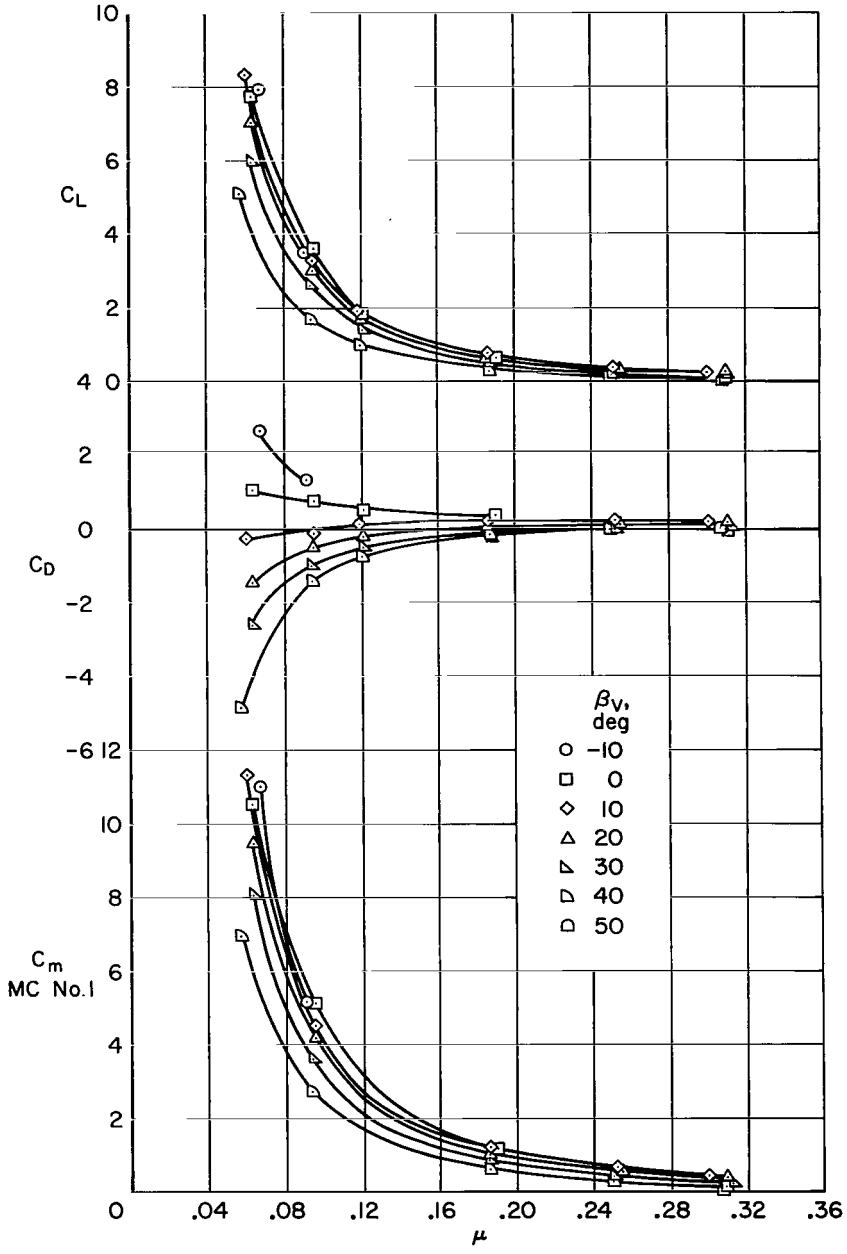

Figure 29.- The effect of tip-speed ratio on the longitudinal characteristics with the front fans operating; rear fans sealed; tandem lift fan configuration; tail off; $\delta_f = 0^\circ$; $\alpha = 0^\circ$.

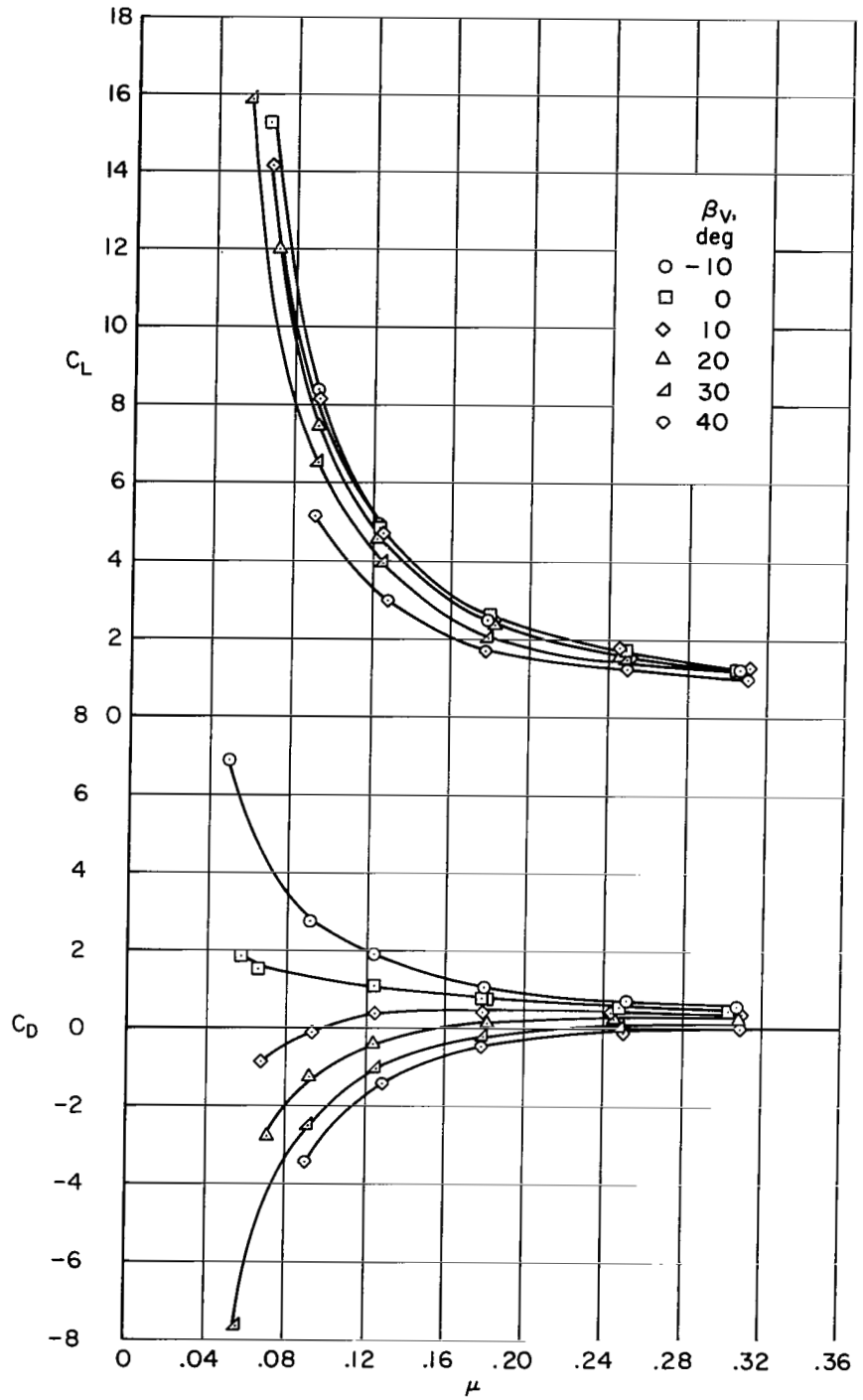

(a) Lift and drag coefficients.

Figure 30.- The effect of tip-speed ratio on the longitudinal characteristics for the complete tandem lift fan configuration; $i_t = 0^\circ$, $\delta_f = 45^\circ$, $\alpha = 0^\circ$.

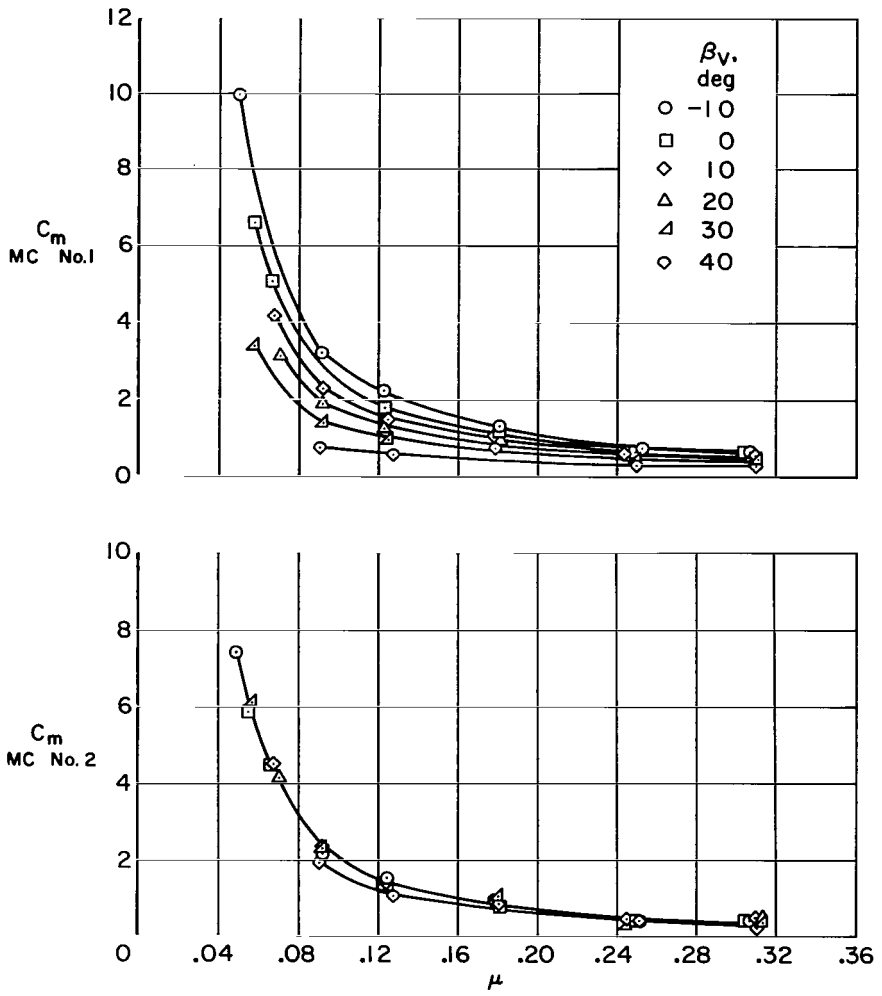

(b) Moment coefficients.

Figure 30.- Concluded.

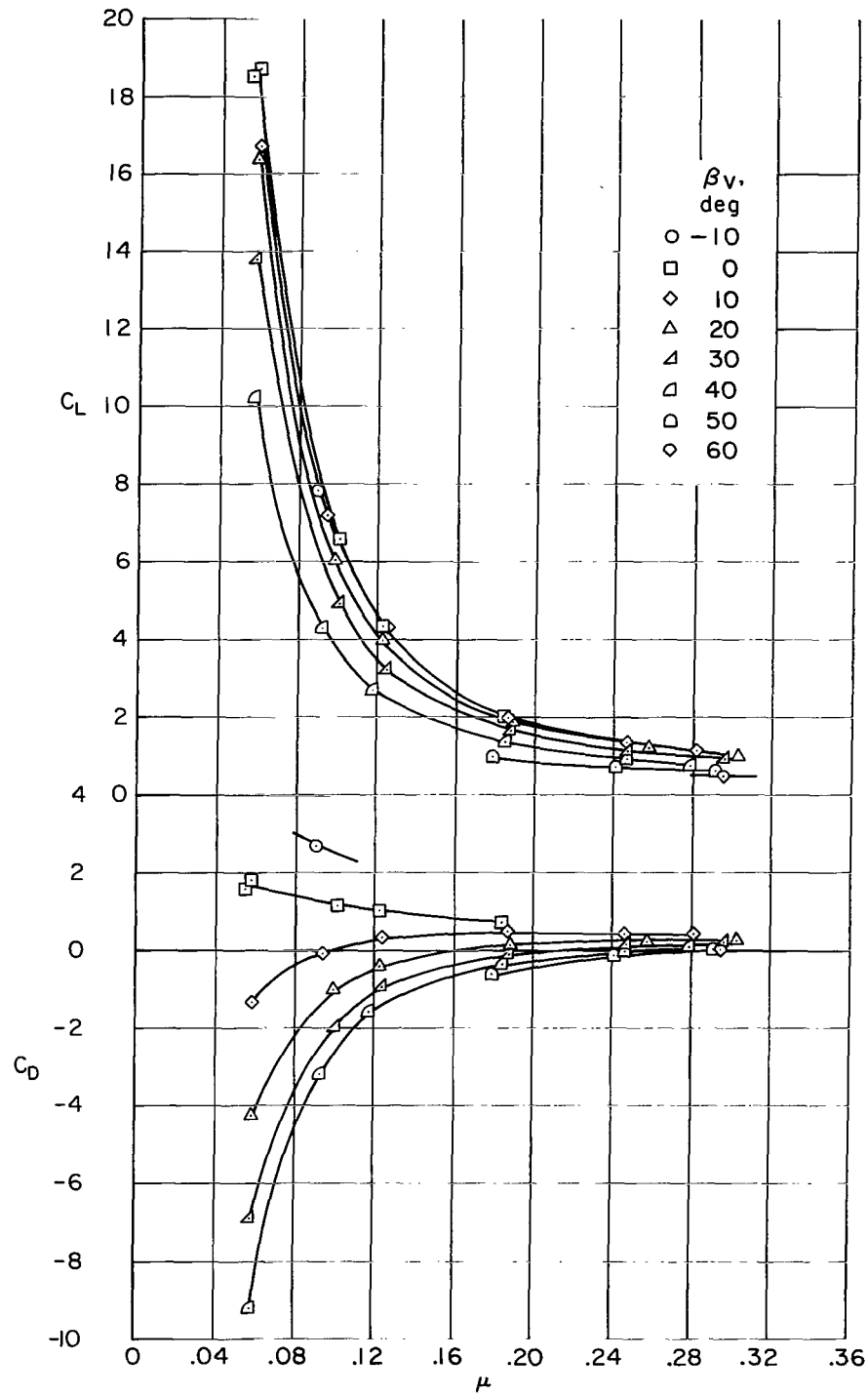

(a) Lift and drag coefficients.

Figure 31.- The effects of tip-speed ratio on the longitudinal characteristics for the complete tandem lift-fan configuration; $i_t = 0^\circ$, $\delta_f = 0^\circ$, $\alpha = 0^\circ$.

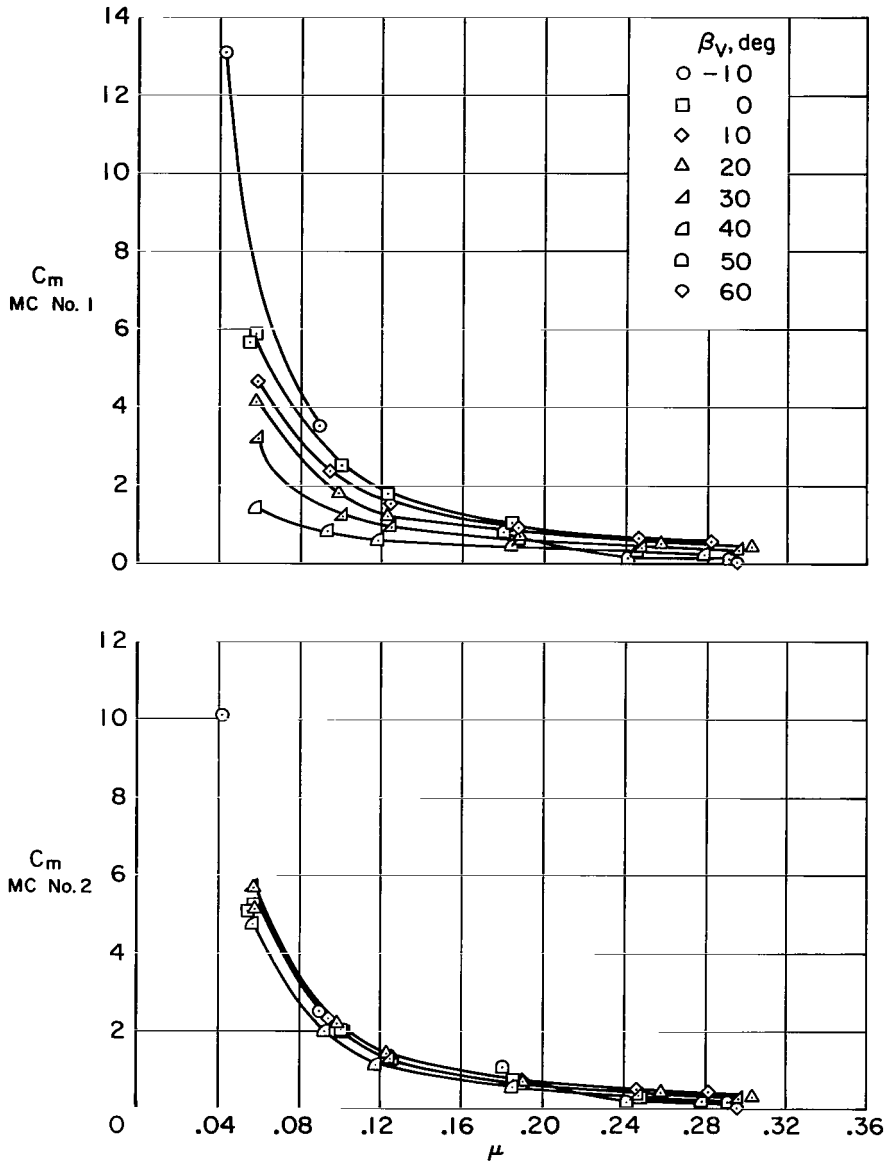

(b) Moment coefficients.

Figure 31.- Concluded.

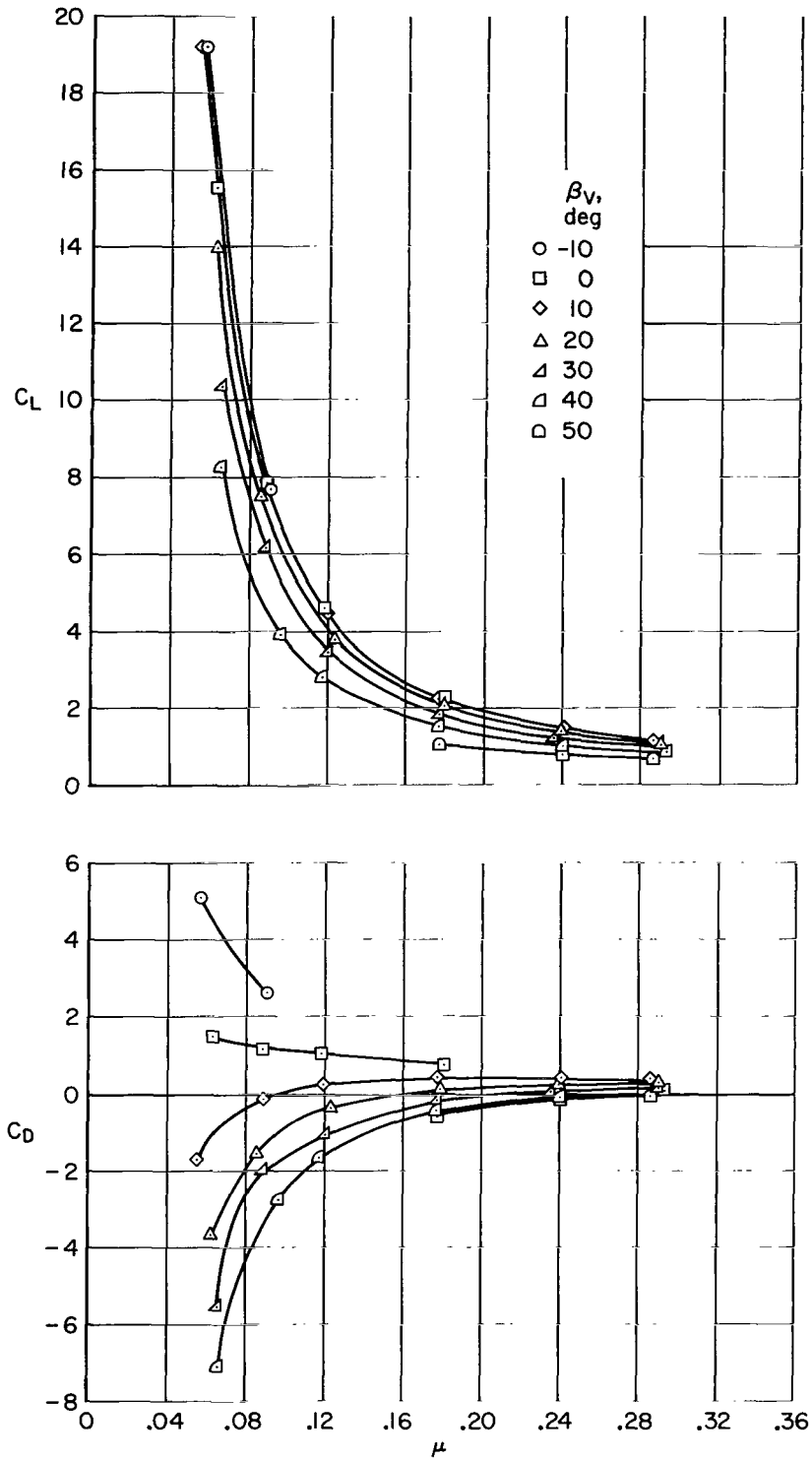

(a) Lift and drag coefficients.

Figure 32.- The effect of tip-speed ratio on the longitudinal characteristics for the tandem lift-fan configuration; tail off, $\delta_f = 0^\circ$, $\alpha = 0^\circ$.

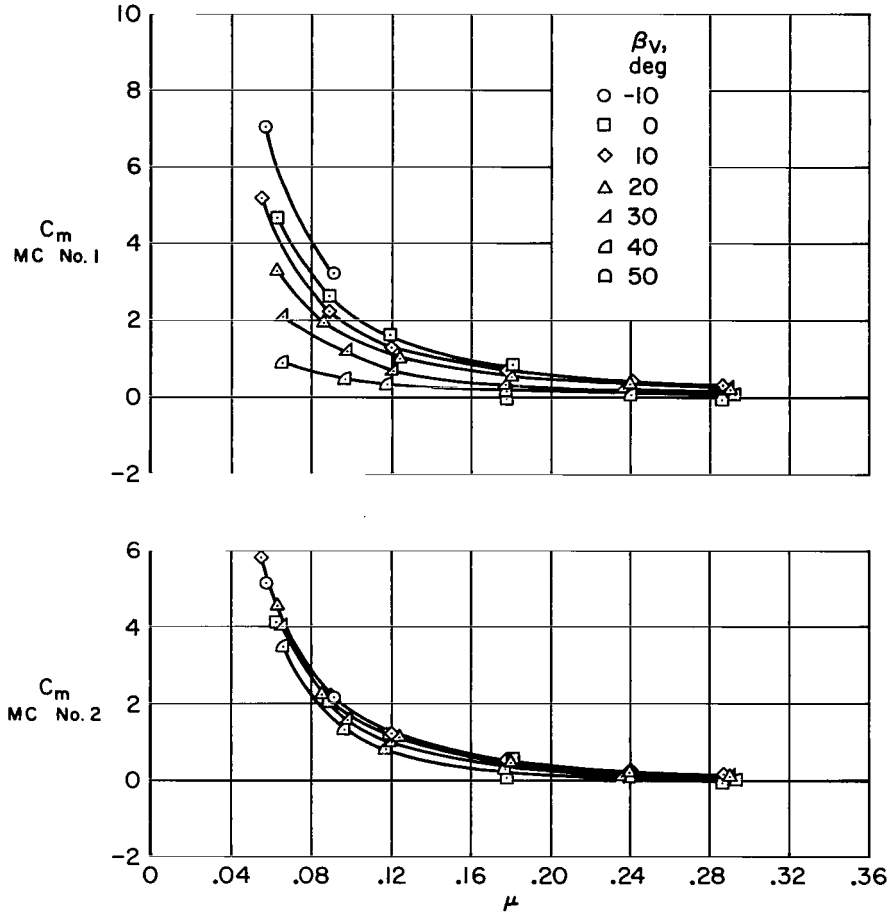

(b) Moment coefficients.

Figure 32.- Concluded.

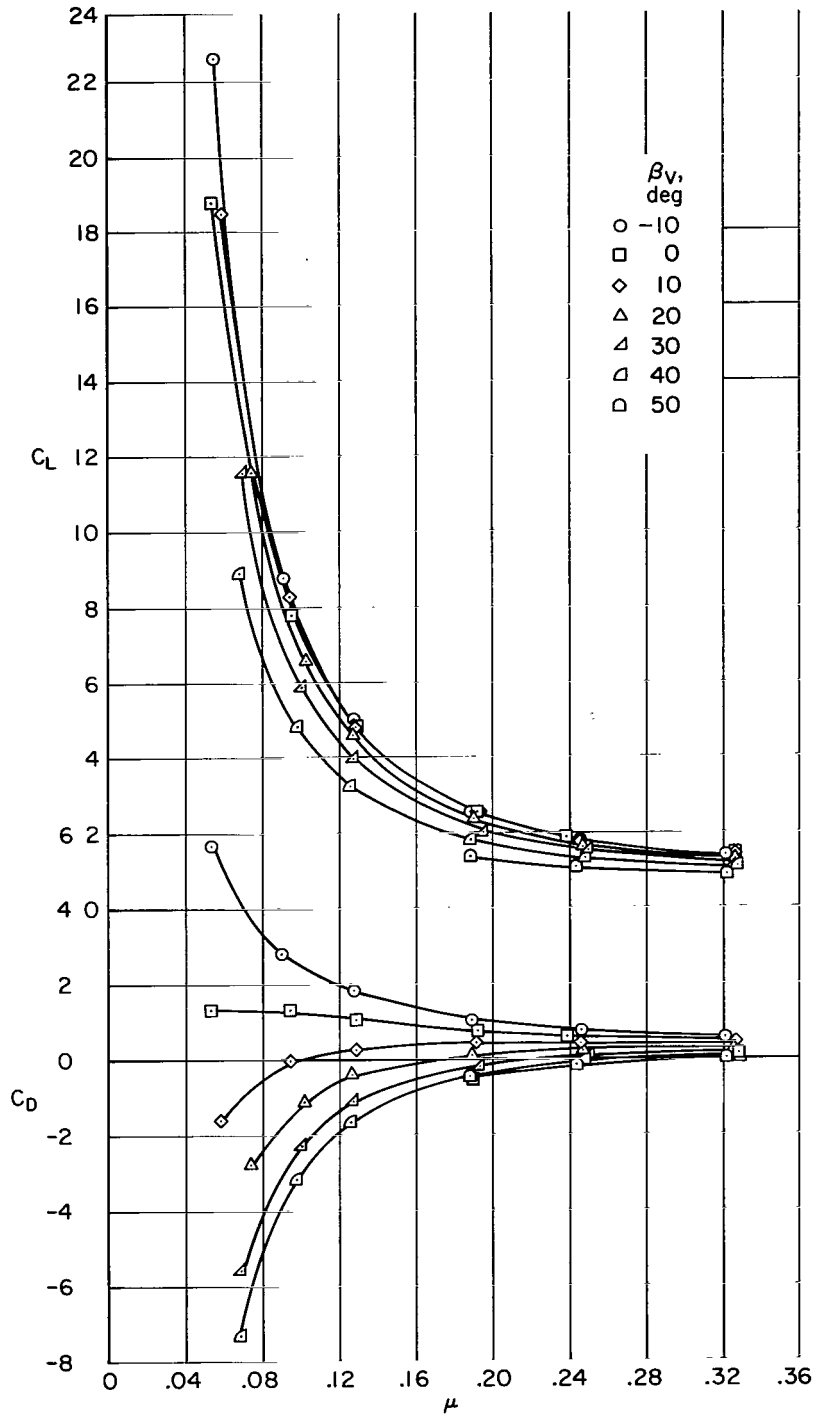

(a) Lift and drag coefficients.

Figure 33.- The effect of tip-speed ratio on the longitudinal characteristics with four tandem lift-fans operating; fairings off, tail off, $\delta_f = 45^\circ$ (part span), $\alpha = 0^\circ$.

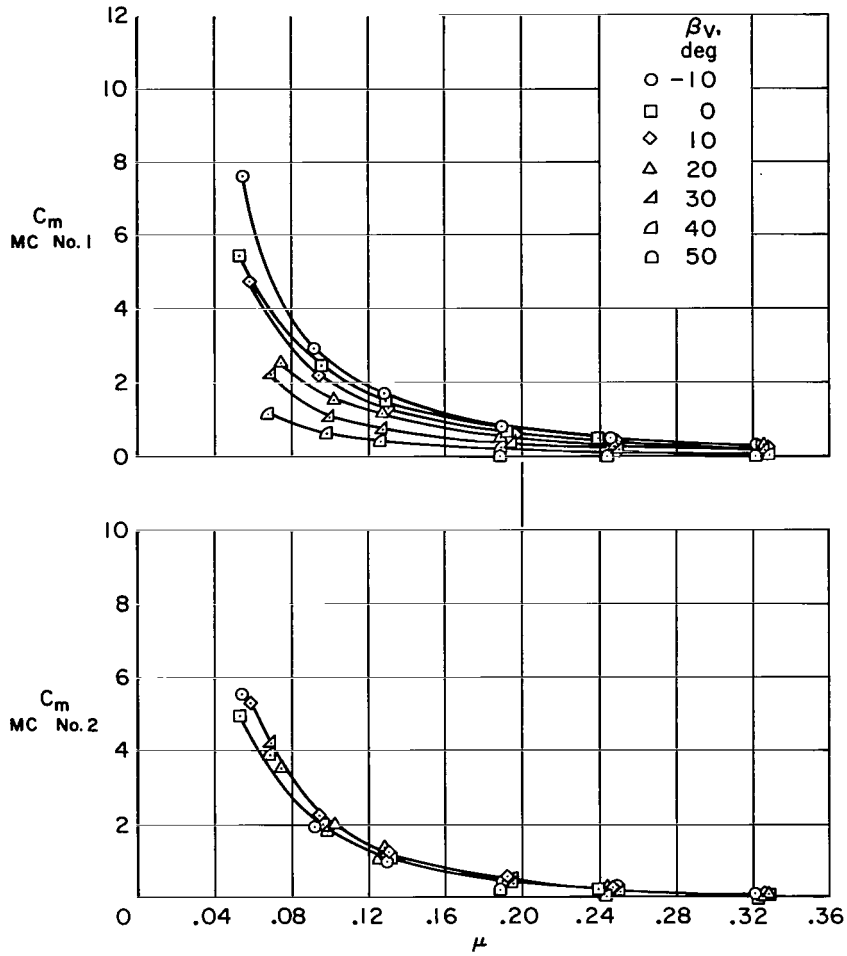

(b) Moment coefficients.

Figure 33.- Concluded.

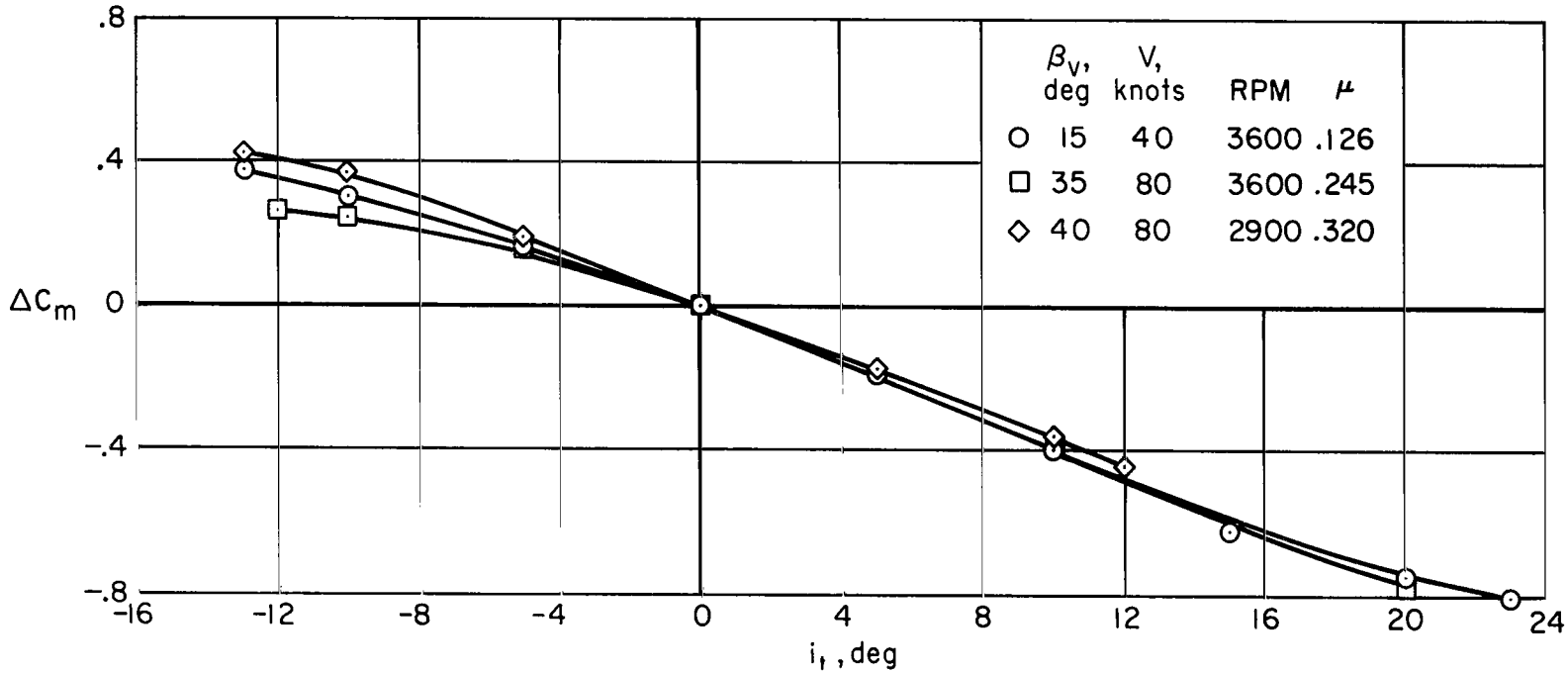

Figure 34.- Trim effectiveness of the horizontal tail for the complete tandem lift-fan configuration operating at various tip-speed ratios; $\delta_f = 45^\circ$, $\alpha = 0^\circ$.

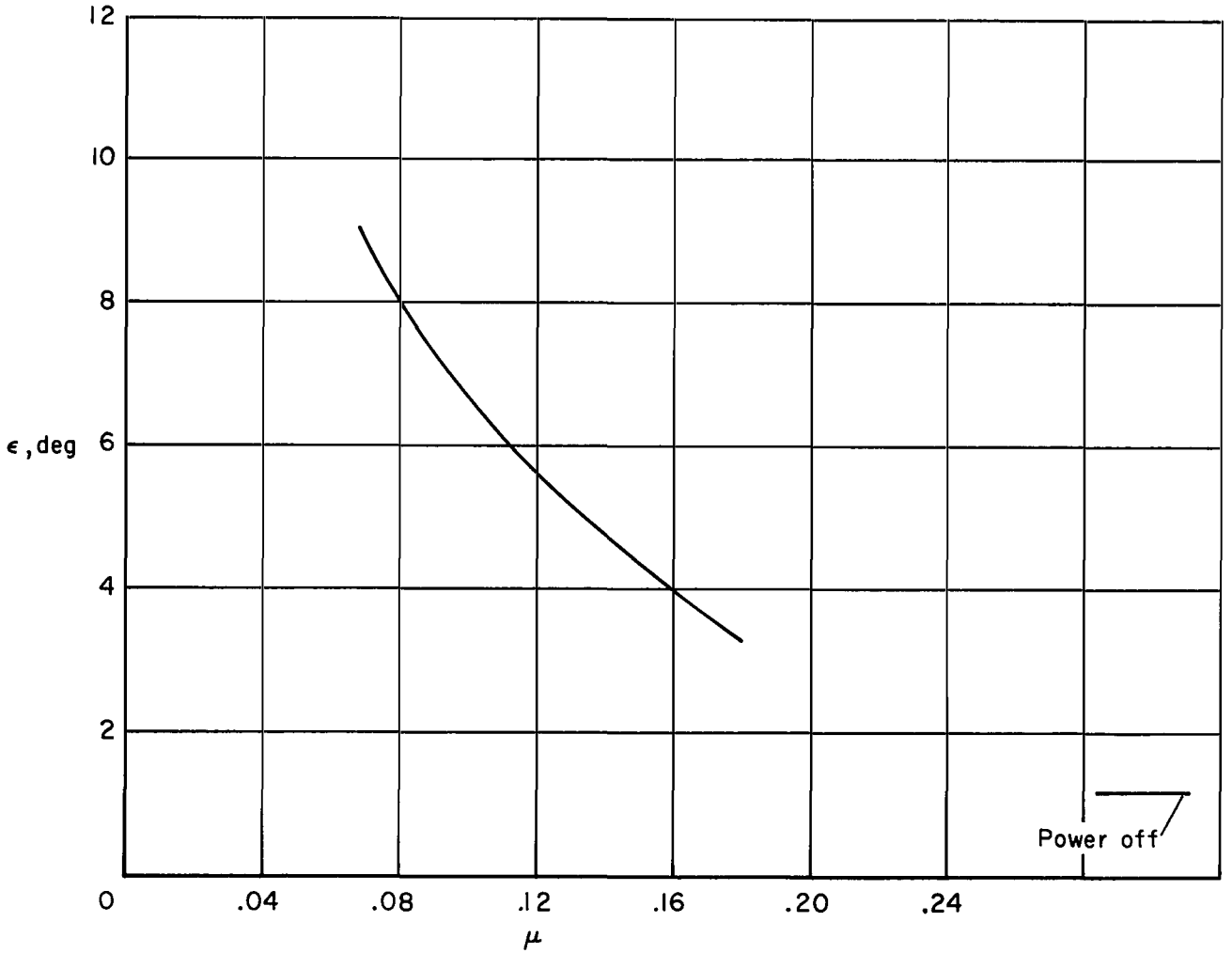

Figure 35.- Variation of average downwash at the horizontal tail for the complete tandem lift-fan configuration; $\delta_f = 0^o$, $\beta_V = 0^o$, $\alpha = 0^o$.

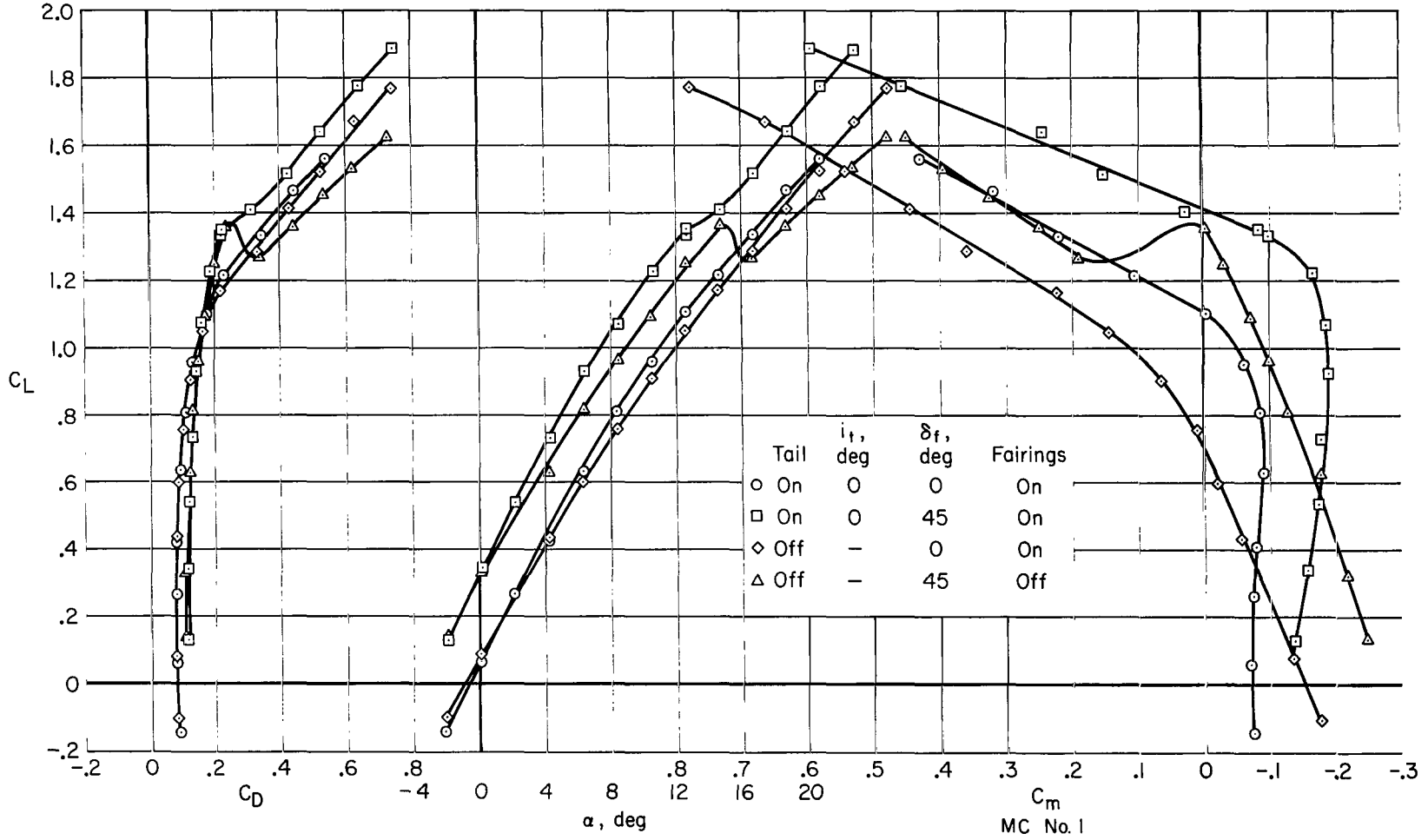

Figure 36.- Longitudinal characteristics with power off for the tandem lift-fan configuration; V = 80 knots.

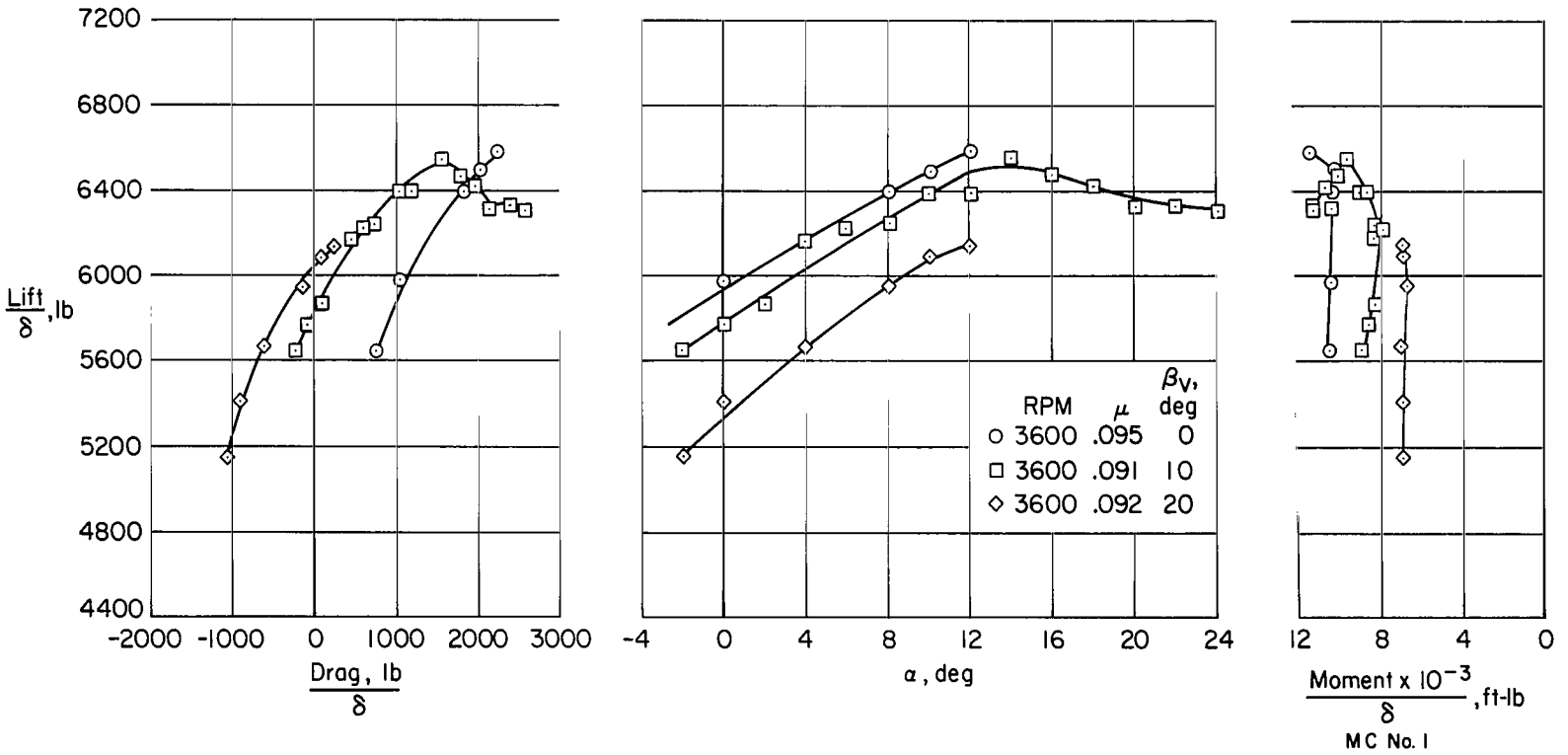

(a) V = 30 knots, $i_t = 15^\circ$.

Figure 37.- Longitudinal characteristics for the complete tandem lift-fan configuration at various tip-speed ratios; tail on, $\delta_f = 45^\circ$.

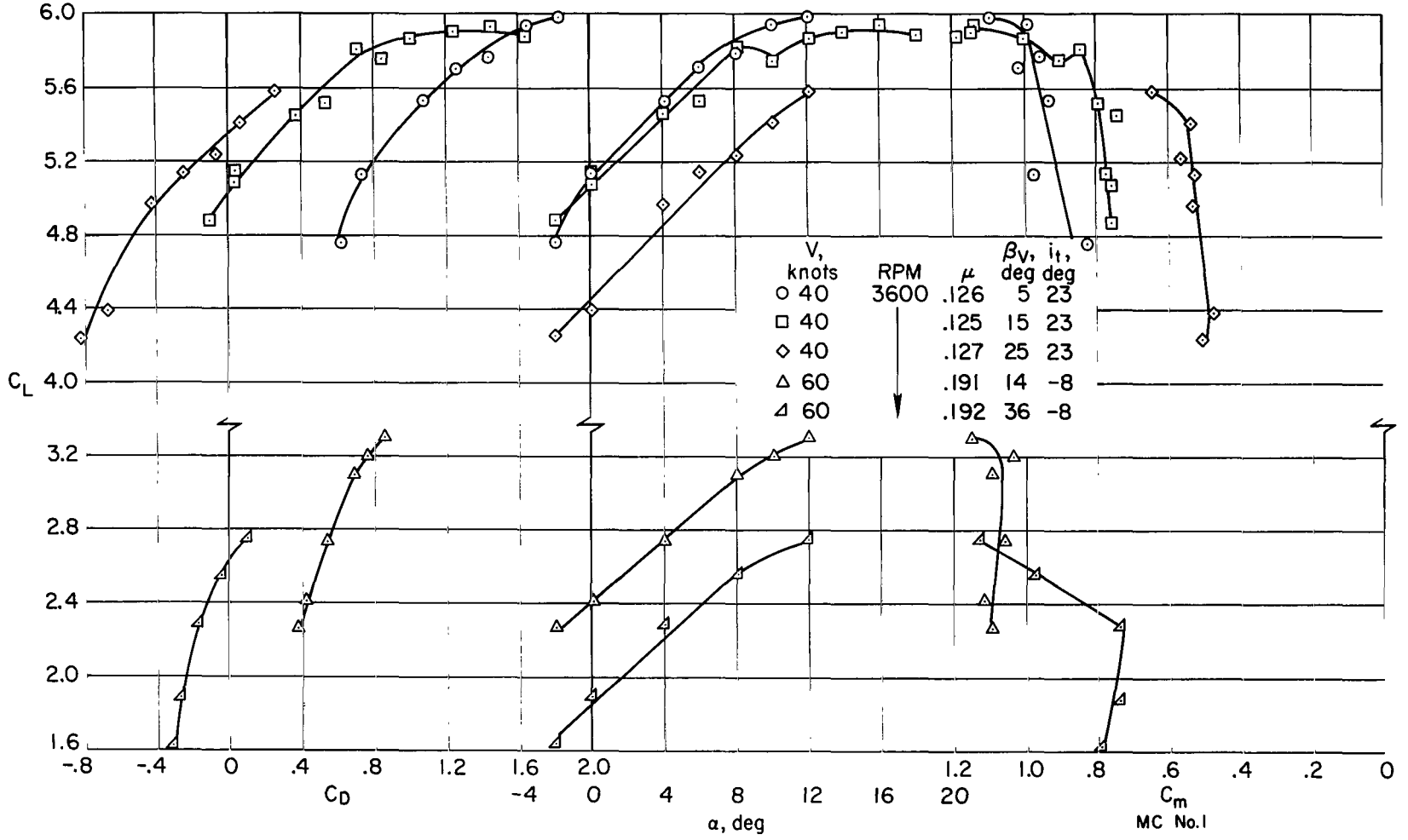

(b) V = 40 and 60 knots.

Figure 37.- Continued.

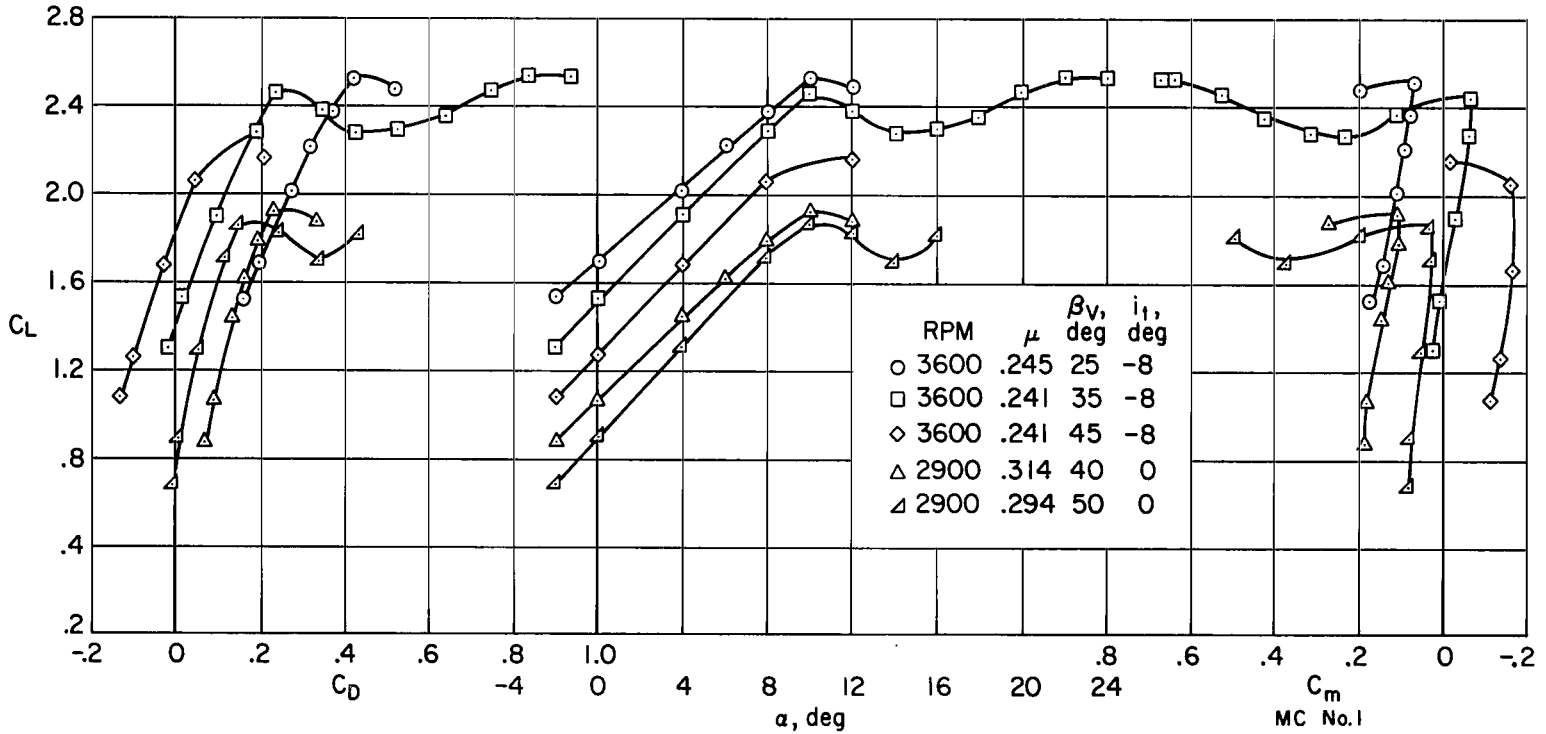

(c) V = 80 knots.

Figure 37.- Concluded.

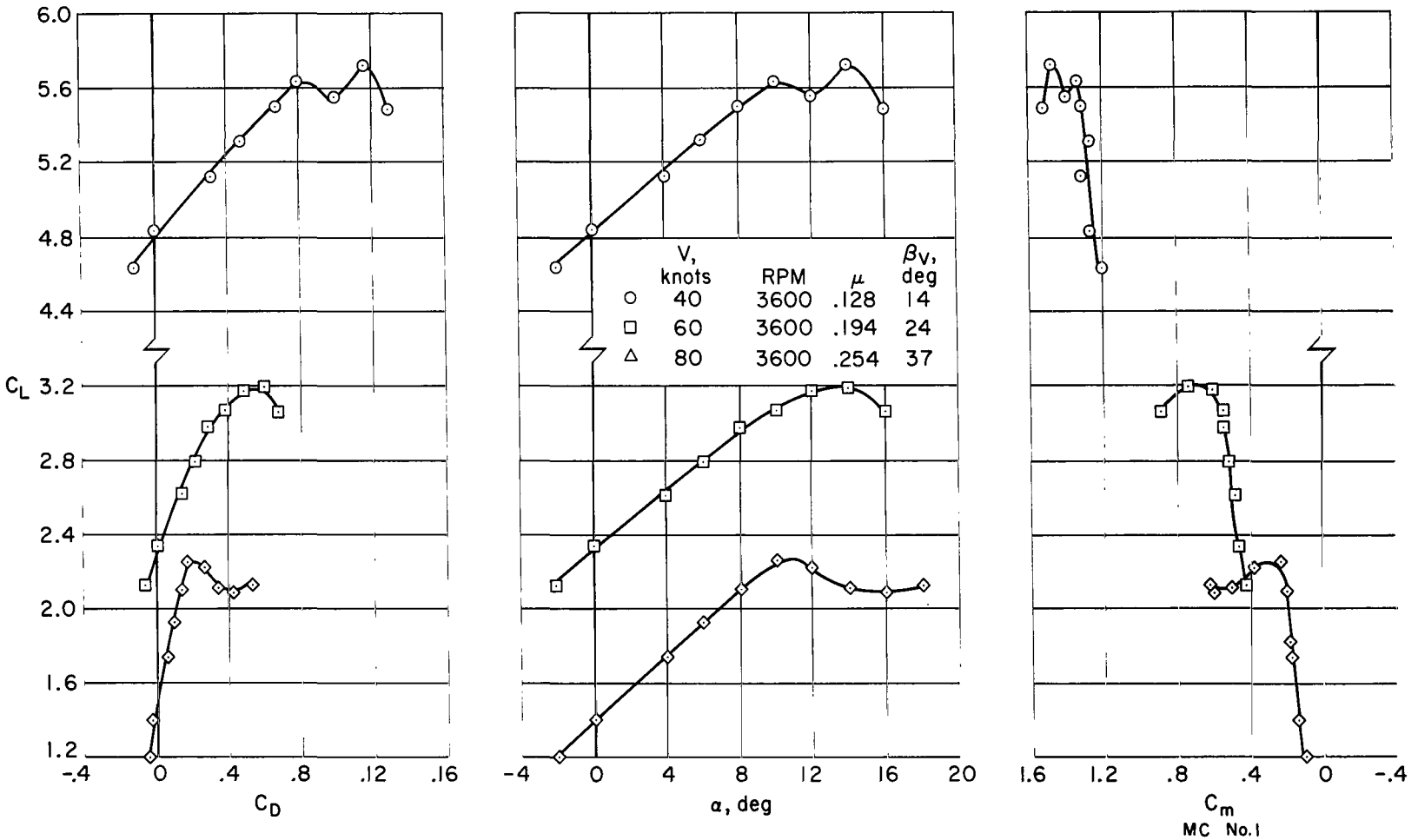

Figure 38.- Longitudinal characteristics with four tandem lift-fans operating at various tip-speed ratios; fairings off, tail off, $\delta_f = 45^\circ$ (part span), $\alpha = 0^\circ$.

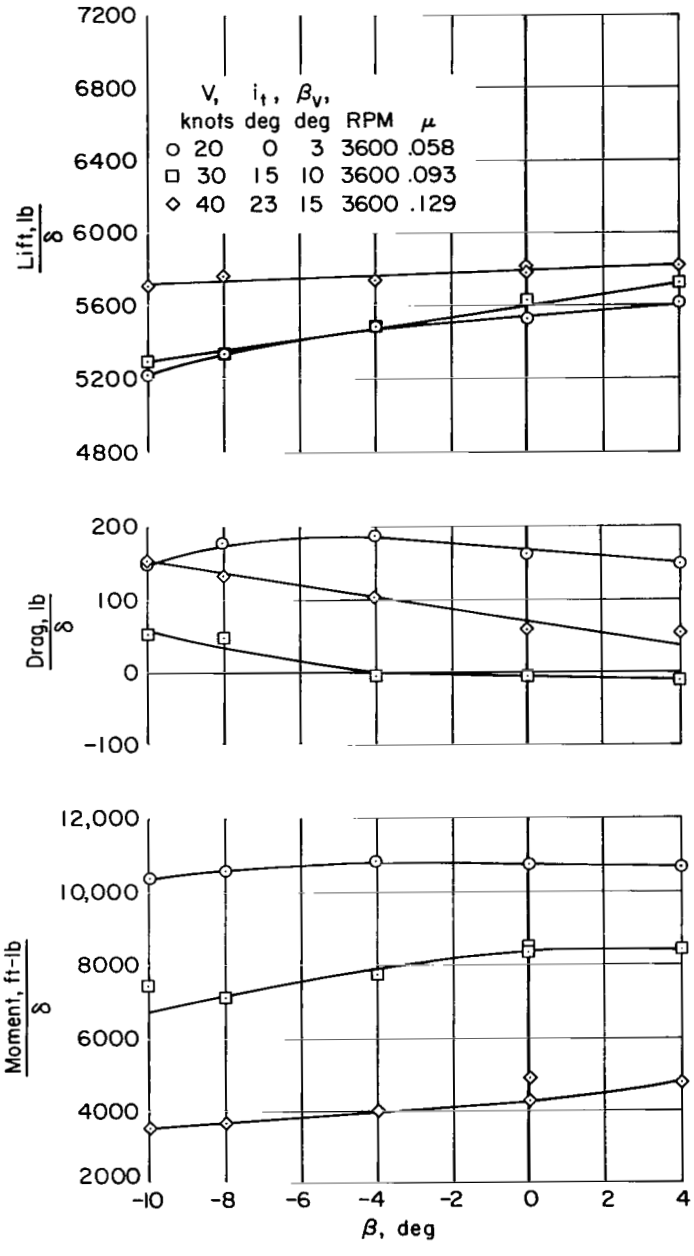

(a) Longitudinal characteristics.

Figure 39.- The effect of sideslip angle on longitudinal and lateral characteristics for the complete tandem lift-fan configuration operating at low tip-speed ratios; tail on, $\delta_f = 45^\circ$, $\alpha = 0^\circ$.

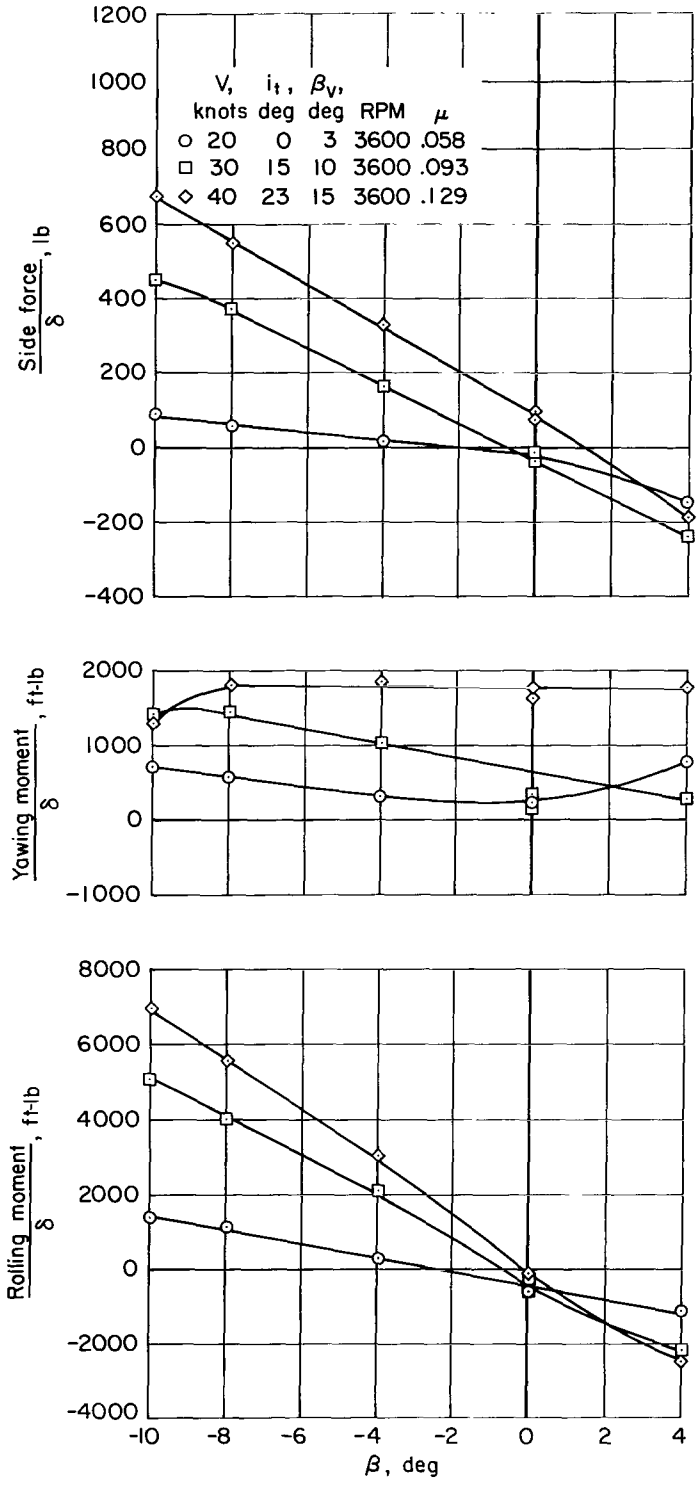

(b) Lateral characteristics.

Figure 39.- Concluded.

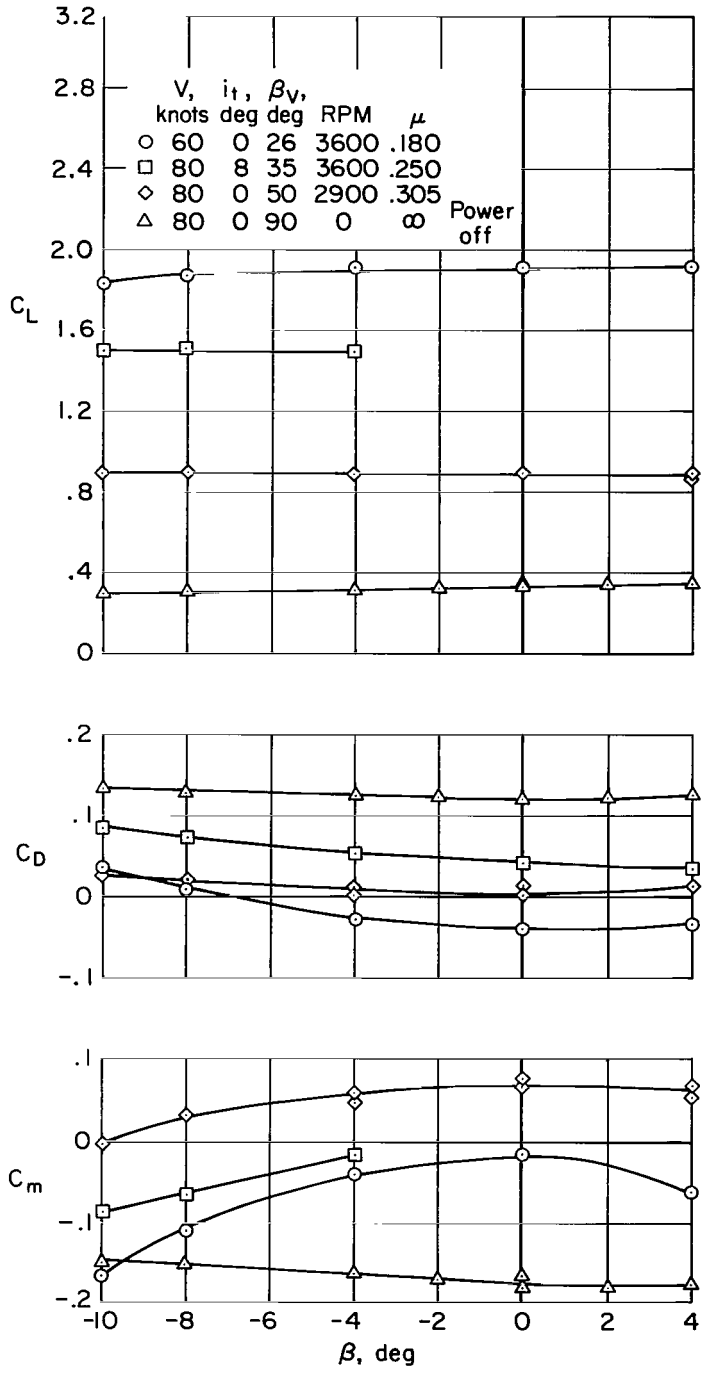

(a) Longitudinal characteristics.

Figure 40.- The effect of sideslip angle on longitudinal and lateral characteristics for the complete tandem lift-fan configuration at various tip-speed ratios; tail on, $\delta_f = 45^\circ$, $\alpha = 0^\circ$.

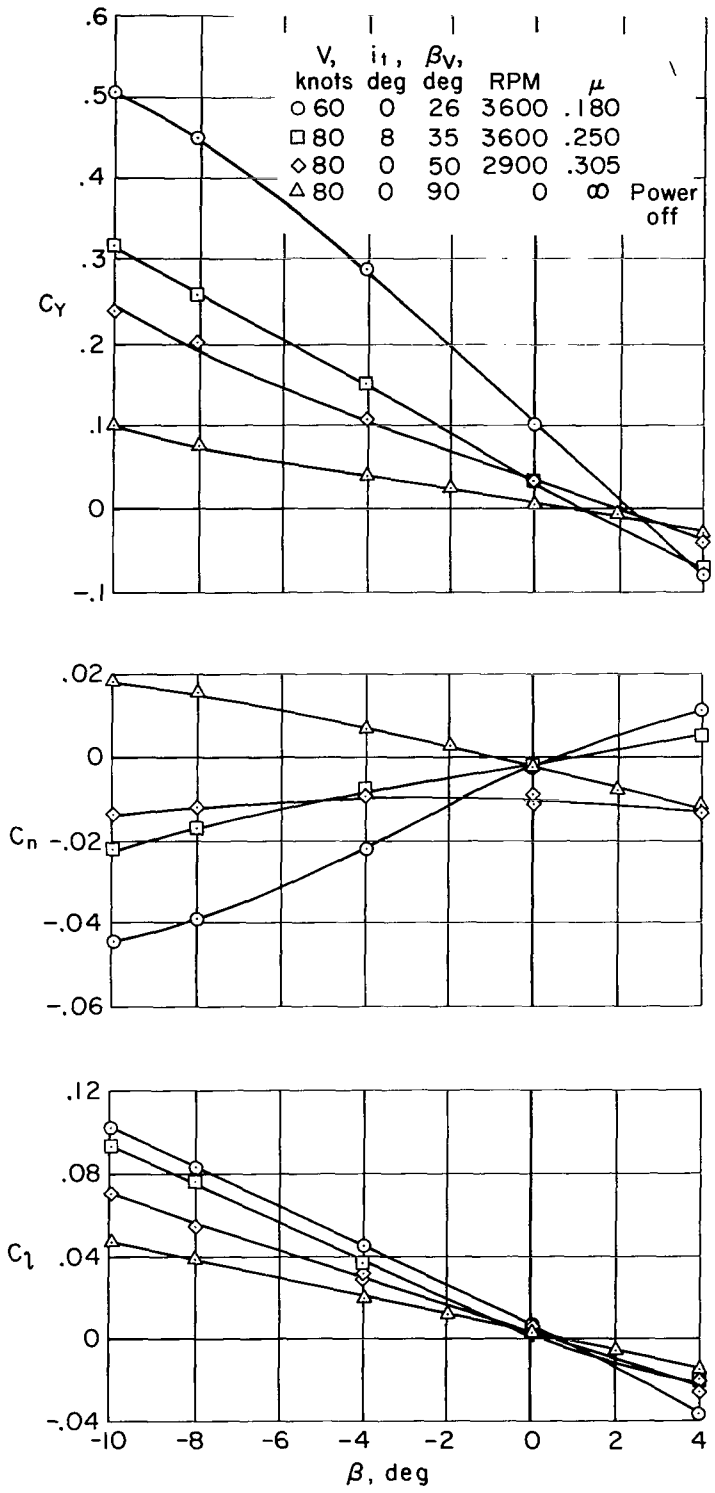

(b) Lateral characteristics.

Figure 40.- Concluded.

"The aeronautical and space activities of the United States shall be conducted so as to contribute . . . to the expansion of human knowledge of phenomena in the atmosphere and space. The Administration shall provide for the widest practicable and appropriate dissemination of information concerning its activities and the results thereof."

—NATIONAL AERONAUTICS AND SPACE ACT OF 1958

NASA SCIENTIFIC AND TECHNICAL PUBLICATIONS

TECHNICAL REPORTS: Scientific and technical information considered important, complete, and a lasting contribution to existing knowledge.

TECHNICAL NOTES: Information less broad in scope but nevertheless of importance as a contribution to existing knowledge.

TECHNICAL MEMORANDUMS: Information receiving limited distribution because of preliminary data, security classification, or other reasons.

CONTRACTOR REPORTS: Scientific and technical information generated under a NASA contract or grant and considered an important contribution to existing knowledge.

TECHNICAL TRANSLATIONS: Information published in a foreign language considered to merit NASA distribution in English.

SPECIAL PUBLICATIONS: Information derived from or of value to NASA activities. Publications include conference proceedings, monographs, data compilations, handbooks, sourcebooks, and special bibliographies.

TECHNOLOGY UTILIZATION PUBLICATIONS: Information on technology used by NASA that may be of particular interest in commercial and other non-aerospace applications. Publications include Tech Briefs, Technology Utilization Reports and Notes, and Technology Surveys.

Details on the availability of these publications may be obtained from:

SCIENTIFIC AND TECHNICAL INFORMATION DIVISION

NATIONAL AERONAUTICS AND SPACE ADMINISTRATION

Washington, D.C. 20546